REPORT DOCUMENTATION PAGE

Form Approved
OMB No. 0704-0188

1. REPORT DATE *(DD-MM-YYYY)*	**2. REPORT TYPE**	**3. DATES COVERED** *(From - To)*
16-12-2009	Final	01-12-2006 to 30-11-2009

4. TITLE AND SUBTITLE
Numerical Modeling of Inverse Problems for Damage Detection in Aircraft Structures

5a. CONTRACT NUMBER

5b. GRANT NUMBER
FA9550-06-1-0542

5c. PROGRAM ELEMENT NUMBER

6. AUTHOR(S)
Prof. Ariosto Bretanha Jorge (P.I.)

5d. PROJECT NUMBER

5e. TASK NUMBER

5f. WORK UNIT NUMBER

7. PERFORMING ORGANIZATION NAME(S) AND ADDRESS(ES)

UNIFEI (Federal University of Itajubá) / IEM (Mechanical Engineering Institute) Av. BPS 1303, Itajuba, MG, 37500-903 Brazil

FAPEPE - FUND DE APOIO ENS PESQ E EXT ITAJUBA (University Foundation) Av. Paulo Carneiro Santiago, 472 - Itajuba, MG, 37500-191 BRAZIL

8. PERFORMING ORGANIZATION REPORT NUMBER

9. SPONSORING / MONITORING AGENCY NAME(S) AND ADDRESS(ES)
AFOSR - Air Force Office of Scientific Research

SOARD - Southern Office of Aerospace Research & Development

10. SPONSOR/MONITOR'S ACRONYM(S)
AFOSR / SOARD

11. SPONSOR/MONITOR'S REPORT NUMBER(S)

12. DISTRIBUTION / AVAILABILITY STATEMENT
Unlimited / Unrestricted

13. SUPPLEMENTARY NOTES

14. ABSTRACT

Structural health monitoring (SHM) is a competitive approach for damage detection in aircraft structures, wherein online information is collected and compared with an existing database for the undamaged structure, to obtain real-time information about the presence of damage. The goal of this research is to develop numerical models of inverse problems for damage detection in aircraft structures, which could later be part of an on-board system for SHM. In this work, the numerical modeling has two main branches: I. The direct problem: a model is required to obtain information on the distribution of the quantity of interest throughout a given damaged structure. The model of the direct problem, using the boundary element method (BEM), is expected to reproduce the reality of an aircraft structure. II. The inverse problem: a model is required to locate the structural damage given the information on the quantity of interest at particular locations (sensor locations). To increase the reliability of the detection approach, a combination of independent optimization and identification procedures can be used. Some treatment of the model uncertainties is required, due to the stochasticity in the problem variables and parameters.

15. SUBJECT TERMS

16. SECURITY CLASSIFICATION OF:			**17. LIMITATION OF ABSTRACT**	**18. NUMBER OF PAGES**	**19a. NAME OF RESPONSIBLE PERSON**
a. REPORT	**b. ABSTRACT**	**c. THIS PAGE**			Ariosto B Jorge (PI)
Unrestricted	Unrestricted	Unrestricted	Unlimited	68	**19b. TELEPHONE NUMBER** *(include area code)* (+5535) 3629-1462

Sponsor: AFOSR – Air Force Office of Scientific Research
(SOARD - Southern Office of Aerospace Research & Development)

Final Report: Years 2006/2009

Project title:
Numerical Modeling of Inverse Problems for Damage Detection in Aircraft Structures

Research Interest Category:
Structural Mechanics

Structural Mechanics Program Manager:
David Stargel, PhD

Director - SOARD (Southern Office of Aerospace Research & Development):
James M. Fillerup, PE

Research developed at UNIFEI / UNICAMP (Brazil)

Prepared by:

Prof. Ariosto B. Jorge. PhD (P.I.)
UNIFEI, Brazil

Date: Dec 16, 2009

Index

Abstract

Structural health monitoring (SHM) is a competitive approach for damage detection in aircraft structures, wherein online information is collected and compared with an existing database for the undamaged structure, to obtain real-time information about the presence of damage. The goal of this research is to develop numerical models of inverse problems for damage detection in aircraft structures, which could later be part of an on-board system for SHM. In this work, the numerical modeling has two main branches: I. The direct problem: a model is required to obtain information on the distribution of the quantity of interest throughout a given damaged structure. The model of the direct problem, using the boundary element method (BEM), is expected to reproduce the reality of an aircraft structure. II. The inverse problem: a model is required to locate the structural damage given the information on the quantity of interest at particular locations (sensor locations). To increase the reliability of the detection approach, a combination of independent optimization and identification procedures can be used. Some treatment of the model uncertainties is required, due to the stochasticity in the problem variables and parameters.

1. Introduction / research outline

1.1 Background

Aircraft structures are subject to damage during their useful life. The timely detection of damages in aircraft structures is an important feature for flight safety. The usual inspection procedures during regular maintenance intervals may lead to problems such as:

- Inspection intervals might be too large, thus allowing damage to propagate unnoticed for an unacceptable time interval or through an unacceptable extension;
- Critical structural components might be difficult to access, thus imposing disassembly / assembly procedures which are time-consuming and expensive, sometimes requiring jigs and other special tools for proper assembly of the structure;
- Some non-destructive techniques (such as eddy current, for example) may be portable, not requiring full disassembly of the structure, but might be inaccurate or might depend strongly on the technician's experience for a damage to be detected properly;
- Other non-destructive techniques (such as X-Ray, or magnetic particles, for example) might require full component disassembly and removal to an industrial facility to perform the structural inspection.
- Some structural components, for example those made of composite materials, may present internal damage which is difficult to detect using standard inspection techniques, as ultrasonic tests.

1.2 Scientific Challenge

Structural health monitoring (SHM) is a competitive approach for damage detection, wherein online information is collected, compared with an existing database for the undamaged structure, and from this comparison, real-time information about the presence of damage is obtained, its

location, length, speed of propagation, and, ultimately, the remaining operational life of the structural component.
Some challenges related to an efficient on-board structural health monitoring system include:

- The system must be small in size and weight, must consume a small amount of power, and must not interfere with the aircraft electrical system;
- The system must be reliable, and the information on the located damage must also be reliable: thus, the system must have redundancies in the built-in numerical codes, which must be based on separate independent numerical models.

1.3 Objective

To study and develop numerical models of inverse problems for damage detection in aircraft structures, which could later be part of an on-board system for structural health monitoring.

1.4 Approach

The approach in this research work is to investigate the feasibility of numerical procedures for damage detection in aircraft structures. The numerical modeling consists in two main parts:

I. **The direct problem:** a model for the structure is required to obtain information on the distribution of the quantity of interest (for example, the acoustic pressure or the stress field) throughout the structure, given the boundary conditions and the presence of the damage. The modeling of the structures is carried out using the boundary element method (BEM). The advantages of the Boundary Element Method over other numerical methods (such as finite elements) are well known from the literature, especially for the treatment of high gradient problems, such as the stress gradient due to cracks. Numerical models for potential, acoustics, or elasticity can be used in combination or independently, to simulate the multiple physics present in lamb waves, stress waves, acoustic emission, etc, involved in the usual structural monitoring techniques ([1] – [3]).

II. **The inverse problem:** a model is required for the procedure of locating the damage in the structure given some (partial) information on the quantity of interest (for example, the stress field) at some particular locations (for example, where some sensors are placed). For this inverse problem, both optimization procedures (local and global optimization) and identification techniques can be used.

Also, both the direct and the inverse problems are in fact stochastic, and involve some level of treatment of the randomness of the parameters and variables of the models.

The research project concentrates on three main problems:

1. **The direct problem:** the model of a structure with a known, assumed damage. For this problem, the numerical codes to investigate must include the model of reinforced panel structures, both metallic and composite. Some possibilities for these models are:
    - The elastic modeling of cracked anisotropic plates using boundary element methods. Further study might include elastoplastic and elastodynamic behaviors;
    - The acoustic modeling of damaged anisotropic plates using boundary element methods. The study might include acoustic propagation from a generated signal or from existing aerodynamic noise.

- The dynamic modeling of the vibration signature of the damaged structure, including natural frequencies and modes of vibration.

2. **The inverse problem:** a global optimization procedure to minimize a functional, obtained from differences between measured values and values generated by the numerical code at different assumed damage locations. The minimum value of the functional will occur when the distance between the real damage and the assumed damage location in the numerical code is also a minimum, thus giving an indication of the damage location and size. Some possibilities to model this optimization problem include heuristics such as evolutionary algorithms (genetic algorithms, or differential evolution, for example). Additionally to the optimization procedures, identification techniques, such as artificial neural networks (ANN), can also be used for this inverse problem, by setting the desired location and size of the damage as parameters.
3. **The modeling of uncertainties:** some variables involved in the process (such as the aerodynamic loads), do not present determinist values and must be treated as random variables. Also, some parameters of the structure, such as the elastic properties and constitutive behavior, are also non-deterministic and must be identified. The treatment of the stochastic nature of the problem leads to parameter identification procedures (such as Kalman filter identification, for example) and to stochastic optimization procedures (such as response surface methodology or Monte Carlo simulation). Procedures to obtain the response surface might include design of experiments combined with regression, or the learning of the structural behavior through a neural network procedure.

The research covered a three-year period (from 2006 to 2009), as a collaborative effort between researchers working in the computational mechanics area from UNIFEI (Federal University of Itajubá) and UNICAMP (State University of Campinas), both in Brazil. During the three years of the project, the research also lead to advising graduate students, both at UNICAMP (with the research concentrated in the study of the behavior of cracked composite plates using boundary element methods) and at UNIFEI (with the research concentrated in the use of deterministic and stochastic optimization and identification techniques for a given direct modeling (elasticity and acoustics, for example).

The modeling of uncertainties was incipient in this work, and is an on-going effort, which is planned to continue as a collaborative research work. Also, a combination of FEM and BEM as direct models was not covered in this research project, and is being planned as an on-going research work, too.

1.5 Resources / Research team

- Professors Ariosto Bretanha Jorge (PI – Principal Investigator) and Sebastião Simões da Cunha Jr. (UNIFEI);
- Professors Paulo Sollero and Eder Lima de Albuquerque (UNICAMP);
- Students from the Computational Mechanics groups (both from UNIFEI and UNICAMP);
- Computational mechanics laboratories at UNIFEI;
- Computational mechanics laboratories at UNICAMP.

1.6 Air Force Relevance

This research investigates numerical models for detection of damages in aircraft structures. The timely detection of damage is an important feature for flight safety. This research is also relevant in aircraft maintenance, with the possibility for using such on-board structural health monitoring system as a substitute for some costly structural inspections during regular, scheduled maintenance.

1.7 Cost / Funding

For this project, a grant of U$70,000.00 was awarded (U$ 20,000.00 for the first year, and U$ 25,000.00 per year, for the second and third years). The funding was directed to finance research expenses (both for the researchers and the students), evenly divided for each university, during these three years of collaborative work. Expenses covered included stipends for students, and also general expenses related to the project (for example, travel expenses, computers, software, computer consumables, books, etc).

1.8 Contact Information for the P.I.

Prof. Dr. Ariosto Bretanha Jorge
UNIFEI - Universidade Federal de Itajubá
Instituto de Engenharia Mecânica
Av. BPS 1303
37500-903 - Itajubá, MG - Brazil
Tel (Brazil): +(35) 3629-1462 (office); +(35) 3629-1152 (secretary);
Fax: +(35) 3629-1148 (secretary)
Email: ariosto.b.jorge@unifei.edu.br
Home page: http://www.gemec.unifei.edu.br/ariosto/

2. Research description

Modeling the damage detection problem: general aspects

The detection of damage (or failure) in structures is an important area in engineering, with several fields of application, among which one can point out: flight safety and aircraft maintenance, piping and containers in the oil industry, structures in nuclear power plant industry, etc. The development of damage detection techniques can bring up technological advances in order to increase the structural reliability (safety), contributing to a better structural integrity analysis and to a better evaluation of the remaining service life (or useful life) of a structure. The analysis of a damaged structure must involve the numerical treatment of data gathered from sensors spread throughout critical points in the structure, and the comparison of this data with numerical results used as reference (for example, results from the same structure without damage of with given (known) damage). These damage detection techniques could involve monitoring (in real time) of the integrity of structural elements which are critical and are difficult to access

(poor accessibility), such as some elements in an airframe, or in an oil piping, or in nuclear or oil installations.

2.1 Damage detection: overview of the Direct and Inverse Problems

To analyze a damage detection problem in a structure, first the modeling of the direct problems is required, to obtain the behavior of this structure in the presence of one or more pre-established damages, with assumed format and size, and at given positions (see references [4] e [5] for damage detection problems).
In this work, two methods of analysis were given particular attention, for the direct method:
1) The study of the stress and strain distributions in structural elements, performed through the BEM (boundary element method) modeling of elastostatics problems (for defects modeled as holes in the structure) or through the BEM modeling of linear elastic fracture mechanics problems (for cracked structures) (see references [6] to [13] for the boundary element method applied to fracture mechanics);
2) The study of the distribution of some scalar field throughout the structure, modeled using BEM. For problems governed by the Laplace or Poisson equations, a potential field, such as the temperature distribution, is the quantity of interest. Other potential fields, such as the sound pressure in the structure due to sound waves (emitted from a pre-established source) were also investigated. The presence of the defect in the structure influences the distribution of these scalar fields. BEM models were used both for Laplace / Poisson problems (heat transfer by conduction in the structure) and for the modeling of the acoustic problem (see references [14] to [17] for the boundary element method applied to acoustics).
The study of other modeling approaches is being planned as an on-going research work, and is not covered in this report. The methods of interest, for this future research, include damage detection approaches based on vibration analysis, and also based on a combination of Finite Element and Boundary Element Methods as a FEM/BEM direct model (the BEM model being best suited for large gradients in the field being considered, while the FEM accommodating well properties/material changes throughout the structure).
For the study of the inverse problem, the model consists of two parts:

a) Monitoring the structural integrity, from experimental measurements, with a certain number of sensors spread throughout the structure. With this, some knowledge is obtained about the distribution of stresses or strains (for example, by means of strain-gages) or about the distribution of a variable derived from the acoustic pressure throughout the structure (for example, by means of microphones, accelerometers, or other sensors).
b) Computation of a functional obtained from adding differences (evaluated in all measurement points) between the values evaluated using the numerical model from the direct problem, for a given damage that was assumed, and the experimental values measured in the same points for the structure with the real damage or crack. This functional is a function of the crack or damage location, either numerical or measured from the real structure. This functional is expected to increase in value when the assumed numerical defect is far away from the real defect. Also, this functional is expected to reach its minimum value when both defects (for example, the numerical and real cracks) coincide. Thus, the inverse problem is, in fact, an optimization problem for the search of a global minimum for this functional. In this work, local optimization methods (such as

linear or quadratic sequential programming) were used to compare with global optimization heuristics (such as genetic algorithms and differential evolution).

The study of the randomness of the variables involved in these problems is of great importance, in order to the computational modeling being used to be representative of the real structure. The study of the randomness was incipient in this work, using stochastic optimization techniques. To account for these uncertainties, future work is planned, for the use of parameter identification techniques (such the Kalman filter approach), together with the treatment of the uncertainties of the variables (using fuzzy optimization techniques) or the treatment of the randomness of these variables (using stochastic optimization techniques, such as response surfaces, or using Monte Carlo simulation).

2.2 Direct Problem

The boundary element method is a numerical procedure well adapted for the modeling of a cracked structure made of an isotropic material (aluminum, for example) or made of orthotropic materials (such as composite materials). In this method, the distribution of the quantities of interest in the domain is obtained from the information of the distribution of some quantities in the boundary. Thus, in this method, the problem is described based on what happens in its boundaries, reducing the dimension of the problem and simplifying numerically the treatment. Furthermore, the boundary element method offers an additional advantage for the fracture mechanics problem, as the scalar and vector fields of the variables of interest can be described with reasonable accuracy, even when these fields are singular, as it is the case for the stress field near the crack ends (near crack tip in 2D, or near crack contour in 3D).

In the case of the approach for the damage detection problem made by means of the analysis of the acoustic response of the structure under excitation, perturbations in the expected response imply in the presence of damage. Thus, the defects and damage in the structure shall characterize its dynamic behavior. The modeling of the direct problem may include also the study of the damage evolution through time (such as, for example, the velocity of crack propagation), in order to estimate the remaining useful life (safe life) of the structure.

2.3 Inverse Problem

The inverse problem might be modeled by means of optimization techniques or by identification techniques. In the following discussion, some aspects of these techniques are detailed. For the discussion, a simple Laplace problem for the distribution of a potential field in a domain is considered. The damage is simulated by the presence of small holes in the domain, and the goal is to obtain the size (diameter of the hole) and the location (vector position of the center of the hole) of the damage.

The direct method (BEM) provides one piece of information (the potential) for any desired point in the domain. Without the hole, the distribution of the potential is known a priori. If a small hole is included, the potential distribution is unknown and must be obtained numerically from the BEM solution. The goal in this problem is to implement two inverse methods (optimization and identification) and to discuss the difficulties in the implementation and advantages of each method, to find out which one is more appropriate to solve the problem. The results obtained for the inverse method by means of this two independent techniques (genetic algorithm (GA) for the optimization procedure and artificial neural networks (ANN's) for the identification procedure)

are compared to analyze the efficiency of each method in finding the location and dimension of the hole.
Increasing the problem complexity, the BEM for the elasticity problem can be used, with some given boundary conditions for the displacement and traction. Differently from the BEM for the potential, the BEM for elasticity (in a 2D problem) provides two pieces of information at a single interior point – one normal stress and one shear stress. But this information cannot be used directly in the optimization problem, as it depends on the system of coordinates being used, or on the normal direction of the cutting plane that passes through the point of interest. Therefore, a choice was made to adopt the stress invariants of the stress tensor at the point of interest– in 2D, the mean stress and the octahedral stress – as the vector field to be analyzed and used in the optimization problem.
A comparison of different (and independent) optimization and identification techniques for this inverse problem of damage detection is also desirable, to check for the robustness of the different approaches in finding the damage. The global optimization techniques that can be used include: genetic algorithm (GA), differential evolution (DE), ant colony (AC), etc. The parameter identification techniques that can be used include: artificial neural networks (ANN's) and Kalman filter (KF).
In order to increase the complexity of the damage detection problem using the BEM formulation for elasticity, the goal could be to identify and locate (using one or more of the inverse problems approaches) the presence in the plate of one or more circular holes (number of holes, radius and location of each hole) and also one or more ellipses (number of ellipses, axis orientation and size (large and small axis) and location of center for each ellipse). To increase even further the complexity of the damage detection modeling, the BEM for fracture mechanics can be used, in order to locate cracks in the plate (number of cracks, and their size, orientation, and location).
For all the different direct problems, the same global optimization techniques and/or parameter identification procedures can be used to solve the inverse problem for damage detection. From the point of view of the inverse problem, the direct model is just a '*black box*' to be supplied to give the numerical information needed to be used in the optimization or identification procedure.
The starting point in the research is to analyze and discuss the detection of just one hole in the structure. Later in the research, by modifying the implementation of the inverse problem, the model would be able to detect more than one damage in a particular structural element.
Concomitant to this research, several different configurations for the direct problem are evaluated (BEM for cracked orthotropic materials, material interfaces, etc). The goal is to implement BEM codes representing situations that emulate better a real aircraft structure (including structural patches, reinforcements, etc). These BEM formulations for the direct problem are being developed mostly by the researchers at UNICAMP. On the other hand, the implementation of the inverse method is being developed mostly at UNIFEI. The two research fronts are under way in parallel, so that the final code would include as many direct codes as possible (to allow for a representative number of possible combinations of damages / airframes to be evaluated), as well as a number of different (independent) inverse models, to increase the reliability in the damage information (quantity, location, and size).

Damage detection by means of optimization techniques

In an experimental analysis, the data gathered come from sensors spread throughout the structure, located at a number of points. The experimental analysis is not being undertaken at this

moment, thus the size and location of the real damage in the plate are being assumed and simulated by using the BEM. In this first example problem, BEM for the potential is being used, and the temperature values at some interior points replace the information that would have been collected by the sensors at these points in the plate.

In order to solve the inverse problem for damage detection, an optimization algorithm (GA, for example) is used. The evaluation function (fitness function) for the GA is formulated as a functional defined as a difference between measured values (simulated, in this case) of the local difference in the potential (between the undamaged plate and the plate with the damage) and the values of the same differences in potential calculated at the same points by the damage detection code (assuming several different locations and sizes for the 'numerical' damage). The minimization of the functional allows the damage detection code to find the unknown parameters of the damage. A general formulation for the functional is shown in Equation (1).

$$J_j = \frac{1}{2}\sum_{i=1}^{n}(measured_i - calculated_{ji})^2 \qquad \textbf{(1)}$$

Where:

n - Number of sensors placed in the plate (number of internal points *i* where differences are evaluated);

$measured_i$ - Vector of simulated values for the differences in potential (obtained using BEM, these values represent the values measured in the plate points for a given damage location and size);

$calculated_{ji}$ - Vector of values for the differences in potential calculated by the damage detection code for each individual *j*.

Figure 1 represents an undamaged thin plate with four sensors indicating the points where the measurement of the quantities of interest (differences in potential, in this case, or stresses, for example, in the elasticity case) is being performed.

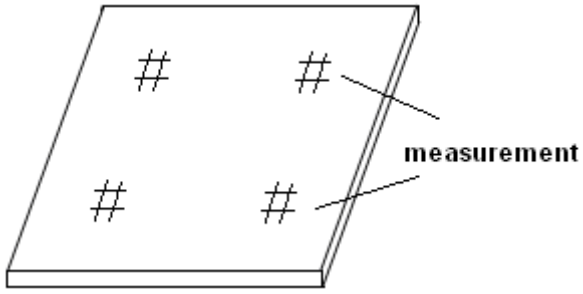

Figure 1 – Undamaged plate with four representative sensors

In order to solve the damage detection problem, an initial population is given to the GA. This initial population is formed by individuals which constitute a possible solution for the problem. These individuals are represented by chromosomes which are themselves constituted by genes. Each gene in a chromosome represents one variable in the problem (for example, the *x* and *y* coordinates and the radius *r* of the hole). As an example, Figure 2(*a*) to 2(*c*) represents three possible configurations of chromosomes. While the location and size of the hole varies, the number of sensors and their locations are always the same, for all chromosomes (these are also

the locations of the 'real' sensors for the measurements). The information on the quantity of interest is collected at these sensor locations for all cases.

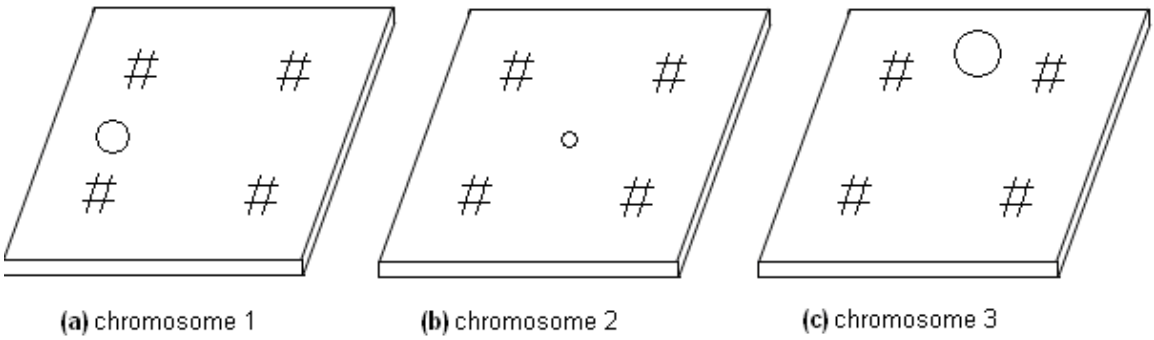

Figure 2 – Plate with a hole: three possible configurations for the chromosomes

Some of the plate properties (such as material properties and geometry) may not be known exactly a priori (due to randomness in the manufacturing or fabrication processes, for example). Material properties (such as elasticity modulus E, and Poisson's ratio υ, in the elastic problem) and geometric parameters (see Figure 3, for example) are suited to be obtained in the real structure by means of parameter identification procedures (such as ANN, for example).

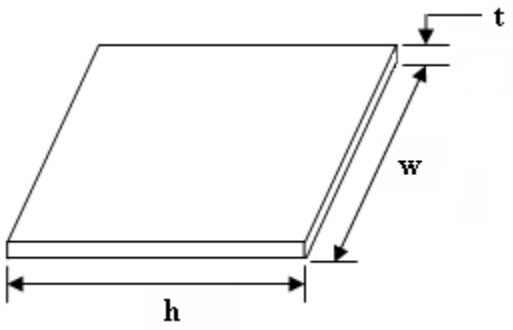

Figure 3 – Plate geometry: possible parameters to be identified

Other variables (such as the loading (shown in Figure 4) and the boundary conditions) may contain uncertainties and randomness and may need to be treated as random variables in the damage detection code.

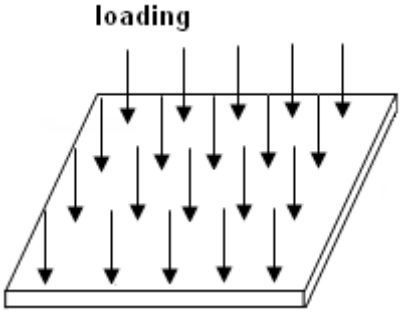

Figure 4 – Loading: possible variables to be treated as random

Also, the number, size and location of the different damages may need to be treated either by parameter identification or as random variables.
For a straight crack, its parameters may be (see Figure 5):
- size = a;
- orientation = θ;
- position = (x_0,y_0).

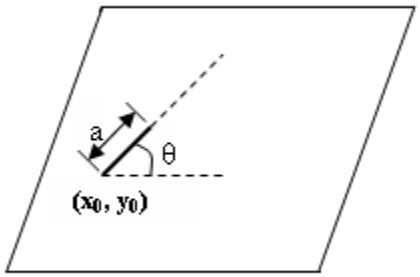

Figure 5 – Crack parameters: size, orientation, position

The treatment of randomness is detailed in the next session (Modeling of Uncertainties). A result expected from the on-going research is the discussion on which method for modeling of uncertainties (identification procedures versus probabilistic methods) is best suited for each of the different variables and parameters of the problems.

For the transition from the plate with a hole to a cracked plate, the direct model using BEM is the only subroutine that changes in the code (from BEM for elasticity to BEM for linear elastic fracture mechanics). The procedures for the inverse problem (either optimization or identification techniques) remain unchanged. Thus, for the simulation, the position, orientation and size of the 'real' crack are assumed (see Figure 6). Also, the numerical solutions for the different chromosomes are obtained in the same way as before (see Figure 7 for three possible chromosomes).

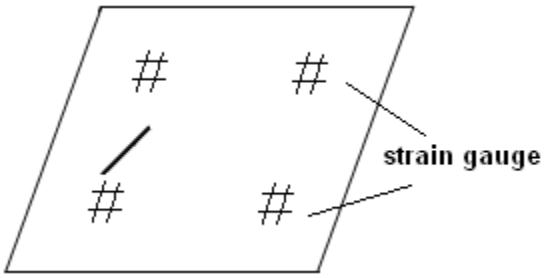

Figure 6 – Cracked plate: size, orientation, position of the 'real' crack (simulated, in this case)

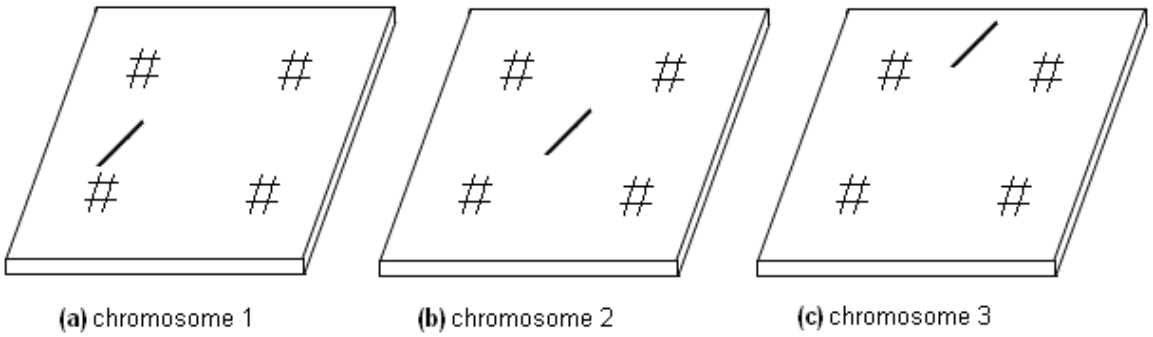

Figure 7 – Cracked plate: three possible configurations for the chromosomes

2.4 Modeling of Uncertainties

This part of the research involves the numerical modeling of an engineering optimization problem with two basic features:

i) the various parameters and variables of the system being studied are not deterministic, and a proper treatment of this variability leads to robust optimization techniques, where the goal is to obtain not only optimum values for the objective functions, but also minimum variations in these objective functions in the neighborhood of these optimum points. In this context, the words '*stochastic optimization*' and '*robust optimization*' lead to the same idea, as the goal of the treatment of the stochasticity of the variables and parameters of the problem is to obtain robust optima. In this case, the optima are points in the feasible region, wherein the values of the objective functions are insensitive to variations around these points;

ii) the fact that the model has to look not only for the optimum values of the objective functions but also for robustness (that is, a small variability of these objective functions around these optima) shows that, in each problem, there is always more than one objective function. Thus, there is a need for decision-making procedures with respect to these multiple objectives, which may involve the use of different multiple-objective optimization techniques, such as weighting, prioritizing (goal programming), the use of objective functions as constraint equations, the use of fuzzy membership functions, obtaining Pareto limiting regions or curves, etc.

Thus, the modeling of uncertainties of the damage detection problem in an aeronautical structure involves stochastic multi-objective optimization techniques in the modeling of the inverse problem.

Modeling the multiple-objective optimization problem: general aspects

The traditional optimization methods usually treat the variables of the problems as deterministic. For a review of traditional calculus-based algorithms (for the search of local optima), see references [18] and [19].

Heuristics that search for global optima have been proposed in the literature, several of which based in the imitation of behaviors found in nature. An example of this is the '*survival of the fittest*', found in heuristics such as evolutionary algorithms, genetic algorithms, differential evolution, particle swarm optimization, etc (see references [20] to [27]).

But in several cases, these algorithms still consider as deterministic the problem variables (for example, the loading, boundary conditions, material properties, geometry etc) and/or parameters (for example, the coefficients in the objective functions or in the constraint equations).

Treatment of stochasticity of variables and parameters

The modeling of stochasticity both in the variables and in the parameters of a problem involves the use of probabilistic methods in engineering, such as Monte Carlo simulation, Response Surface techniques, Design of Experiments, First Order Reliability Methods (FORM) or Second Order Reliability Methods (SORM), logistic regression, etc.
The stochasticity can be also used in identification procedures in two steps: first, a set of random information is used to identify the system parameters (for example, via Kalman filter), and second, an independent set of stochastic data is used for the treatment of the random variables of the problem (see references [28] to [32] on different probabilistic methods in engineering).

Decision techniques in the treatment of multiple objectives

Decision techniques regarding the multiple objectives of an optimization problem may include: weighting, assignment of priorities, the use of objective functions as constraint equations, the use of fuzzy membership functions in the decision-making process, obtaining regions or curves of Pareto limits, etc.
In certain cases, objectives of different natures may need to be considered, and their combination (through weighting, for example) may not be possible. For example, on a particular problem, one objective may happen to be written as a real function, while another objective may involve only integer numbers, and a third objective may involve only a qualitative response. In this case, a promising technique for a proper combination of these objectives of different natures could be the use of fuzzy membership functions for each objective function, looking for the optimization of one function only, namely, the summation of all the fuzzy membership functions. This technique could even allow the designer to include a bias through one or another objective function, if this is considered necessary (see references [33] and [34] on the use of fuzzy logic in optimization).

3. Main accomplishments

This research is a collaborative effort between the Computational Mechanics groups at UNIFEI (Itajubá) and UNICAMP (Campinas). The research on the direct problem has been performed under supervision of Professors Paulo Sollero and Eder Lima, at UNICAMP, while the research on the inverse problem and on the modeling of uncertainties has been performed under supervision of Professors Ariosto and Sebastião Simões, at UNIFEI.
As results directly related to this research, several publications and monographs were obtained, as detailed in the Appendix. The publications were concentrated on conference papers and journal articles, while the monographs were concentrated on thesis and dissertations defended by the students working on the research groups, both at UNIFEI and UNICAMP. Besides the published work and the defended thesis and dissertations, some research papers and student thesis/dissertation defenses are also expected to occur in the near future, related to this work. The list in the Appendix includes the on-going research, leading to student dissertations / thesis.

3.1 Main accomplishments on the direct and inverse models

Throughout the research project, the complexity of the modeling of the direct and inverse problems has increased, pursuing two goals:

- The goal for the direct model is to be improved in order to reproduce as close as possible the reality of an aircraft structure.
- The goal for the inverse model is to be as reliable as possible. For that, a combination of independent optimization and identification procedures is deemed necessary. The reliability of the damage detection procedure is expected to be high, if two or more independent approaches indicate the same location and size for the structural damage.

In addition, the current inverse models already include some stochastic modeling, but the proper treatment of the uncertainties is an on-going research, and is also the object of collaborative research planned for the near future.

The main accomplishments of this research project can be summarized as follows:

- For the direct problem:
    - BEM models implemented: cracked composite plates with repair patches (static and dynamic), evaluation of adhesive shear stress, anisotropic fundamental solution using numerical integration (Radon transformation);
    - Comparison between Dual Reciprocity BEM and cell domain integration to treat remaining domain integrals (due to the shear interaction forces).
- For the inverse problem:
    - Damage detection algorithm implemented for standard BEM models (potential, elasticity, acoustics);
    - Optimization methods (Sequential Quadratic Programming – SQP; Genetic Algorithms - GA) and identification techniques (Artificial Neural Networks - ANN) were compared for structures with deterministic parameters.

The models implemented are detailed in the several published works (conference papers and journal articles) cited in the Appendix. Some illustrative results for the direct model research are shown below, in Figures 8 to 11. Figure 8 shows the boundary element model for a cracked plate with a composite patch. The remaining domain integrals (due to the shear interaction forces) need to be evaluated either by a Dual Reciprocity approach of by cell domain integration.

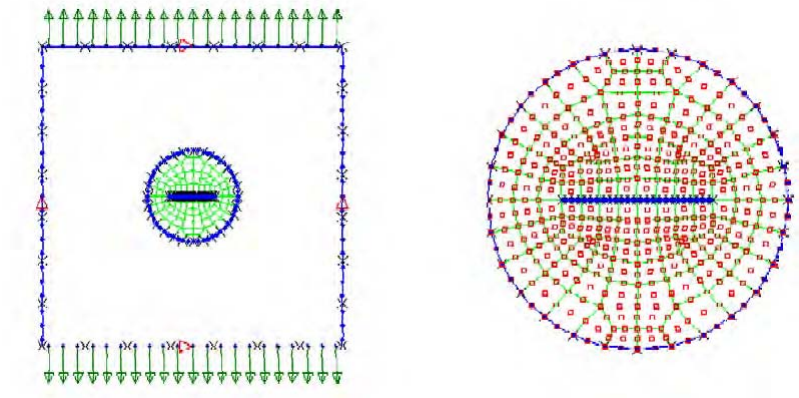

Figure 8: Circular composite patch over a cracked square sheet: BEM model

Figure 9 shows the stress distribution obtained with the BEM model. The presence of the circular patch has alleviated the stresses on the cracked region of the plate.

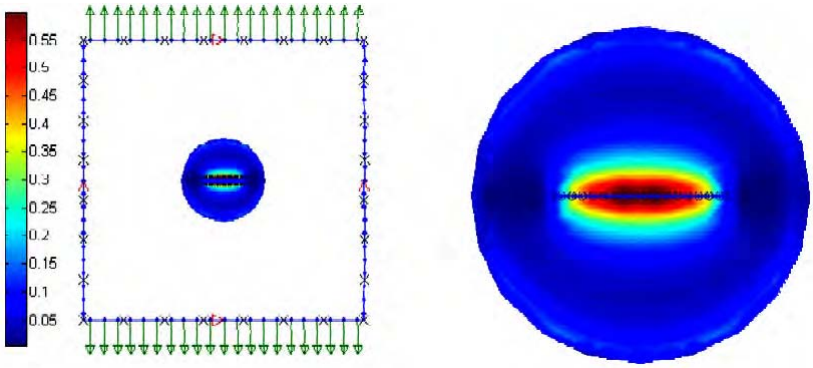

Figure 9: Circular composite patch over a cracked square sheet: stress results using BEM

Figure 10 shows a representation of the problem being modeled, in which there is an adhesive layer between the composite patch (anisotropic) and the metallic plate (isotropic). The adhesive layer was treated in the BEM model implemented.

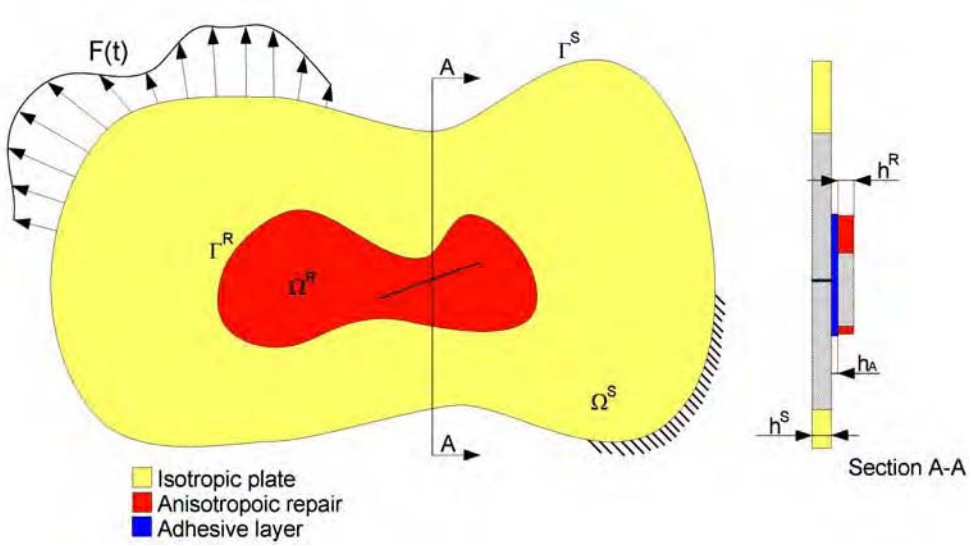

Figure 10: Dynamic analysis model: plate, composite patch, adhesive layer

Figure 11 shows the numerical integration results to obtain the anisotropic fundamental solution in 3D using the Radon transformation, pointing out the need to increase the number of Gauss points in this numerical integration, in order to obtain a proper reconstruction of the smooth anisotropic fundamental solution, to be used with the BEM formulation.

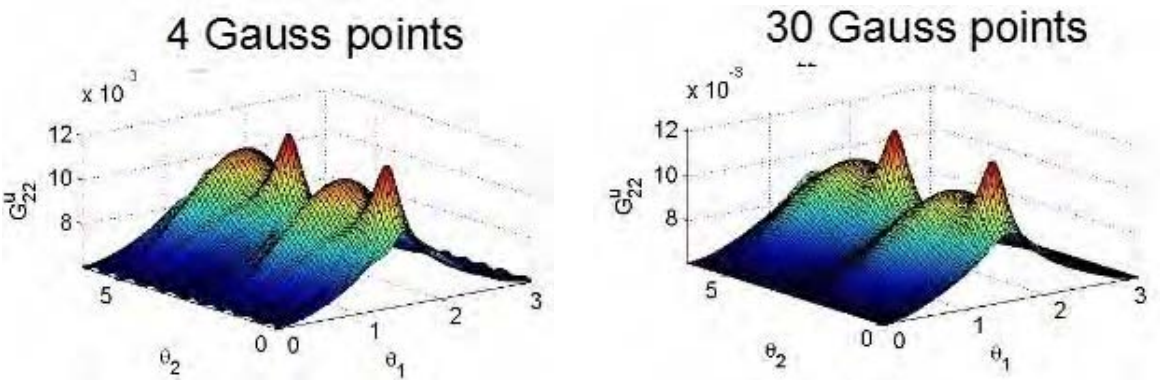

Figure 11: Anisotropic fundamental solution 3D: numerical integration requires 30 or more Gauss points.

Regarding the research on the inverse model, some illustrative results are shown below, in Figures 12 to 14. Figure 12 shows the convergence pattern of the inverse method using the genetic algorithm (GA) as the optimization approach, and the BEM model of the Laplace equation as the direct model for the potential distribution along the plate. Besides the usual operations of mutation and cross-over, the use of elitism improves the accuracy of the damage localization results.

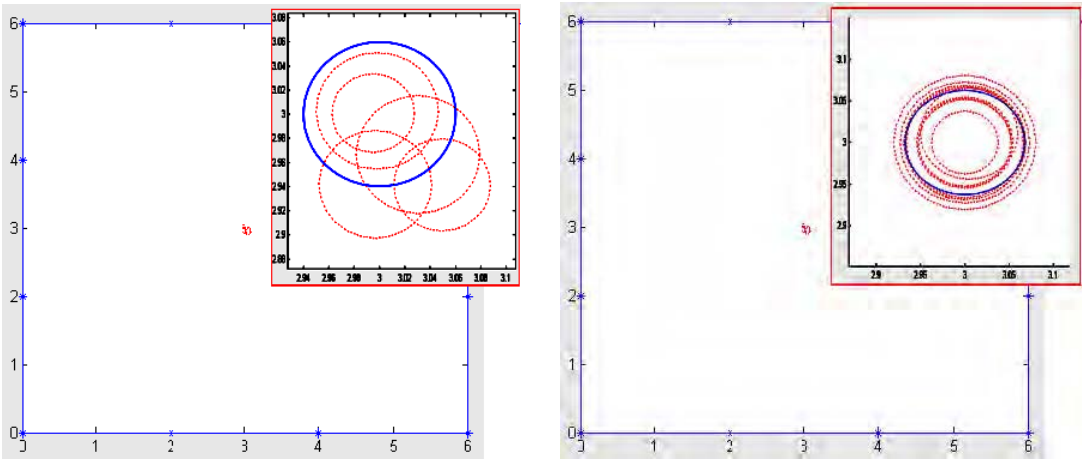

Figure 12: Influence of GA parameters: high elitism is better

Figure 13 shows the convergence pattern of the inverse method using the genetic algorithm (GA) as the optimization approach, and the elastostatics BEM as the direct model. The localization results present smaller variability when the distribution of a scalar quantity along the plate is used (in this case, the mean stress or the octahedral stress, which are the invariants of the stress tensor), instead of a vector quantity (in this case, the stress components, which are direction-dependent).

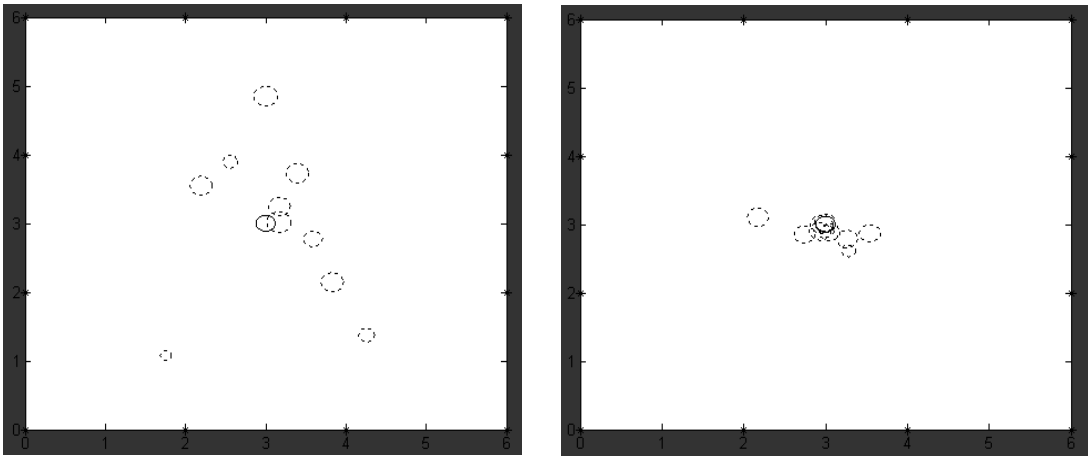

Figure 13: Stress invariants: better results (less variability) than stress vector components

For the acoustics model, the acoustic pressure is a potential field. This acoustic potential at a particular location (the sensor location) is a function of time, and can be measured for the case of the real hole, and can be simulated using BEM, for the case of the numerical hole. A functional can be built as differences in the areas below the curves of the potential for the real and measured cases. Figure 14 shows that this functional correlates directly with the distances between the numerical and the real hole (the value of this functional gets smaller as the numerical hole approaches the real hole).

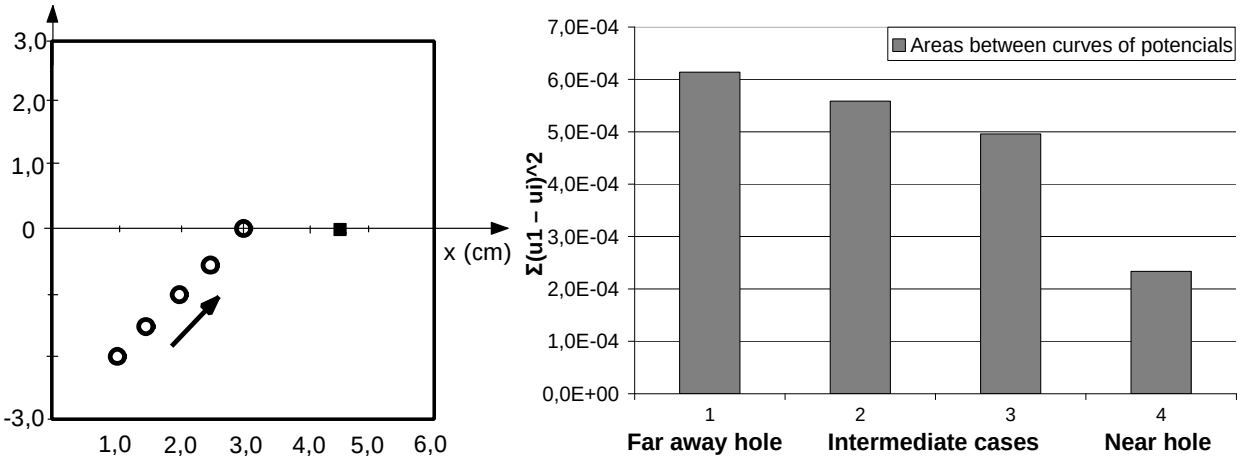

Figure 14: Acoustics model: "numerical" holes approaching the "real" hole. The inverse model identifies the numerical hole closest to real hole.

3.2 Establishment of collaborative research work (on-going work)

The research on the modeling and simulation of the inverse problem has involved some collaborative work with Prof. G. Walker and with Professor P. K. Basu, both from Vanderbilt University (Nashville, TN). This collaboration was very important for discussing modeling techniques for the inverse problem. Furthermore, this collaboration has created a synergy between the computational mechanics group from UNIFEI in Brazil and Vanderbilt University, important for the planned modeling of the uncertainties of the damage detection problem.

To accomplish this collaborative work, Prof. Ariosto spent some time in 2009 at Vanderbilt University, as a visiting scholar, while continuing to coordinate the research work being done by the students and researchers from the UNIFEI research group, in Brazil. Funding for the expenses of this visit to Vanderbilt University was obtained through a Brazilian agency, CNPq.

References

[1] Raghavan, A & Cesnik, CES (2005): Lamb Wave-based Structural Health Monitoring, Book Chapter in '*Damage Prognosis*'. Editors: Inman, DJ; Farrar, CR; Lopes Jr., V; & Steffen Jr., V. Wiley.

[2] Cesnik, CES & Raghavan, A (2008): Fundamentals of Guided Elastic Waves in Solids, Chapter in '*Encyclopedia of Structural Health Monitoring*'. Editors: Cheng, F-K & Boller C, Wiley, to appear.

[3] Giurgiutiu, V; Joshi, S, et al. (2007): Structural health monitoring with piezoelectric wafer active sensors for space applications, AIAA JOURNAL, V. 45, p. 2838-2850.

[4] Banks, HT; Inman, DJ; Leo, DJ & Wang, Y (1996): An experimentally validated damage detection theory in smart structures, *Journal of Sound and Vibration*, 191, 5 (1996), 859-880.

[5] Burczynski, T & Beluch, W (2001): The identification of cracks using boundary elements and evolutionary algorithms, *Engineering Analysis with Boundary Elements*, 25 (2001), pp. 313-322.

[6] Aliabadi, MH & Rooke, DP (1991): *Numerical fracture mechanics*, Computational Mechanics Publications. Dordrecht: Kluwer Academic Publishers.

[7] Blandford, GE; Ingraffea, AR & Liggett, JA (1981): Two-dimensional stress intensity factor computations using the boundary element method, *Int. J. Num. Meth. Eng*. 17, 387-404.

[8] Cruse, TA (1978): Two-dimensional BIE fracture mechanics analysis, *Appl. Math. Model*., 2, 287-293.

[9] Cruse, TA (1988): *Boundary Element Analysis in Computational Fracture Mechanics*, Kluwer Academic Publishers.

[10] Cruse, TA & Novati, G (1992): Traction boundary integral equation (BIE) formulations and applications to nonplanar and multiple cracks, *Fracture Mechanics: Twenty-second Symposium*, ASTM, 314-332.

[11] Mi, Y & Aliabadi, MH (1992): Dual boundary element method for three-dimensional fracture mechanics analysis, *Engineering Analysis with Boundary Elements*, 10, pp. 161-171.

[12] Tada, H; Paris, PC & Irwin, GR (2000): *The stress analysis of cracks handbook*, 3rd edn, ASME: ASME, New York.

[13] Weaver, J (1977): Three dimensional crack analysis, *Int. J. Solids Struct*.; 12, 201-218.

[14] Kane, JH; Mao, S; Everstine, GC (1991): A Boundary element formulation for acoustic shape sensitivity analysis. *J Acoustics Soc. Am.*, 90(1): 561-573.

[15] Wu, TW; Seybert, AF (1991): Acoustics radiation and scattering. In: Ciskowski RD, Brebbia CA, editors. *Boundary element methods in acoustics.* Amsterdam: Computational Mechanics Publications-Elsevier Applied Science,61-67.

[16] Soares, D; Mansur, WJ; Von Estorff, O (2007): An efficient time-domain FEM/BEM coupling approach based on FEM implicit Green's functions and truncation of BEM time convolution process, *Computer Methods in Applied Mechanics and Engineering*, V. 196, 9-12, p. 1816-1826.

[17] Soares, D; Mansur, WJ (2007): An efficient stabilized boundary element formulation for 2D time-domain acoustics and elastodynamics, *Computational Mechanics*, V. 40, 2, p. 355-365.

[18] Nash, SG; Sofer, A (1996): *Linear and nonlinear programming*, McGraw-Hill.

[19] Vanderplaats, GN (1984): *Numerical optimization techniques for engineering design*, Mcgraw-Hill.

[20] Bäck, T; Schwefel, H-P (1993): An overview of evolutionary algorithms for parameter optimization, *Evolutionary Computation* 1, 1 (1993), 1-23.

[21] Ding, Y (1986): Shape Optimization of structures: a literature survey. *Comput. Struct*, 24(6):985-1004.

[22] Goldberg, DE (1989): *Genetic Algorithms in Search, Optimization and Machine Learning*. Addison-Wesley.

[23] Holand, JH (1975): *Adaptation in Natural and Artificial Systems*. University of Michigan Press.

[24] Houck, CR; Joines, JA; Kay, MG (1995): *A genetic algorithm for function optimization: a MATLAB implementation*. Tech. Rep. NCSU-IE 95-09, North Carolina State University.

[25] Michalewicz, Z (1995): *Genetic Algorithms + Data Structures = Evolutionary Programs*, 3rd ed. Springer.

[26] Muñoz, A; Martorell, S; Serradel, V (1997): Genetic algorithms in optimizing surveillance and maintenance of components, *Reliability Engineering and System Safety*, 57 (1997), 107-120.

[27] Toffolo, A; Lazzaretto, A (2002): Evolutionary algorithms for multi-objective energetic and economic optimization in thermal system design. *Energy*. V.27, no.6, pp. 549-567.

[28] Hosmer, DW; Lemeshow, S (1989): *Applied Logistic Regression*, John Wiley & Sons,Inc.

[29] Haldar, A; Mahadevan, S (1999): *Probability, Reliability, and Statistical Methods in Engineering Design*, Wiley.

[30] Mahadevan, S.; Cruse, TA (1994): System reliability computational under progressive damage. *Structural Safety & Reliability*. In: Schueller, Shinozuka & Yao, Balkema, Rotterdam, p.1287-1292.

[31] Sengupta, D (2004): On the Kalman filter with possibly degenerate and correlated errors. *Linear Algebra and its Applications*. V. 388, no. 1, pp. 327-340.

[32] Montgomery, DC; Runger, GC (2007): *Applied Statistics and Probability for Engineers*, 4th Edition, Wiley.

[33] Rao, SS; Xiong, Y (2005): Mixed-Discrete Fuzzy Multiobjective Optimization of Structures using a Hybrid Genetic Algorithm, *6th World Congress on Structural and Multidisciplinary Optimization*, Rio de Janeiro, 30 May - 03 June 2005, Brazil.

[34] Xion, Y; Rao, SS (2004): Fuzzy nonlinear programming for mixed-discrete design optimization through hybrid genetic algorithm, *Fuzzy Sets and Systems*, 146, pp. 167–186.

Appendix

Related Publications: Conference papers

1. Gouvêa, AR; Albuquerque, EL; Sollero, P; Palermo Jr, L (2007): A new formulation for bending analysis of laminate composite plates by the boundary element method *CMNE/CILAMCE 2007*, Porto, June 13 - 15.

2. Useche J, Sollero P, Albuquerque, EL, Palermo Jr, L (2007): Boundary element analysis of cracked thick plates repaired with adhesive composite patches, *Advances in Boundary Element Techniques VII – BeTeq 2007* (V. Minutolo e M.H. Aliabadi eds.) Napoles, pp. 117-122.

3. Useche, J; Sollero, P; Albuquerque, EL (2007): Fracture analysis of Reissner plates using the dual boundary element method, *Proceedings of 19th International Congress of Mechanical Engineering - COBEM 2007*, November 5-9, Brasília, DF.

4. Useche J, Sollero P, Albuquerque, EL (2007): Boundary element analysis of cracked thick plates repaired with adhesive bonded patches, *Proceedings of 19th International Congress of Mechanical Engineering – COBEM 2007*, November 5-9, Brasília, DF.

5. Lopes, PS; Cunha Jr, SS; Jorge, AB (2007): Damage detection using global optimization and parameter identification techniques, *Proceedings of 19th International Congress of Mechanical Engineering* - COBEM 2007, November 5-9, Brasília, DF.

6. Jorge, AB; Lopes, PS; Cunha Jr, SS (2008): Modeling of a damage detection problem in a structure subject to uncertainties using multi-objective stochastic optimization techniques, *15th Int. Conf. on Computational & Experimental Engineering & Sciences* - ICCES'08, March 16-22, Honolulu, HI, USA

7. Lopes, PS; Jorge, AB; Cunha Jr, SS (2008): Detection of holes in a plate using global optimization and parameter identification techniques, *International Conference on Engineering Optimization* - EngOpt 2008, June 1-5, Rio de Janeiro, Brazil

8. Jorge, AB; Lopes, PS; Lopes, ME (2008): On the use of Boundary Element Methods for Inverse Problems of Damage Detection in Structures, *Boundary Element Techniques Conference* - BeTeq2008,9-11 July,Sevilla, Spain

9. Useche, J, Sollero, P, Albuquerque, EL, Palermo Jr, L (2007). Computational modeling of cracked plates repaired with adhesively bonded composite patches using the boundary element method. In: *19o Congresso de Engenharia Mecânica*, Brasília.

10. Barros, RSV, Sollero P, Useche, J, Albuquerque, EL (2007). Análise estrutural de juntas coladas e de fadiga em reparos de materiais compósitos em chapas trincadas. *X Encontro de Modelagem Computacional*, Nova Friburgo.

11. Santos, RR, Sollero, P, Useche, J, Albuquerque, EL (2007). Análise estática de chapas trincadas com reparo de material compósito. *X Encontro de Modelagem Computacional*, Nova Friburgo.

12. Gouvêa, AR, Albuquerque, EL, Palermo Jr, L, Sollero, P (2008). Computation of stresses on the boundary of laminate composite plates by the boundary element method. In: International Conference on Boundary Element Techniques VIII, Seville. *Advances in Boundary Element Techniques*. London: EC LTD.

13. Torsani, F, Gouvêa, AR, Albuquerque, EL, Sollero, P (2008). Stress analysis of composite laminated plates by the boundary element method. In: International Conference on Boundary Element Techniques VIII, Seville. *Advances in Boundary Element Techniques*. London: EC LTD.

14. Mauler, M, Sollero, P, Albuquerque, EL (2008). Boundary element formulation for dynamic analysis of cracked sheets repaired with anisotropic patches. In: International Conference on Boundary Element Techniques VIII, Seville. *Advances in Boundary Element Techniques*. London: EC LTD.

15. Albuquerque, EL, Aliabadi, MH (2008). A boundary element analysis of symmetric laminate composite shallow shells. In: International Conference on Boundary Element Techniques VIII, Seville. *Advances in Boundary Element Techniques*. London: EC LTD.

16. Albuquerque, EL, Baiz, PM, Aliabadi, MH (2008). Stability analysis of composite plates by the boundary element method. In: International Conference on Boundary Element Techniques VIII, 2007, Seville. *Advances in Boundary Element Techniques*. London: EC LTD.

17. Albuquerque, EL, Aliabadi, MH (2008). A boundary element formulation for boundary only analysis of thin shallow shells. In: International Conference on Boundary Element Techniques VIII, 2008, Seville. *Advances in Boundary Element Techniques*. London: EC LTD.

18. Souza, CAO, Sollero, P, Santiago, AG, Albuquerque, EL (2009). Analysis of composite bonded joints using the 3D boundary element method. In: International Conference on Boundary Element Techniques IX.

19. Santana, AP, Sousa, KR, Albuquerque, EL, Sollero, P (2009). A dynamic formulation of the boundary element method for transient analysis of laminated composite thin plates. In: International Conference on Boundary Element Techniques IX.

20. Santiago, AG, Sollero, P, Albuquerque, EL (2009). Telles transformation applied to the evaluation of 3D anisotropic fundamental solution. 20th International Congress of Mechanical Engineering, COBEM 2009, Gramado, RS, Brazil.

Related Publications: Journal articles

1. Useche, J, Sollero, P, Albuquerque, EL (2008). Boundary element analysis of cracked sheets repaired with bonded anisotropic patches. *Key Engineering Materials*, v. 383, p. 97-108.
2. Lopes, PS, Jorge, AB, Cunha Jr, SS (2009). Detection of holes in a plate using global optimization and parameter identification techniques, *Inverse Problems in Science & Engineering*, accepted for publication.
3. Gouvea, AR, Albuquerque, EL, Torsani, FL, Palermo, L, Sollero, P (2009). Computation of moments and stresses in laminated composite plates by BEM, *Engineering Analysis with Boundary Elements*, submitted.

Note: the above three journal articles are attached at the end of this report, for completeness.

Related Student Dissertations / Thesis (defended)

1. **Title:** Damage detection in structures using artificial neural network techniques and genetic algorithms (in Portuguese) (Detecção de danos em estruturas por meio de técnicas de redes neurais artificiais e algoritmos genéticos). **Type of monograph:** Masters Thesis in Mechanical Engineering (UNIFEI). **Author:** Patricia da Silva Lopes. **Advisor:** Prof. Ariosto Bretanha Jorge. **Co-advisor:** Prof. Sebastião Simões da Cunha Jr. (Prof. Eder Lima de Albuquerque acted as committee member for the defense). **Defense date:** March 2007.

2. **Title:** Implementation of the stress calculations in laminate composite plates using the Boundary Element Method (in Portuguese) (Implementação do Cálculo das Tensões em Placas Compósitas Laminadas usando o Método dos Elementos de Contorno). **Type of monograph:** Masters Thesis in Mechanical Engineering (UNICAMP). **Author:** Fernando Luiz Torsani. **Advisor:** Prof. Eder Lima de Albuquerque. **Co-advisor:** Prof. Paulo Sollero. **Defense date:** July 2007.

3. **Title:** Boundary element method analysis of cracked Reissner plates repaired with composite bonded patches (in Portuguese) (Análise pelo método dos elementos de contorno de Placas de Reissner trincadas e reparadas com compósitos colados). **Type of monograph:** Doctoral Dissertation in Mechanical Engineering (UNICAMP). **Author:** Jairo F. Useche. **Advisor:** Prof. Paulo Sollero. **Co-advisor:** Prof. Eder Lima de Albuquerque. **Defense date:** November 2007. (Prof. Dr. Ariosto Bretanha Jorge acted as committee member for the defense).

4. **Title:** Dynamic formulations of the Boundary Element Method applied to the analysis of thin laminate composite plates (in Portuguese) (Formulações dinâmicas do Método dos

Elementos de Contorno aplicado a análise de Placas Finas de Compósitos Laminados). **Type of monograph:** Masters Thesis in Mechanical Engineering (UNICAMP). **Author:** André Pereira Santana. **Advisor:** Prof. Eder Lima de Albuquerque. **Co-advisor:** Prof. Paulo Sollero. **Defense date:** November 2008.

5. **Title:** Modeling of an acoustic problem for aeronautical structures by the boundary element technique, with application to damage detection (in Portuguese) (Modelagem de Problema de Acústica para Estruturas Aeronáuticas pela Técnica dos Elementos de Contorno, com Aplicação para Detecção de Danos). **Type of monograph:** Masters Thesis in Mechanical Engineering (UNIFEI). **Author:** Mauricio Eduardo Lopes. **Advisor:** Prof. Ariosto Bretanha Jorge. **Co-advisor:** Prof. Sebastião Simões da Cunha Jr. **Defense date:** February 2009. (Prof. Eder Lima de Albuquerque acted as committee member for the defense).

6. **Title:** Dynamic analysis of cracked plates with composite patches using the Boundary Element Method (in Portuguese) (Análise Dinâmica de Chapas Trincadas com Reparos de Material Compósito Através do Método de Elementos de Contorno). **Type of research:** Masters Studies in Mechanical Engineering (UNICAMP). **Student:** Martim Mauler Neto. **Advisor:** Prof. Dr. Paulo Sollero. **Defense date:** May 2009.

7. **Title:** Numerical modeling by 3D boundary elements of bonded patches in aeronautical structures made of composite material (in Portuguese) (Modelagem numérica por elementos de contorno 3D de juntas coladas em estruturas aeronáuticas de material compósito). **Type of research:** Masters Studies in Mechanical Engineering (UNICAMP). **Student:** Carlos Alexandre Oliveira de Souza. **Advisor:** Prof. Dr. Paulo Sollero. **Co-advisor:** Prof. Eder Lima de Albuquerque. **Defense date:** July 2009.

8. **Title:** Stress analysis in thin composite plates under dynamic loading using the Boundary Element Method (in Portuguese) (Análise de Tensões em Placas Finas de Materiais Compósitos sob Carregamento Dinâmico usando o Método dos Elementos de Contorno). **Type of monograph:** Masters Thesis in Mechanical Engineering (UNICAMP). **Author:** Kerlles Rafael Pereira Sousa. **Advisor:** Prof. Eder Lima de Albuquerque. **Co-advisor:** Prof. Paulo Sollero. **Defense date:** November 2009.

Related Student Dissertations / Thesis (on-going research)

1. **Title:** Damage detection in structures by parameter identification and global optimization techniques (in Portuguese) (Detecção de danos estruturais por meio de técnicas de identificação de parâmetros e de otimização global). **Type of research:** Doctoral Studies in Mechanical Engineering (UNIFEI). **Student:** Patricia da Silva Lopes. **Advisor:** Prof. Ariosto Bretanha Jorge. **Co-advisor:** Prof. Sebastião Simões da Cunha Jr. (Prof. Paulo Sollero is intended to act as committee member for the defense).

Key Engineering Materials Vol. 383 (2008) pp 97-108
online at http://www.scientific.net

Boundary element analysis of cracked sheets repaired with bonded anisotropic patches

J. F. Useche, P. Sollero and E. L. Albuquerque

Faculty of Mechanical Engineering, State University of Campinas
Campinas, Brazil, sollero@fem.unicamp.br

Keywords: cracked sheet; composite repair; adhesive patch; dual boundary element method; dual reciprocity boundary element method.

Abstract. A boundary element formulation for the analysis of isotropic cracked sheets, repaired with adhesively bonded anisotropic patches is presented. The sheet and the patch are modeled using the boundary element method. The crack in the isotropic sheet is modeled using the dual boundary element method. The interaction between the isotropic sheet and the patch is modeled considering shear body forces uniformly distributed on the interaction zone using a linear elastic relationship. Two different techniques are used in the present boundary element implementation to treat the domain integrals that arise in the formulation due to shear interaction forces. These techniques are the cell domain integration and the dual reciprocity boundary element method. Examples show that results obtained for the shear stress distribution in the adhesive layer are in good agreement with analytical solution.

Introduction

Adhesively bonded composite patches are increasingly used in aircraft structure repairs in order to extend the life of cracked structures and avoid high expenses owing to the replacement of cracked components. In aeronautical applications, when a non-destructive technique detects a crack, it is usually necessary to drill the crack tip region in order to decrease the stress concentration and then apply a layer of adhesive patch on this region to avoid the crack growth. The patch transfers the load from the cracked structure to the repair, avoiding crack opening and crack propagation. The main advantages of bonded patches, when compared to other types of repairs such as riveted patches, are the homogeneous load transfer between the cracked plate and the repair and the absence of holes, which are stress concentrators, as shown by Rose and Wang [1].

Bonded patches in cracked structures have been studied by many researchers. In general, the sheet, the patch, and the adhesive layer are considered to be thin, so that the whole component does not bend out of its plane, and the problem can be solved using the two dimensional elasticity theory. The initial works analyzing isotropic patches in structures were presented by Erdogan and Arin [2] and Ratwani [3], in the seventies. These works presented the study of bonded repairs in infinite plates with cracks. They used analytical solutions for the deformations and displacement compatibility between the cracked plate and the repair.

Mitchell, Wooley and Chwiruth [4] used the finite element method (FEM) to study the reinforcement of plates induced by the application of repairs. They used two-dimensional finite elements with constant stress distribution and the plate and repair were coupled through nodes where conditions of displacement compatibility were imposed. They also analyzed the presence of a crack in the plate. However, they did not consider the stress singularity at the crack tip and did not evaluate the stress intensity factors. Jones and Callinan (see References [5], [6], [7]) used the FEM for the analysis of metallic plates repaired with a layer of composite material. They developed a stiffness matrix to couple the plate, the adhesive layer, and the composite repair. Special singular elements were used at the crack tip.

Young, Cartwright and Rooke [8] modeled the cracked plate and the repair using the boundary element method (BEM). Shear stresses in the adhesive layer and body forces acting on the plate and on the repair were modeled using the cell integration technique. A special Green function for domains

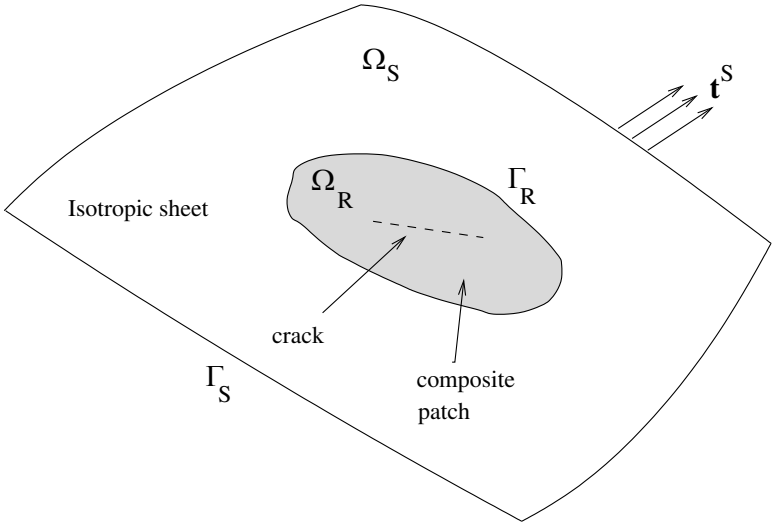

Figure 1: Cracked sheet repaired with adhesive patch

with cracks was used to model straight cracks, which limits the applicability of the model.

Tarn and Shek [9] studied the problem of cracked plates repaired with bonded composite patches. A spring was used to couple the cracked plate model with the repair model. The repair was modeled using the FEM and the crack using the BEM. Young [10] modeled the distributed interaction force between the plate and the repair by discretizing the bonded repaired area using internal cells in the boundary element formulation.

Salgado and Aliabadi [12] introduced the dual boundary element method (DBEM) to model the metallic cracked plate and the boundary element method to model the metallic repair. The distributed forces between the plate and the repair were modeled using the dual reciprocity boundary element method (DRBEM). This formulation was applied by Salgado and Aliabadi [13] to the analysis of metallic thin plates reinforced with bonded isotropic repairs. The reinforced plate was modeled using the BEM. Shear stresses in the adhesive layer were modeled as action-reaction body forces exchanged between the plate and the repair. Widagdo and Aliabadi [14] extended this formulation to model mechanically fastened composite repair patches. The fasteners were considered as linear springs coupling the cracked sheet and the anisotropic repair and their interaction loading was modeled as a summation of discrete point forces. Widagdo and Aliabadi [15] apply this formulation for the analysis of cracked sheet repaired with adhesively bonded orthotropic repairs.

The current work analyses a composite repair patch adhesively bonded in a metallic cracked sheet. The DBEM is used to model the isotropic cracked sheet and the BEM is used to model the anisotropic composite patch. The interaction loading between the sheet and the patch is modeled considering the shear forces in the adhesive layer uniformly distributed using a linear elastic relationship. Two different techniques are used to treat domain the integrals that arise in the formulation due to the interaction shear forces: the cell domain integration and the DRBEM.

Numerical examples of the adhesive stress analysis in cracked plate, repaired with a circular and rectangular composite patches, are presented. The shear stress distributions obtained with the current techniques are compared to the analytical solution of Rose [16] with good agreement. Stress intensity factors are calculed using the displacement extrapolation technique.

1 Boundary element formulation

Figure 1 presents a finite isotropic sheet, containing an inner crack and an adhesive patch. In this case, the interaction forces can be treated as unknown body forces exchanged by the sheet and the patch in the attachment sub-region. Considering that the sheet and the patch remain flat after deformation, the two-dimensional elasticity theory can be used to model this problem. In this case, displacements

at the sheet and at the patch have to be compatible with the shear deformation of the adhesive layer connecting them.

When the sheet is deformed due to applied loads on its boundaries, interaction forces occur between the sheet, with contour Γ_S, and the repair patch, with contour Γ_R (see figure 1). In this two-dimensional case, interaction forces in the plate directly underneath the repair patch, and in the patch itself, can be treated as unknown body forces (action-reaction pair). As shown by Salgado and Aliabadi [13], the boundary integral equation for the displacement of a source point **x'** on the sheet is given by:

$$c_{ij}^{S}\left(\mathbf{x}'\right) u_{j}^{S}\left(\mathbf{x}'\right) + \int_{\Gamma_S} T_{ij}^{*S}\left(\mathbf{x}', \mathbf{x}\right) u_{j}^{S}\left(\mathbf{x}\right) d\Gamma = \int_{\Gamma_S} U_{ij}^{*S}\left(\mathbf{x}', \mathbf{x}\right) t_{j}^{S}\left(\mathbf{x}\right) d\Gamma + \frac{1}{h_S} \int_{\Omega_R} U_{ij}^{*S}\left(\mathbf{x}', \mathbf{x}\right) b_{j}^{S}\left(\mathbf{x}\right) d\Omega_R \qquad i,j = 1,2 \tag{1}$$

where c_{ij}^{S} is a coefficient which depends on the position of the source point in relation to the boundary of the sheet Γ_S; $U_{ij}^{*S}(\mathbf{x}', \mathbf{x})$ and $T_{ij}^{*S}(\mathbf{x}', \mathbf{x})$ are Kelvin's isotropic fundamental solutions for displacements and tractions, respectively, for the two-dimensional sheet media; u_j^S and t_j^S are displacement and traction vectors at the boundary of the sheet; b_j^S are interaction forces exchanged between the sheet and the patch in the domain Ω_R of the patch; h_S is the thickness of the sheet.

Similarly, the displacement of a source point $\mathbf{x}'$ on the repair is given by:

$$c_{ij}^{R}\left(\mathbf{x}'\right) u_{j}^{R}\left(\mathbf{x}'\right) + \int_{\Gamma} T_{ij}^{*R}\left(\mathbf{x}', \mathbf{x}\right) u_{j}^{R}\left(\mathbf{x}'\right) d\Gamma = \int_{\Gamma} U_{ij}^{*R}\left(\mathbf{x}', \mathbf{x}\right) t_{j}^{R}\left(\mathbf{x}'\right) d\Gamma + \frac{1}{h_R} \int_{\Omega_R} U_{ij}^{*R}\left(\mathbf{x}', \mathbf{x}\right) b_{j}^{R}\left(\mathbf{x}'\right) d\Omega_R \qquad i,j = 1,2 \tag{2}$$

where c_{ij}^{R} is a coefficient which depends on the position of the source point in relation to the boundary of the sheet Γ_R; $U_{ij}^{*R}(\mathbf{x}', \mathbf{x})$ and $T_{ij}^{*R}(\mathbf{x}', \mathbf{x})$ are anisotropic fundamental solutions for the two-dimensional composite repair; u_j^R and t_j^R are displacement and traction vectors at the boundary of the repair; b_j^R are the interaction forces exchanged between the sheet and the patch in the domain Ω_R of the patch; h_R is the thickness of the sheet.

In this work, the anisotropic fundamental solutions for two-dimensional elastic media was used to model the mechanical response of the composite patch (see Aliabadi and Sollero [17]).

The crack in the isotropic sheet was modeled using the DBEM. The traction integral equation is applied in one of the crack faces and the displacement integral equation is applied in the other crack face. The traction integral equation is given by:

$$\frac{1}{2} t_{j}^{S}\left(\mathbf{x}'\right) + n_i\left(\mathbf{x}'\right) \int_{\Gamma_S} S_{ijk}^{*S}\left(\mathbf{x}', \mathbf{x}\right) u_{j}^{S}\left(\mathbf{x}\right) d\Gamma = n_i\left(\mathbf{x}'\right) \int_{\Gamma_S} D_{ijk}^{*S}\left(\mathbf{x}', \mathbf{x}\right) t_{j}^{S}\left(\mathbf{x}\right) d\Gamma + \frac{1}{h_S} \int_{\Omega_R} D_{ijk}^{*S}\left(\mathbf{x}', \mathbf{x}\right) b_{j}^{S}\left(\mathbf{x}\right) d\Omega_R \qquad i,j = 1,2 \tag{3}$$

where $S_{ijk}^{*S}(\mathbf{x}', \mathbf{x})$ and $D_{ijk}^{*S}(\mathbf{x}', \mathbf{x})$ are linear combinations of derivatives of fundamentals solutions for traction and displacement $T_{ij}^{*R}(\mathbf{x}', \mathbf{x})$ and $U_{ij}^{*R}(\mathbf{x}', \mathbf{x})$, respectively, and n_i are the components of a unit vector outward to the boundary in the collocation point.

Now, considering a uniform shear deformation through the adhesive thickness, as proposed by Salgado and Aliabadi [13], and neglecting shear deformations in the sheet and in the patch, the body force $b_j(\mathbf{x}')$, that is equal to the shear stress in the adhesive $\tau_j(\mathbf{x}')$, can be written as a function of the difference Δu_j between the displacements u_j^S of a point $\mathbf{x}'$ ($\mathbf{x}' \in \Omega_R$) on the sheet and u_j^R of a corresponding point on the repair patch, as:

$$b_j\left(\mathbf{x}'\right) = \tau_j\left(\mathbf{x}'\right) = \frac{G_A}{h_A}\left\{u_j^S\left(\mathbf{x}'\right) - u_j^R\left(\mathbf{x}'\right)\right\} \qquad j = 1,2 \tag{4}$$

where h_A is the thickness of the adhesive layer, G_A is the transversal stiffness modulus of the adhesive material.

2 Domain integral techniques

As can be seen, equations (1) and (2) require the calculation of domain integrals. Two different techniques were used and compared to treat the domain integrals that arise in the formulation due to the shear interaction forces. These techniques are the cell domain integration method and the DRBEM.

2.1 Cell domain integration

In the cell domain technique, the attachment region Ω_R is subdivided in elementary cells. The distribution of the shear stress $\tau_j(\mathbf{x}')$ in the adhesive is described in terms of nodal values associated to each cell. In this work two types of cells were used. Since there exist two coincident nodes at crack elements (one for each crack edge), these nodes can't be used as collocation points because no coincidents nodes exist in the patch. Then, constants cells with a central node has been used to aproximate the shear stress distribution at neibourghood of the crack. Nine node quadrilateral isoparametric cells were used to approximate the variation of the adhesive shear stress in the remaining attachment area.

Consequently, in the cell integration method, the domain integral in the equation (1) can be expressed as (see Salgado and Aliabadi [13]):

$$\frac{1}{h_S}\int_{\Omega_R} U_{ij}^{*S}\left(\mathbf{x}',\mathbf{x}\right) b_j\left(\mathbf{x}\right) d\Omega_R \cong \frac{1}{h_S}\sum_{k=1}^{ncells}\int_{\Omega_k} U_{ij}^{*S}\left(\mathbf{x}',\mathbf{x}\right) b_j\left(\mathbf{x}\right) d\Omega_k \tag{5}$$

and the integration is carried out on each cell. Using equation (4) and the bi-quadratic isoparametric approximation proposed in this work, we can write:

$$\frac{1}{h_S}\sum_{k=1}^{ncells}\int_{\Omega_k} U_{ij}^{*S} b_j\left(\mathbf{x}\right) d\Omega_k \cong \frac{1}{h_S}\sum_{k=1}^{ncells}\left[\int_{\Omega_k} \underline{\mathbf{U}}^*\underline{\mathbf{N}} d\Omega_k\right]\mathbf{a}_k \tag{6}$$

where, $\underline{\mathbf{N}}$ is the matrix of bi-quadratic Lagrange shape functions and $\mathbf{a}_k = \left\{\mathbf{u}_d^S, \mathbf{u}^R\right\}^T$ is the vector of nodal displacements at cell k. In this vector, $\mathbf{u}_d^S$ refers to sheet displacement at Ω_R and $\mathbf{u}^R$ refers to repair displacements. Similar expression can be obtained for domain integrals at equations (2) and (3).

In this work the integral on the right hand side of equation (6) is evaluated using ten-point Gaussian quadrature. However, when the source point $\mathbf{x}'$ is placed within the cell, this integral becomes weakly singular which will cause numerical error if Gaussian quadrature is used directly. In this case the integrand in (6) can be regularized at the singular point by substracting suitable singular term, which may be treated separately as follow (see Young and Rooke [11]):

$$\int_{\Omega_k} U_{ij}^{*S} N_{jk} d\Omega_k = \int_{-1}^{1}\int_{-1}^{-1}\left\{U_{ij}^{*S} N_{jk} J - \lambda_{ij}\ln\left(R\right) J\right\} d\xi d\eta + \lambda_{ij} J \int_{-1}^{1}\int_{-1}^{-1}\ln\left(R\right) d\xi d\eta \tag{7}$$

where, $R = \sqrt{(\xi - \xi_o)^2 + (\eta - \eta_o)^2}$. The second integral on the right hand side can be evaluated analytically. The constant λ_{ij} is given by:

$$\lambda_{ij} = -\frac{1}{16\pi}\frac{(3-v)}{G_S}\delta_{ij} \tag{8}$$

where G_S is the shear modulus of the sheet.

2.2 DRBEM integration technique

In the DRBEM, interaction forces are approximated as a sum of unknown coefficients α_k^d multiplied by approximating functions $f_{jk}^d(\mathbf{x}', \mathbf{x})$, so that:

$$b_j(\mathbf{x}) = \sum_{d=1}^{D} \alpha_k^d f_{jk}^d\left(\mathbf{x}^d, \mathbf{x}\right) \tag{9}$$

The cofficients α_k^d have no physical meaning. But they are related to attachment shear forces through equation (4):

$$u_j^S(\mathbf{x}') - u_j^R(\mathbf{x}') = \frac{h_A}{G_A}\sum_{d=1}^{D} \alpha_j^d f_{jk}^d\left(\mathbf{x}^d, \mathbf{x}\right) \qquad j = 1, 2 \tag{10}$$

In this work, a linear approximation function $f_{jk}^d(\mathbf{x}', \mathbf{x})$ was used for the isotropic sheet:

$$f_{jk}^d\left(\mathbf{x}^d, \mathbf{x}\right) = (1 - r)\,\delta_{jk} \tag{11}$$

For the anisotropic patch, an approximation function given by Albuquerque, Sollero and Aliabadi [18] was used:

$$f_{jk}^d = C_{jilm}\left[cr\left(r_{,m}r_{,i}\delta_{lk} + \delta_{im}\delta_{lk}\right)\right] \tag{12}$$

Finally, the domain integral of equation (5) can be expressed as:

$$\int_{\Omega_R} U_{ij}^{*S}(\mathbf{x}', \mathbf{x})\, b_j(\mathbf{x})\, d\Omega_R = -\frac{1}{h_S}\sum_{d=1}^{D} \alpha_k^d \left[c_{ij}\left(\mathbf{x}^d\right)\hat{u}_{kj}^d\left(\mathbf{x}^d\right) + \int_{\Gamma_R} T_{ij}^{*S}(\mathbf{x}', \mathbf{x})\,\hat{u}_{kj}^d d\Gamma_R - \int_{\Gamma_R} U_{ij}^{*S}(\mathbf{x}', \mathbf{x})\,\hat{t}_{kj}^d d\Gamma_R\right] \tag{13}$$

where $\hat{u}_{kj}^d$ and $\hat{t}_{kj}^d$ are particular solutions for displacements and tractions corresponding to a predefined function f_{kj}^d for the sheet. A similar approach was used to model body forces in the patch.

3 Matrix formulation

3.1 Cell integration technique

In matrix form, equation (6) can be written as:

$$\frac{1}{h_S}\sum_{k=1}^{ncells}\left(\int_{\Omega_k} \underline{\mathbf{U}}^* \cdot \underline{\mathbf{N}} d\Omega_k\right)_k \mathbf{a}_k = \underline{\mathbf{F}}_c^S \mathbf{u}_d^S - \underline{\mathbf{F}}_c^S \mathbf{u}^S \tag{14}$$

Discretizing the boundary, the equations for isotropic sheet (including traction equation) can be written in compact form as:

$$\underline{\mathbf{H}}_c^S \mathbf{u}_c^S = \underline{\mathbf{G}}_c^S \mathbf{t}_c^S + \underline{\mathbf{F}}_c^S \mathbf{u}_d^S - \underline{\mathbf{F}}_c^S \mathbf{u}^R$$

$$\underline{\mathbf{I}} \mathbf{u}_d^S + \underline{\mathbf{H}}_d^S \mathbf{u}_c^S = \underline{\mathbf{G}}_d^S \mathbf{t}_c^S + \underline{\mathbf{F}}_d^S \mathbf{u}_d^S - \underline{\mathbf{F}}_d^S \mathbf{u}^R \tag{15}$$

where subindex c and d identify boundary and domain collocation points on the sheet. The matrix of influence coefficients $\underline{\mathbf{H}}^S$ and $\underline{\mathbf{G}}^S$ are defined as:

$$\underline{\mathbf{H}}^S = \sum_{e=1}^{nelem} \int_{\Gamma_e} T_{ij}^{*S} \phi_j d\Gamma_e$$

$$\underline{\mathbf{G}}^S = \sum_{e=1}^{nelem} \int_{\Gamma_e} U_{ij}^{*S} \phi_j d\Gamma_e \tag{16}$$

In these integrals, ϕ_j are shape functions for the elements. In this work, quadratic discontinuos elements are used to interpolate the displacement and traction variations in the boundaries of the plate and the repair.

In a similar way, matrix equations for repair can be written as (without considering traction forces applied at boundary repair):

$$\underline{\mathbf{H}}_c^R \mathbf{u}_c^R = \underline{\mathbf{F}}_c^R \mathbf{u}^R - \underline{\mathbf{F}}_c^R \mathbf{u}_d^P$$

$$\underline{\mathbf{I}} \mathbf{u}_d^R + \underline{\mathbf{H}}_d^R \mathbf{u}_c^R = \underline{\mathbf{F}}_d^R \mathbf{u}^R - \underline{\mathbf{F}}_d^R \mathbf{u}^P \tag{17}$$

In this case, similar significance has the $\underline{\mathbf{H}}^R$ and $\underline{\mathbf{G}}^R$ matrices as those in the sheet case. In the general case, when the sheet and the patch are made of different materials, the $\mathbf{F}^S$ and $\mathbf{F}^R$ matrices in equations (15) and (17) are not equals.

After some mathematical manipulation, the coupling equations for the sheet and the repair using the cell integration technique can be written as:

$$\begin{bmatrix} \underline{\mathbf{M}}^S & \underline{\mathbf{F}}^S \\ \underline{\mathbf{M}}^R & \underline{\mathbf{Q}}^R \end{bmatrix} \begin{Bmatrix} \mathbf{u}^S \\ \mathbf{u}^R \end{Bmatrix} = \begin{Bmatrix} \underline{\mathbf{G}}^S \mathbf{t}_c^S \\ \mathbf{0} \end{Bmatrix} \tag{18}$$

where $\underline{\mathbf{M}}^P$, $\underline{\mathbf{M}}^R$ and $\underline{\mathbf{Q}}^R$ matrix involving the $\underline{\mathbf{F}}$ matrices for sheet and repair.

3.2 DRBEM integration technique

In DRBEM integration tecnhique, equation (13) can be write in matrix form as:

$$\int_{\Omega_R} U_{ij}^{*S}(\mathbf{x}', \mathbf{x})\, b_j(\mathbf{x})\, d\Omega_R = \left(\underline{\mathbf{H}}^S \hat{\mathbf{U}}^S - \underline{\mathbf{G}}^S \hat{\mathbf{T}}^S \right) \alpha^S \tag{19}$$

In this equation, the influence matrices $\underline{\mathbf{H}}^S$ and $\underline{\mathbf{G}}^S$ are those defined in equation (16) with functions $\hat{u}_{kj}^d$ and $\hat{t}_{kj}^d$ approximated within each boundary element by using interpolation functions and nodal values as done for $u_j^S(\mathbf{x})$ and $t_j^S(\mathbf{x})$ in equation (15).

Discretizing the boundary, equations for the sheet (including traction equation) can be written in a compact form as:

$$\underline{\mathbf{H}}_c^S \mathbf{u}_c^S - \underline{\mathbf{G}}_c^S \mathbf{t}_c^S = \underline{\mathbf{A}}_c^S \alpha^S$$

$$\underline{\mathbf{I}} \mathbf{u}_d^S + \underline{\mathbf{H}}_d^S \mathbf{u}_c^S = \underline{\mathbf{A}}_d^S \alpha^S \tag{20}$$

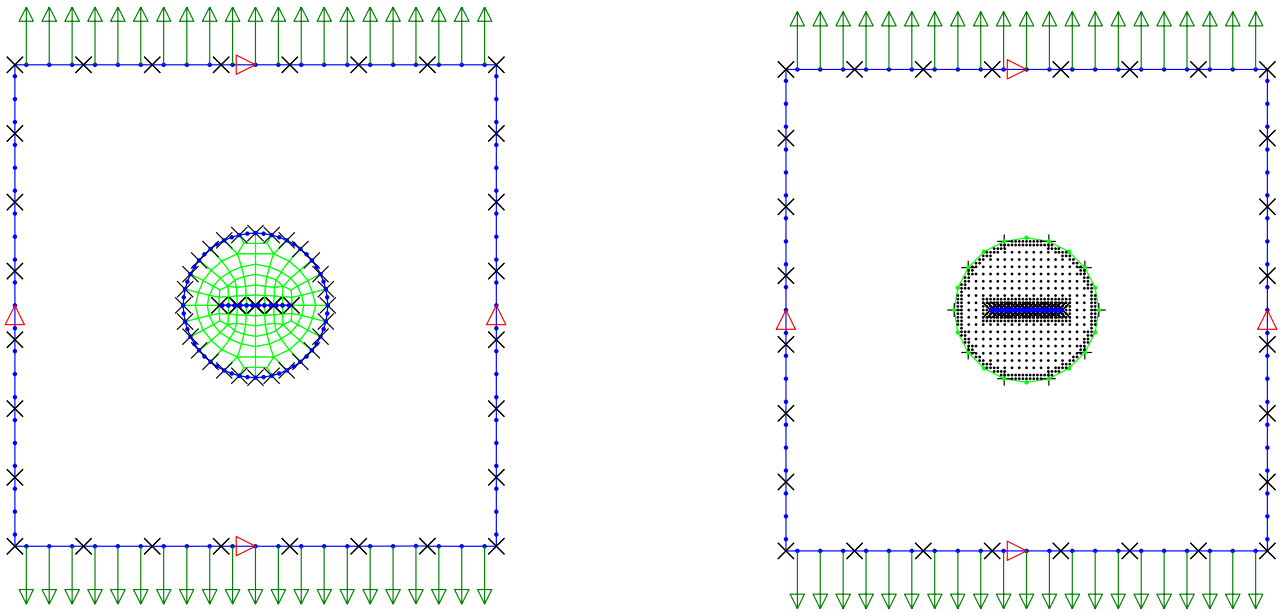

Figure 2: Model of cracked sheet reapired with adhesive patch using bi-quadratic interpolation cells. Left: cell model. Right: DRBEM model

where matrix $\underline{\mathbf{A}}^S$ is given by: $\underline{\mathbf{A}}^S = \underline{\mathbf{H}}^S \hat{\mathbf{U}}^S - \underline{\mathbf{G}}^S \hat{\mathbf{T}}^S$. In similar way, equations for repair are:

$$\underline{\mathbf{H}}_c^R \mathbf{u}_c^R - \underline{\mathbf{G}}_c^R \mathbf{t}_c^R = \underline{\mathbf{A}}_c^R \alpha^R$$

$$\underline{\mathbf{I}} \mathbf{u}_d^R + \underline{\mathbf{H}}_d^R \mathbf{u}_c^R = \underline{\mathbf{A}}_d^R \alpha^R \tag{21}$$

Now, equation (10) can be written in a matrix form for the sheet and the repair as:

$$\mathbf{u}_d^S - \mathbf{u}^R = \frac{h_A}{G_A} \underline{\mathbf{F}}^S \alpha^S$$

$$\mathbf{u}^R - \mathbf{u}_d^S = \frac{h_A}{G_A} \underline{\mathbf{F}}^R \alpha^R \tag{22}$$

Finally, coupling equations for the sheet and the repair using the DRBEM integration technique are given by,

$$\begin{bmatrix} \left(\underline{\mathbf{H}} - \underline{\mathbf{A}}\underline{\mathbf{F}}^{-1}\right)^S & \left(\underline{\mathbf{A}}\underline{\mathbf{F}}^{-1}\right)^S \\ \left(\underline{\mathbf{H}} - \underline{\mathbf{A}}\underline{\mathbf{F}}^{-1}\right)^R & \left(\underline{\mathbf{A}}\underline{\mathbf{F}}^{-1}\right)^R \end{bmatrix} \begin{Bmatrix} \mathbf{u}^S \\ \mathbf{u}^R \end{Bmatrix} = \begin{Bmatrix} \underline{\mathbf{G}}^S \mathbf{t}^S \\ \mathbf{0} \end{Bmatrix} \tag{23}$$

4 Numerical results

4.1 Circular composite patch over a cracked square sheet

A square sheet whose edge length is 200 mm is subjected to a uniform constant tension of 1 GPa in the direction of the y-axis. The sheet has a central crack of length $2a = 30$ mm and thickness equal to 1.5 mm. A circular repair of radius equal to 30 mm and thickness equal to 1.5 mm is bonded at the center of the sheet using an adhesive with 0.15 mm of thickness and shear modulus $G = 0.6$ GPa. Properties of the sheet and the patch are given in Table 1.

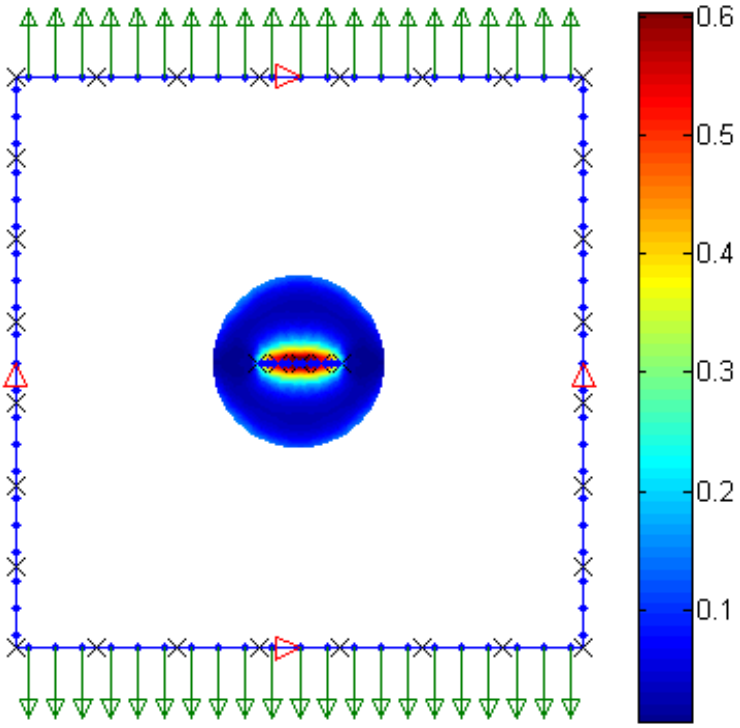

Figure 3: Normalized shear stress force in the adhesive.

Table 1: Mechanical properties of the sheet and the composite patch

Sheet	**Patch**
Young modulus $(E) = 72400$ Mpa	$E_1 = 25000$ MPa
Poissons ratio$(v) = 0.3$	$E_2 = 208000$ MPa
	$G_{12} = 72400$ MPa
	$\nu_{12} = 0.02$

The problem was analyzed using the method of cells and the DRBEM. In both cases, the mesh comprises of 28 discontinuous quadratic elements on the edge of the plate and on the edge of the repair. As shown in Figure 2, quadratic continuos cells with nine nodes were used to discretize de load transfer domain between the sheet and the patch except in crack neighborhood, where constants cells were used. Ten-point Gauss quadrature rule was used to evaluate the domain integral at quadratic cells.

Also, figure 2 shows the used DRBEM model. In this model, DRBEM collocations points have been concentrated near the crack and towards boundary repair. The shear stress distribution in the adhesive layer obtained using the DRBEM is shown in Figure 3. As was expected, shear stress gradients appear near crack's border where the difference between sheet and repair displacements is higher. Shear distribution map obtained in the model with cells is similar and it's not show here.

The resultant for the shear stress in the adhesive is showed in the Figure 4 normalized with respect to the sheet far field stresses (i.e. 1 GPa). This stresses has been obtained using the equation:

$$\tau^* = \frac{1}{\sigma_0}\sqrt{\tau_{zx}^2 + \tau_{zy}^2} \tag{24}$$

where σ_0 is the far stresses applied in the y-axis, τ_{zx} and τ_{zy} are shear stresses in the x and y-axis directions. As can be seen in this figure the convergence of the solution is obtained as the number of internal points increases. Further refining in the boundary mesh hasn't significantly affects the results. Obtained results are compared with analytical solution given by Rose [16] for an infinity orthotropic

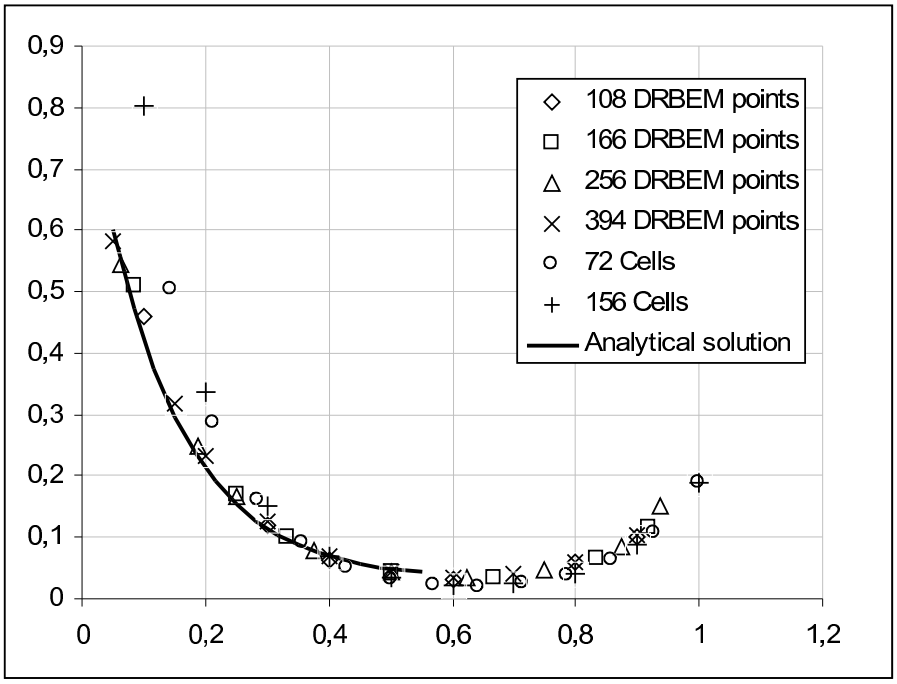

Figure 4: Normalized shear stress in the adhesive layer x=0 and $0 \leq y \leq R \leq 1$.

patches bonded to an infinity orthotropic sheet for patch with elliptic (circular) geometry:

$$\tau(y) = \sigma_0 \Lambda t e^{(-\Lambda|y|)} \tag{25}$$

again, σ_0 is the stress applied in the y-axis (i.e. 1 GPa) and the parameter Λ is given by:

$$\Lambda^2 = (G_A/h_A)\left\{\left(E^S h_S\right)^{-1} + \left(E_y^R h_R\right)^{-1}\right\} \tag{26}$$

It can be seen that good agreement was obtained even for relatively coarse internal points grids when the DRBEM were used. Lower convergence rate to Rose's solution was found with cell method.

4.2 Rectangular orthotropic patch over a square sheet

Consider a thin aluminium sheet with height H_s = of 254mm, width W_s = 254 mm, thickness equal to 5 mm with a central crack of length $2a$ = 13 mm repaired with boron-epoxi patch having dimensions: W_r = 130 mm; H_r = 75 mm. The sheet is subjected to a remote uniaxial tensile load of σ = 70 MPa, plane stress condition are assumed. The material properties of the plate, patch and adhesive are showed in table 2.

Table 2: Mechanical properties of the sheet and the composite patch

Sheet	**Patch**
Young modulus (E) = 72000 Mpa	E_1 = 19600 MPa
Poissons ratio(v) = 0.33	E_2 = 210000 MPa
	G_{12} = 5460 MPa
	ν_{12} = 0.3

The problem was analyzed using the cell method. The mesh comprises of 28 discontinuous quadratic elements on the edge of the plate. A convergence analysis for shear stress in the adhesive layer as function of number of cells and elements at boundary of the repair was performed. Figure 5 shows the used model.

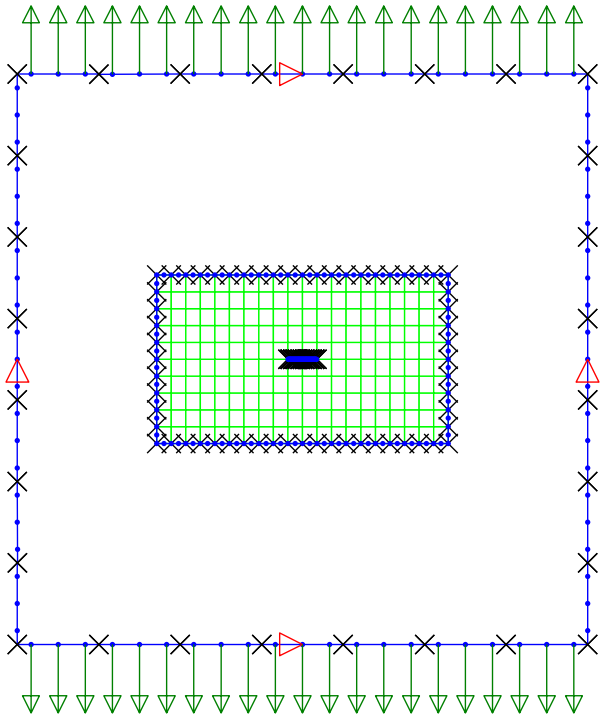

Figure 5: DBEM model for square sheet with rectangular patch.

Figure 6 shows the shear stress distribution in the adhesive layer. Again, shear stress gradients appear near crack's border where the difference between sheet and repair displacements is higher.

The displacement extrapolation technique is used for the evaluation of stress intensity factors as described in Salgado and Aliabadi [13]. When discontinuos elements are used for modelling crack surfaces, SIF values are extrapolated to the crack tip using relationship (see figure 7):

$$\{K\}^{tip} = \frac{r_{AA'}}{r_{AA'} - r_{BB'}} \left(\{K\}^{BB} - \frac{r_{BB'}}{r_{AA'}} \{K\}^{AA'} \right) \tag{27}$$

Three cases were considered, with $2a = 13$, 15 and 20mm, respectively. Table 3 shows the stress intensity factors in mode I obtained with 12 quadratic discontinuos boundary elements on each surface of the crack. In this table, SIFs are compared with those reported in Belhouari et al. [19].

Table 3: KI stress intensity factor for rectangular orthotropic patch over a square sheet

2a(mm)	K_I**-BEM**	K_I**-Ref.[19]**	**error**
13	7.60	8.10	6.17%
15	11.30	11.90	5.04%
20	11.95	12.50	4.40%

5 Conclusions

A new boundary element formulation for modelling cracked sheets repaired with composite patches was developed. The cracked sheet was modelled with the DBEM and the patch was modelled with

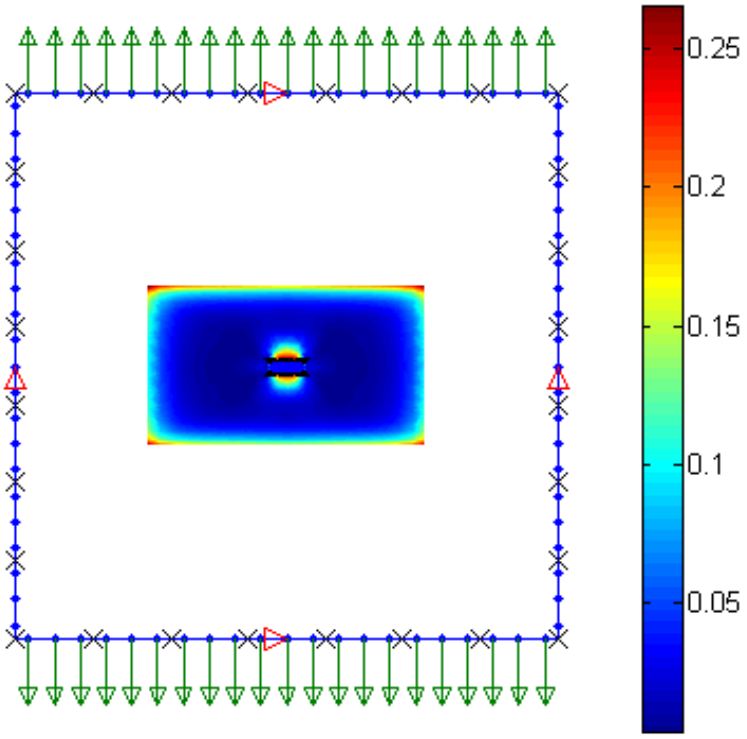

Figure 6: Normalized shear stress in the adhesive layer.

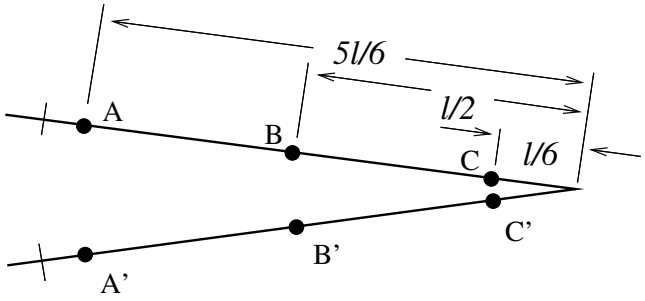

Figure 7: Discontinuous crack tip element.

the BEM. The interaction between the isotropic sheet and the patch was modeled considering shear body forces uniformly distributed on the interaction zone using a linear elastic relationship. The cell domain integration and the dual reciprocity have been used to treat the domain integrals that arise in the formulation due to shear interaction forces. The DRBEM showed higher convergence rate to analytical solution than the cell method. It can be concluded that the new formulation can be used with reasonable accuracy to study the mechanical behaviour of adhesively bonded repairs.

References

[1] Rose L. R. F., Wang, CH. Analytical methods for designing composite repairs. In Advances in the Bonded Composite Repair of Metallic Aircraft Structure, Vol. 1, Baker A, Rose F, Jones R, eds. Elsevier, Oxford, (2002).

[2] Erdogan, F., Arin, K. A sandwich plate with a part-through and debonding crack. *Engineering Fracture Mechanics*, **4**: 449-458, (1972).

[3] Ratawani, M. N. Analysis of cracked adhesivelly bonded laminate structures. *AIAA Journal*, **17**: 988-994, (1979).

[4] Mitchell, R. A., Wooley, R. M., Chwiruth, D. J. Analysis of composite reinforced cutouts and cracks *AIAA Journal*, **13**(6): 744-749, (1975).

[5] Jones R. and Callinan, R. J. On the use of special crack tip elements in cracked elastic sheets. *International Journal of Fracture*, **3**(1): 51-64, (1977).

[6] Jones R. and Callinan, R. J. Finite element analysis of patched cracks. *Journal of Structural Mechanics*, **7**(2): 107-130, (1979).

[7] Jones R. and Callinan, R. J. A design study in crack patching. *Fibre Science and Technology*, **14**: 99-111, (1981).

[8] Young, A., Cartwright, D. J, Rooke, D. P. The boundary element method for analysing repairs paletes on cracked finite sheets. *Proceddings of the 4th International conference on numerical methods in fracture mechanics*, Owen D.R.J. and Luxmoore A.R. (eds), 463-479, San Antonio, EUA, (1988).

[9] Tarn, J. G., Shek, K. L. Analysis of cracked plates with a bonded patch. *Engineering Fracture Mechanics*, **40**(6): 1055-1065, (1991).

[10] Young, A. Influence of tapering on the stresses in repair patches. *Proceddings of the 3rd International conference on numerical methods in fracture mechanics*, Owen D.R.J. and Luxmoore A.R. (eds), 741-752, San Antonio, EUA, (1987).

[11] Young, A., Rooke, D. P. Analysis of patched and stiffened cracked panels using the boundary element method. *Int. J. Solid Structures*, **29**(17): 2201-2216, (1992).

[12] Salgado, N. E., Aliabadi, M. H. Dual reciprocity method for the analysis of adhesively patched sheets. *Communications in Numerical Methods in Engineering*, **13**: 397-405, (1997).

[13] Salgado, N. K., Aliabadi, M. H. The boundary element analysis of cracked stiffened sheets, reinforced by adhesively bonded patches. *International Journal for Numerical Methods in Engineering*, **42**(2): 195-217, (1998).

[14] Widagdo, D., Aliabadi, M. H. Boundary element analysis of cracked panels repaired by mechanically fastened composite patches. *Engineering analysis with boundary elements*, **25**(4-5): 339-345 apr-may, (2001).

[15] Widagdo, D., Aliabadi, M. H. Boundary element analysis of composite repair patches *Proc. Advances in Boundary Element Techniques II*, New Jersey, USA, 327-335, (2001).

[16] Rose, L. R. An application of the inclusion analogy for bonded reinforcements. *International Journal of Solids and Structures*, **17**: 827-838, (1981).

[17] Aliabadi M. H, Sollero P. Crack growth analysis in homogeneous orthotropic laminates. *Composite Science and Technology*, **58**: 1697-1703, (1998).

[18] Albuquerque E. L, Sollero P., Aliabadi M. H. The boundary element method applied to time dependent problems in anisotropic materials. *International Journal of Solids and Structures*, **39**: 1405-1422, (2002).

[19] Belhouari, M., Bouiadjra, B., Megueni, A., Kaddouri, K. Comparison of double and single repairs to symmetric composite structures: a numerical analysis. *Composite Structures*, **65**: 47-53, (2004).

Inverse Problems in Science and Engineering
Vol. X, No. X, Month 200X, 000–000

Detection of holes in a plate using global optimization and parameter identification techniques

Patricia da Silva Lopes [*], Ariosto Bretanha Jorge and Sebastião Simões Cunha Jr.

Mechanical Engineering Institute, Federal University of Itajubá, Itajubá, MG, Brazil.

In this work, an inverse problem of damage identification and localization is modeled using independent techniques, both for the direct model and for the inverse model. The damage is characterized by a hole in the structure, which modifies existing temperature and stress fields. Direct models for the thermal (conduction) and elastostatics problems are needed to obtain the distribution of these quantities in the domain, for a particular configuration. The boundary element method is used here as the direct problem, and two different and independent techniques are used for the inverse problem, in order to localize and to identify a damage in a structure. The first technique adopted is a global optimization technique using genetic algorithms and the second approach is a parameter identification technique using artificial neural networks. The identification and localization of a hole in the structure is performed using these two techniques for the inverse problem, with comparable results.

Keywords*:* damage detection; boundary element method; optimization; genetic algorithm; parameter identification; artificial neural network

*Corresponding author. Email: patricia.silva.lopes@gmail.com

1. Introduction

Several types of static and dynamic loads and the structural deterioration process can cause different types of structural damage. The damage can be characterized by a change in the structure, such as the presence of holes and cracks. The knowledge of the change in the material properties corresponding to the damage depends on the type of material and on the structural configuration. The proper assessment of the damage in a structure can be useful to infer its remaining service life. The assessment of the structural damage can be performed through a comparison between measured and simulated data. To provide the simulated data, a numerical code is required, in which a direct model of the problem is consistently used by an inverse problem algorithm. For the direct problem, a model is required to obtain information on the distribution of the quantity of interest throughout the structure, given the boundary conditions and the presence of the damage. For the inverse problem, a model is required for the procedure of locating the damage in the structure given some (partial) information on the quantity of interest at some particular locations (for example, where some sensors are placed).

Numerical methods, such as the boundary element method (BEM) or the finite element method (FEM) can be used for modeling the direct problem. The study or analysis of damage in a plate can be done through the thermal modeling or the distribution of stresses. In this work, two BEM formulations were used, for potential and elastostatics problems, respectively. The BEM was chosen in this work, for two main reasons: *i*) the problem dimension under study is reduced by one, and only meshing of the boundary is required, simplifying the process of re-meshing the domain for the various damages being simulated; *ii*) the integral representation is an exact formulation, and the numerical errors are only due to the boundary discretization into boundary elements. For the potential formulation, the potential values are simulated on the external surface of the plate at given points. These potential values represent the distribution of temperatures on the plate. The use of thermal techniques shows that the distribution of temperatures on a plate changes due to the variations in the mechanical properties of the plate, what could be related to the presence of a given damage. For the elastostatics formulation, the quantities of interest are the interior point displacements and stresses.

The damage detection problem can be considered as a problem of system identification or an inverse problem. The inverse problem of identifying the presence, location and size of damage, such as cracks and holes, in a plate structure can be modeled using optimization and parameter identification techniques. In this work, the genetic algorithm (GA) is used as the optimization procedure, for two reasons: *i*) the algorithm looks for a global optimum, and is not trapped in local optima, which may not locate properly the damage; *ii*) there is no need to evaluate derivatives of the objective function. Also, in this work, the artificial neural network (ANN) approach is used as a parameter identification technique, for three reasons: *i*) ANN does not require a priori the presence of a Gaussian white noise, as it would be the case of Kalman filters, for example; *ii*) ANN is capable of representing non-linear problems; *iii*) ANN provides flexibility in terms of the number of internal layers to be used. By solving the inverse problem using two independent techniques (GA and ANN), a more reliable information on the damage parameters can be obtained, as a comparison of the results from both approaches can provide a means to verify these results.

The presence of damage may induce rapid changes in the field variable of the problem, and even discontinuities in the governing equation in the domain. Classical calculus-based optimization methods require evaluation of derivatives of the objective function, which may not be possible to be obtained, or may be numerically obtained, with unacceptable inaccuracy. Besides, these problems can have several local minima (multiple solutions), and thus a global optimization method (such as GA) is a better choice for the numerical solution [1,2]. In [1], the direct mechanical problem is modeled numerically through BEM, and the inverse problem, to minimize the error (difference between the measured and the computed value), is modeled in two ways: using sequential quadratic programming (SQP), to obtain a local optimum, and using the GA, to obtain a global optimum for the same objective function. SQP is a calculus-based optimization method, in

which the second derivatives are required to obtain the Hessian matrix. In [1], the Hessian matrix was approximated through a finite difference scheme. Also, this method depends on the choice of the starting point, so the algorithm can stop at a local minimum of the function that may not represent the proper damage parameters for the problem. On the other hand, GA uses multiple points to search for the solution, rather than a single point, and a global minimum has a better chance of being obtained. Also, as GA does not require any evaluation of derivatives, no errors are included in the solution due to the approximation of these derivatives.

In the works presented in [3] and [4], the BEM is also used to model the direct mechanical problem numerically. A backpropagation neural network (BPN) for the on-line identification of holes or cracks in composite structures is applied by [3]. In [4], evolutionary algorithms at the identification of crack are used and the problem is formulated as the minimization of the difference between the measured and computed values of displacements or stresses for selected boundary nodes. The work presented in [5] proposes a BPN for the inverse analysis, and a numerical model for the direct method. This direct model is based on a coupling of the FEM with the boundary integral equation (BIE) method, of which the discretized form is also known as the BEM. The BPN uses a backpropagation learning rule, where the adjustment of weights, from input to hidden layers, is made by back-propagating the errors of the neurons, from the output layer to the hidden layers.

In [6], a new method was developed for finding boundary temperatures and heat fluxes, where both quantities may be unknown in some parts of the boundary. This technique requires over-specified thermal boundary conditions, i.e., both the temperatures and the heat fluxes must be specified, on other parts of the boundary. In this case, BEM was used for the direct model, and the program performed automatic non-iterative determination of the thermal boundary conditions (boundary temperature and flux) on the parts of the interior and exterior boundaries where both quantities were unknown. This non-iterative approach was extended in [7] for elastostatics problems using BEM, for finding deformations and tractions on parts of the boundary where these quantities are unavailable. Again, the boundary conditions need to be over-specified on other parts of the boundary, i.e., both the displacements and the tractions must be specified at these other boundary subregions.

In this work, two direct problems are modeled using the BEM approach in 2D: *i*) a potential problem of heat transfer (conduction) on a domain; and *ii*) an elastostatics problem. In both cases, a damage is simulated by the presence of a hole inside the domain. For each run of the direct model, the information about the location and radius of the hole, and also about the boundary conditions, loading, and plate and hole discretization, is also provided. After evaluating the boundary solution, the BEM code evaluates, as a post-processing, some quantities of interest at selected interior points. The selected interior points are candidates to be sensor locations, for a future experimental setting, and the quantities of interest at these points may be the quantities that these sensors are able to measure. Each run of the direct method using the potential formulation provides one piece of information (the potential, i.e., the temperature) at the selected interior points. On the other hand, the elastostatics BEM formulation provides three pieces of information at an interior point – the components of the stress tensor, i.e., two normal stresses and one shear stress. The values of the normal stress and the shear stresses depend on the system of coordinates being used, or on the normal direction of the cutting plane that passes through the point of interest. As the goal of the inverse method is to identify and locate the hole, but not to identify any direction-dependent properties, the desired quantities to be supplied to the inverse model should be scalar quantities obtained at the selected interior points, and not direction-dependent quantities. Scalar quantities of interest can be obtained as the invariants of the stress tensor – in 2D, the mean stress and the octahedral stress – at the selected interior points. The mean stress and the octahedral stress are independent scalar fields, and either one can be used as the variable of interest at the selected interior points. In this work, the mean stress was adopted as the quantity to be provided to the inverse model for the elastostatics problem.

The boundary conditions for the external boundary of the plate may be set as temperatures or fluxes prescribed, for the potential formulation, or displacement or traction prescribed, for the elastostatics formulation. The boundary conditions for the internal boundary of the plate (the hole) were set assuming zero fluxes, for the potential formulation, and zero tractions, for the elastostatics formulation. For the inverse problem, the direct BEM model first evaluates the differences in the quantity of interest (the potential or the mean stress, depending on the problem) between the undamaged plate and the plate with the damage, for all selected interior points. These differences are then supplied as input to the optimization (GA) or identification (ANN) subroutines. The main idea for passing only differences of the quantities of interest is to avoid any possible bias related to the magnitude of these quantities, as only their change (due to the presence of the hole) is important for the inverse problem. The information provided by the BEM model for the direct problem is used for comparison with similar information, which must be available, for a plate with a hole with unknown size and location. Usually, the information on the "real" plate would be available by means of an experimental device, in which sensors would be put in all selected interior point locations. For the purpose of validating this approach, the plate with the "real" hole is also simulated with the BEM model, so the inverse problem algorithm will try to identify and locate this simulated "real" hole. The optimization (GA) and identification (ANN) subroutines are independent approaches for localization (obtaining the center coordinates) and identification (obtaining the radius) of a given simulated "real" hole.

In short, the numerical modelling of the direct problem is performed using two different BEM approaches, for potential and elastostatics formulations, respectively. Also, two different and independent techniques (optimization using GA, and identification using ANN) are used for resolving the inverse problem to obtain the damage location and size, for each BEM model. The comparison between the results obtained using the two different and independent techniques (GA and ANN) for the inverse problem allows for a validation of the inverse procedure. A redundancy in the results, i.e., similar damage identification and localization results, from the two different and independent inverse techniques, will provide a good indication of the correctness of this procedure. A test case using GA, available in the literature, will also be used for comparison purposes. All subroutines in this work were written using the MATLAB® platform.

2. Direct problem: boundary element methods

Numerical methods, such as the boundary element method (BEM) or the finite element method (FEM) can be used for modeling the direct problem. In the FEM, the problem domain is partitioned into a number of subdomains (or finite elements) with connectivity between the elements provided through common nodal points. In the BEM, the governing partial differential equation of a domain is transformed into a set of integral equations, which relate the boundary variables (both known and unknown) [8,9]. The BEM has some advantages with regard to FEM [8]: *i*) BEM discretization is done only in the boundary of the domain, while FEM requires the discretization of the entire domain; *ii*) the number of equations associated with BEM is smaller than in the FEM approach, for the same degree of accuracy; *iii*) BEM is well suited for problems with singularities, such as in linear elastic fracture mechanics.

The BEM is a numerical procedure well adapted for the modeling of a structure with damage. In this method, the distribution of the quantities of interest in the domain is obtained from the information of the distribution of certain quantities in the boundary. Thus, the problem is described based on what happens in its boundaries, reducing the dimension of the problem and simplifying numerically the treatment. In this work, the models investigated include the potential and elastostatics formulations (see references [9] and [10] for both formulations). A simple direct method for a conduction problem is modeled, where the temperature distribution on the external surface of a thin plate is analyzed. Without the hole, the distribution of the potential is known *a priori*. If a small hole is included, the potential distribution is unknown and must be obtained numerically from the BEM solution. Increasing the problem complexity, a BEM model for the

elastostatics problem can be used. Similarly, the distribution of the displacement and stresses without the hole is known *a priori*. If a small hole is included, this information is unknown and must be obtained numerically from the BEM solution. When modeling the damage detection problem by means of an analysis of the elastic response of the structure under excitation, perturbations in the expected response imply in the presence of damage. Thus, the damage in the structure will characterize its behavior, static or dynamic.

2.1. Boundary integral equation for potential and elastostatics problems

For the elastostatics problem, the elastic behavior of a body under static loads is governed by the equilibrium, compatibility and constitutive equations [11]. Considering Γ as the boundary of the body, an integral representation of these equations, can be written as Equation (1), for the case with no volume forces

$$c_k^i(y)u_k(y)=\int_\Gamma\left[u_k^i(x;y)q_k(x)-q_k^i(x;y)u_k(x)\right]d\Gamma(x) \tag{1}$$

where: q_k is the traction vector at a boundary point whose outward normal n_j; u_k is the displacement vector; u_k^i and q_k^i are the displacement and traction vectors of the fundamental solution, respectively (see references, [11], [7], [9] and [10] for more details). When the limit to the boundary is taken for the collocation point y, the equation is called a Boundary Integral Equation (BIE). The term c_k^i is the free term coefficient, which depends on the position of the collocation point, relative to the boundary. For an interior point, $c_k^i=1$; for an exterior point, $c_k^i=0$; for a boundary point on a smooth section of the boundary, $c_k^i=1/2$. For non-smooth boundary points, the free term coefficient depends on the swept angle at this point, when going from the boundary region before the point to the boundary region after the point, following the interior domain. By performing collocation at different boundary points (the nodes), a set of equations is obtained, which can be discretized to obtain a system of algebraic equations to be solved. The set of equations is completed by the boundary conditions, $u_i(x)=\bar{u}_i$ on Γ_u and $q_i(x)=\bar{q}_i$ on Γ_q, where Γ_u and Γ_q are non-overlapping partitions of the boundary Γ ($\Gamma_u\cup\Gamma_q=\Gamma$ and $\Gamma_u\cap\Gamma_q=\varnothing$) ([11,12]). The kernels of the integrands, given by the fundamental solution and its derivative, lead to weakly-singular and singular integrals, respectively, when the collocation point and the integration point coincide. Special integration schemes are incorporated in the BEM code, to account for the evaluation of these singular integrals.

Equation (1) is a component of a vector equation, in the k-direction ($k=1,2$, in the 2D case). A scalar boundary integral equation for the potential problem can be obtained as an integral representation, closely similar to Equation (1), for the case where there are no heat sources in the domain. In this case, due to the scalar nature of the potential field, the symbol k can be dropped, as shown in Equation (2).

$$c(y)u(y)=\int_\Gamma\left[\psi(x;y)q(x)-\frac{\partial\psi}{\partial n}(x;y)u(x)\right]d\Gamma(x) \tag{2}$$

where: $c(y)$ is the coefficient of the free term; u is the potential; q is the flux in the outward normal direction; $\psi=(1/2\pi)\ln(1/r)$ is the fundamental solution for the Laplace equation; $r=|x-y|$ is the distance between the collocation point y and the integration point x; and, $\partial\psi/\partial n=-(1/2\pi r)(\partial r/\partial n)$ is the flux associated to the potential ψ. The boundary conditions are similar to the previous case, with $\bar{u}$ and $\bar{q}$ now representing known values of the potential and flux on Γ_u and Γ_q, respectively [12].

2.2. Boundary element discretization

By evaluating Equation (1) at the collocation points y, by using proper shape functions in the

discretized boundary (in this work, constant boundary elements), and by applying adequate quadrature formulae for the numerical integration (in this work, 4 Gauss points for each element), a system of linear equation is obtained as (Equation (3))

$$[H]\{u\}=[G]\{q\} \tag{3}$$

where $\{u\}$ and $\{q\}$ contains the nodal values of the displacement and traction vectors, for the elastostatics problem, or the nodal values of potential and flux vectors, for the potential problem.

When the boundary conditions of each problem are taken into account properly, after algebraic manipulation, known and unknown quantities are separated, and a system of linear equations, which can be solved for the unknown boundary quantities, is obtained as (Equation (4))

$$[A]\{x\}=\{f\} \tag{4}$$

where $\{x\}$ is the vector of unknown boundary quantities; $\{f\}$ is the right-hand side, obtained after manipulating the known boundary quantities with the proper numerical integration coefficients; and $[A]$ is a matrix with the integration coefficients related to the unknown boundary variables.

After the boundary solution is obtained, by post-processing, the solution for the displacement (elastostatics problem) and for the temperature (potential problem) at selected interior points is obtained by means of a particular case of Equation (1), where c_k^i is equal to 1 [10]. As the integral equation for interior points does not contain singular integrals, special integration schemes are not required in the BEM code, for this case.

Regarding the elastostatics problem, the internal stresses σ_{ij} can be computed by differentiating the displacements at internal points and introducing the corresponding strains into the stress-strain relationships (Equation (5)) (see references [9] and [10]).

$$\sigma_{ij}=\frac{2\mu\nu}{1-2\nu}\delta_{ij}\frac{\partial u_m}{\partial x_m}+\mu\left(\frac{\partial u_i}{\partial x_j}+\frac{\partial u_j}{\partial x_i}\right) \tag{5}$$

where: μ is the shear modulus and ν is the Poisson's ratio.

After a proper substitution of the value of u_k into Equation (5), the internal stresses can be represented in compact form shown in Equation (6)

$$\sigma_{ij}=\int_\Gamma D_{kij}q_k d\Gamma-\int_\Gamma S_{kij}u_k d\Gamma \tag{6}$$

where:

$$D_{kij}=\frac{1}{4\alpha\pi(1-\nu)r^\alpha}\left\{(1-2\nu)\left(\delta_{ki}r_{,j}+\delta_{kj}r_{,i}-\delta_{ij}r_{,k}\right)+\beta r_{,i}r_{,j}r_{,k}\right\}$$

$$S_{kij}=\frac{2\mu}{4\alpha\pi(1-\nu)r^\beta}\left\{\beta\frac{\partial r}{\partial n}\left[(1-2\nu)\delta_{ij}r_{,k}+\nu\left(\delta_{ik}r_{,j}+\delta_{jk}r_{,i}\right)-\gamma r_{,i}r_{,j}r_{,k}\right]+\right. \tag{7}$$

$$\left.+\beta\nu\left(n_i r_{,j}r_{,k}+n_j r_{,i}r_{,k}\right)+(1-2\nu)\left(\beta n_k r_{,i}r_{,j}+n_j\delta_{ik}+n_i\delta_{jk}\right)-(1-4\nu)n_k\delta_{ij}\right\}$$

In Equation (7), $\alpha=1$, $\beta=2$, and $\gamma=4$ for a two-dimensional case. The derivatives indicated by commas are taken at a boundary point x_i^B (Equation (8))

$$r_{,i}=\frac{\partial r}{\partial x_i}=\frac{r_i^B}{r^B} \tag{8}$$

with $r_i^B=x_i^B-x_i^I$, being x_i^I an internal point and $r^B=|r|$. The derivative shown in Equation (8) is equal and opposite in sign to those taken at an internal point [9].

3. Inverse problem: optimization and parameter identification techniques

The inverse problem might be modeled by means of optimization and parameter identification techniques. The damage is simulated by the presence of a small hole in the domain, and the goal is to obtain size and location of the damage.

3.1. Optimization using genetic algorithms

The genetic algorithm (GA) is a search method based on the processes of natural evolution. This method works with a set of possible solutions for a given problem, composing the initial population. In other words, GA uses multiple points to search for the solution rather than a single point in the traditional gradient based optimization method [13]. In this algorithm the problem variables are represented as genes in a chromosome (each chromosome is also denominated an individual of the population). Starting from an initial population, the individuals with better adapted genetic characteristics have higher chances of surviving and reproducing.

According to [4], the GA's are methods that do not depend on the choice of the initial point, increasing the chances of obtaining the optimum global of the system. So that the population is diversified and maintain certain acquired adaptation characteristics by the previous generations, the genetic operators (selection, crossover and mutation) can be used. These operators transform the population through successive generations, extending the search until arriving to a satisfactory result. For more details about how these operators work, see references [14], [15] and [16].

In this work, the optimal solution for unknown parameters of the damage (location and size) is obtained through the GA for potential and elastostatics formulation. Considering the first formulation (potential formulation), a functional can be defined as the difference between the measured (simulated) values of the difference in the potential (between the undamaged plate and the plate with the damage) and the values of the same differences in potential calculated at the same points by the damage detection program. In the second formulation (elastostatics formulation), the functional is defined as the difference between the measured (simulated) values of the local difference in the mean stress (between the undamaged plate and the plate with the damage) and the values of the same differences in mean stress calculated at the same points by the code (assuming several different locations and sizes for the “numerical” damage). The functional corresponds to the fitness function of the GA. The minimization of this fitness function allows the damage detection program to find the unknown parameters of the damage. The functional formulation is shown at Equation (9):

$$J_j = \frac{1}{2}\sum_{i=1}^{n}\left(measured_i - calculated_{ji}\right)^2 \tag{9}$$

being n the number of internal points i (“sensors” placed in the plate) where the differences are evaluated; $measured_i$ the vector of simulated values for the differences obtained using BEM, for a given damage; and, $calculated_{ji}$ the vector of differences in potential (potential formulation) or mean stress (elastostatics formulation) calculated by the code for each individual j.

As mentioned, GA starts with an initial population, representing a set of possible solutions for a given problem. To solve the damage detection problem, each chromosome (individual) of the population can be assembled according to the vector presented in Equation (10):

$$c = \left[g_1\ g_2\ g_3\ g_4 \cdots g_{n+3}\right] \tag{10}$$

where:

g_1 – first gene representing the x-coordinate of the hole;

g_2 – second gene representing the y-coordinate of the hole;

g_3 – third gene representing the hole radius;
g_4 … g_{n+3} – fourth gene and the subsequent genes, representing the measures of the potential difference (potential formulation) or the mean stress difference (elastostatics formulation) between the undamaged plate and the plate with the damage.

As an example, Figure 1 represents three possible configurations of chromosomes. While the location and size of the hole vary, the number and location of the sensors remain the same, for all chromosomes. The information on the quantity of interest is collected at these sensor locations for all cases.

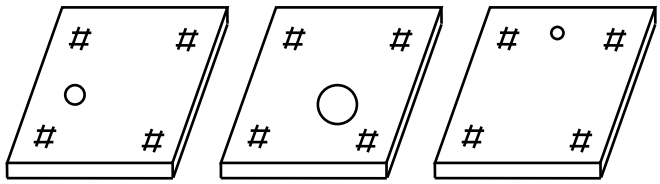

Figure 1. Plate with a hole: three possible configurations for the chromosomes.

3.2. Parameter identification using artificial neural network

The artificial neural networks (ANN's) are computational techniques that present a mathematic model to represent the human brain and to try to simulate the learning process of this brain. An ANN is formed by the interconnected neurons whose inputs can be obtained from the outputs of other neurons or from input nodes. Different configurations of the artificial neuron can be made to develop different network topologies [18]. Among the existent configurations, the ANN can be feedforward or feedback. At the feedforward neural networks, the neurons are interconnected in layers, but the flow of data only occurs in a direction [17]. At the feedback neural networks, a neuron receives the information of neurons of the previous layer and of a subsequent layer. After defining the structure of the ANN, an iterative process of weight adjustment of this network is made. This process is known as training process. Following the training, the ANN learns how to proceed for other input data in the problem domain.

In this work a backpropagation neural network (BPN) is used, through a feedforward configuration and the backpropagation learning algorithm. The backpropagation algorithm carries out a supervised learning where the desired outputs are given as part of the training vector. For more details about how this algorithm woks, see reference [19]. In addition, there is a training function of ANN known as ‘gradient descent with momentum and adaptive learning rate function’ (see, for example the MATLAB® help manual). This function is a backpropagation network training function that combines adaptive learning rate with momentum training. An adaptive learning rate allows the performance of the steepest descent algorithm to improve, attempting to keep the learning step size as large as possible while keeping learning stable. Moreover, momentum training allows a network to respond not only to the local gradient, but also to recent trends in the error surface. Without momentum a network may get stuck in a flat local minimum.

3.3. Formulation of optimization and parameter identification problems

The problem of damage detection in a thin plate can be formularized as an optimization problem (using GA) according to the flowchart in Figure 2, or can be formularized as a parameter identification problem (using ANN) according to the flowchart in Figure 3.

Considering Figure 2, the initial population for the GA approach is formed by the geometric information of a numerical hole (x- and y-coordinates of its center, and also its radius) and also by differences in the quantities of interest, calculated at selected interior points, herein called “Difference 1”. “Difference 1” can be the local difference in the potential or the local difference in the mean stress between the undamaged

plate and the plate with the damage, for potential and elastostatics formulations, respectively. Similarly, a set called “Difference 2” can be evaluated at the same interior points, representing the “measured” differences for the quantity of interest at these points, for the “real” hole. In this work, the “real” hole is also simulated. To validate the damage detection approach, the value of “Difference 2” was not allowed to be in the initial population of the GA approach. The initial population and also “Difference 2” are employed in the fitness function, presented in Equation (9). The goal of the GA approach is to look for a minimum value of this fitness function. For that, the algorithm uses genetic operators to modify the population and subsequently reevaluate the fitness function for the new population. Convergence criteria can be set, including the number of iterations, the differences in the fitness function (the optimum value) between two subsequent populations, or the differences between the hole parameters of location and size (the optimizer) between two populations. When the convergence criterion is met, the numerical holes have reached the vicinity of the “real” hole, and thus the information about the location and size of the “real” hole is obtained. In this work, a criterion for the maximum number of generations (no to exceed 75 in the potential problem and not to exceed 100 in the elastostatics problem) was assumed, together with a default criterion for the tolerance (difference between two fitness functions less than or equal to 1×10^{-6}).

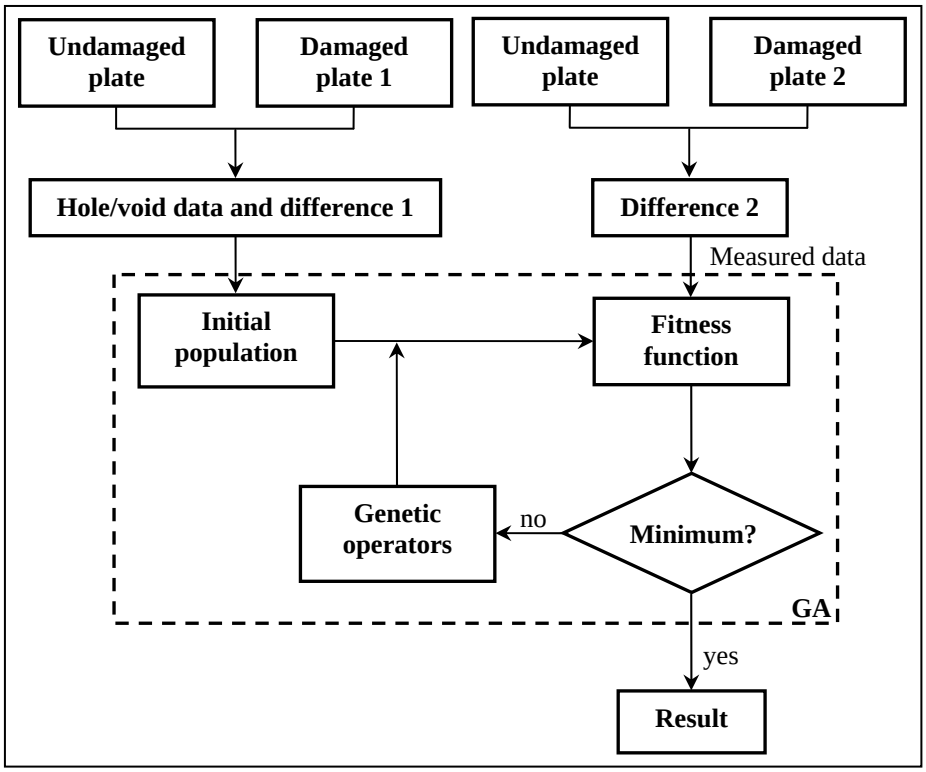

Figure 2. Flowchart for the optimization procedure using GA.

According to Figure 3, a network is created, considering “Difference 1” (the same “Difference 1” as in the GA approach) as the input data and the geometric information for the hole (x- and y-coordinates of the hole center, and its radius) as the output data. The next step is to train the created network, obtaining, as a result, a NET that contains information about how to proceed for another input data in the problem domain. Finally, the trained network is simulated for “Difference 2” (same “Difference 2” as in the GA approach). Similarly to the optimization algorithm, convergence criteria need to be set for this approach. In this work, the error goal was assumed, not to exceed 1×10^{-5} for the potential problem and 1×10^{-2} for the elastostatics

problem. The order of magnitude of these assumed error goals follows the order of magnitudes in the differences of the quantities of interest, namely the potential and the stress. A convergence criterion in terms of the maximum number of iterations (not to exceed 5000 epochs) was also assumed. When the convergence criterion is met, the ANN has identified the "real" hole, providing the information about its location and size.

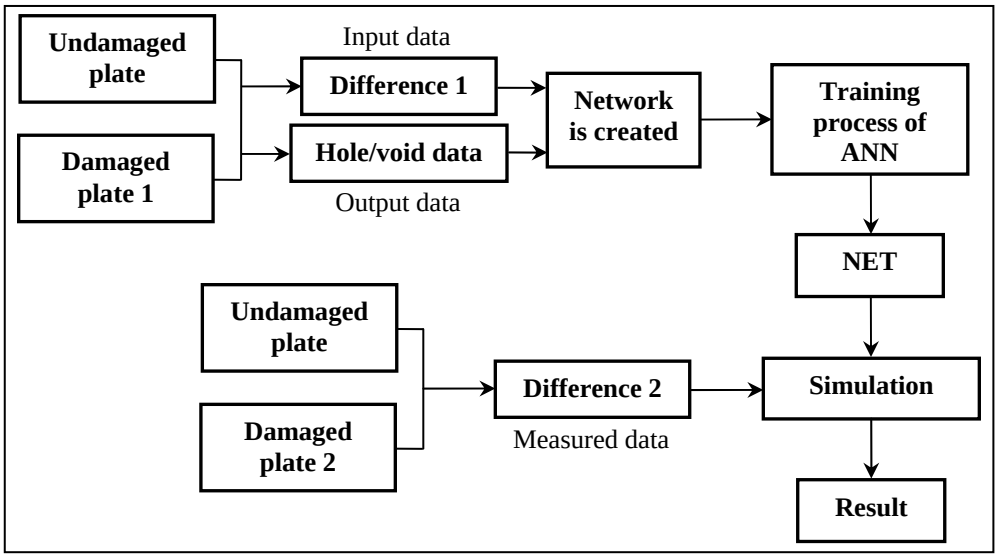

Figure 3. Flowchart for the parameter identification procedure using ANN.

4. Numerical results and discussion

For the potential problem, the results obtained by the damage detection program are analyzed for a problem of heat flow in a thin plate. Initially, a plate without damage and with the dimensions $(0.06\times0.06)\ m$ was simulated through the boundary element method (BEM), as illustrated in Figure 4. The boundary of the plate was discretized into 12 elements and the value of the potential was evaluated at 49 internal points (Figure 4(b)). The contour conditions for the problem are represented in this figure, where q represents the heat flow and u represents the temperature at the boundary. Then, a plate with a central hole of radius $0.06\ cm$, with the same dimensions and boundary conditions, was also simulated, and the obtained results for the potential were compared with the plate without damage.

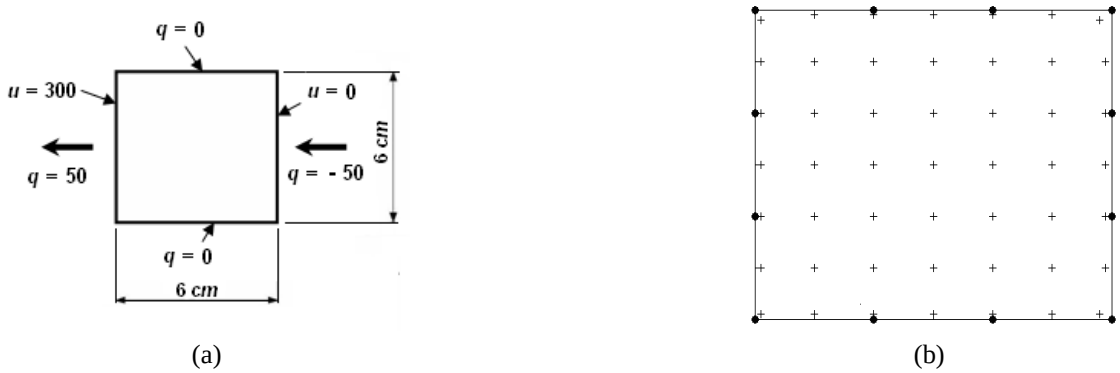

Figure 4. Plate model for the potential problem: (a) dimensions, loading, and boundary conditions. (b) boundary discretization and sensor locations.

For the elastostatics problem, a BEM model was built for the plate with a hole with the boundary conditions illustrated in Figure 5(a). Two discretizations were implemented for the external contour, a coarse mesh with 12 constant elements and a fine mesh with 48 constant elements. Figure 5(b) shows the discretization for the case of 48 elements in the outer boundary and 12 elements in the hole, as well as the position of the nine sensors. At the present work, the sensors were uniformly distributed on the plate and no positioning study of the sensors was performed. The plate was simulated with shear modulus equal to $94{,}500\ MPa$ and a Poisson's ratio for plane strain equal to 0.1.

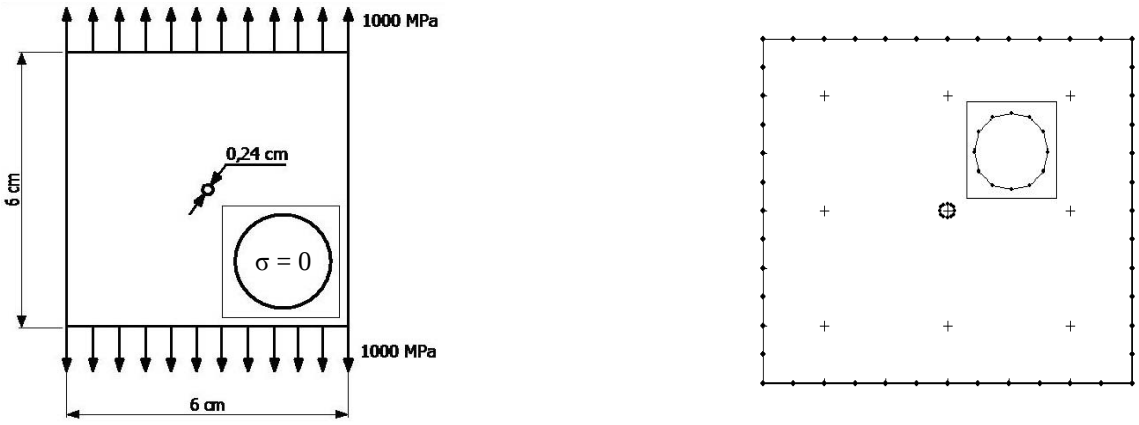

Figure 5. Plate model for the elastostatics problem: (a) dimensions, loading, and boundary conditions. Insert shows a stress-free hole; (b) boundary discretization (fine mesh) and sensor locations. Insert shows hole discretization.

The influence of the numerical errors due to the BEM discretization in the optimization results can be seen in Figure 6. A comparison was made for the optimization results (using 10 runs of a GA approach) and for two meshes (a coarse mesh and a fine mesh) using the elastostatics formulation for the plate shown in Figure 5(a). Figure 6 presents illustrative results for the mean values of the error in the location (*x* and *y* coordinates) and size (radius *r*) of a central hole [20].

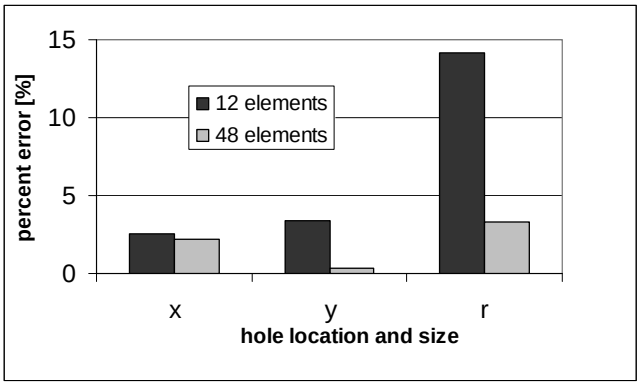

Figure 6. Mean values for the error in location and size of a center hole.

4.1. Assembly of data for the GA and ANN procedures

For the potential formulation, holes with radius equal to 0.15 *cm*, 0.03 *cm* and 0.09 *cm*, respectively,

were considered to assemble the initial population of the GA. For each one of these radius, the coordinate x of the center of the hole was varied from 0.5 *cm* to 5.0 *cm* and the coordinate y of the center of the same hole was varied from 0.5 *cm* to 5.5 *cm*, both coordinates with a step size of 0.5 *cm*. Then, 110 different positions for each radius in the plate were simulated and the respective values of the potential difference were stored for *a-posteriori* processing.

For the ANN, initially 25 internal points, representing the sensors on the plate, were considered to the assembly of the input data of this network. After, the number of sensors was subsequently decreased to 15, 9 and 5, respectively. In the present work, the sensors were uniformly distributed on the plate and no positioning study of the sensors was performed; only a study regarding the reduction on number of the sensors was done. The distribution of the sensors on the plate, for each case, is shown in Figures 7(a), 7(b), 7(c) and 7(d), respectively.

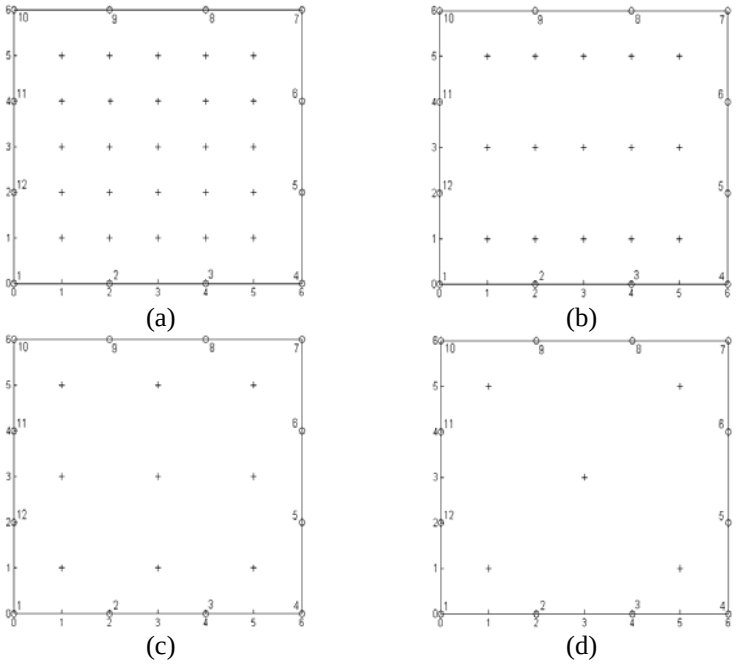

Figure 7. Sensor distribution for the ANN: (a) 25, (b) 15, (c) 9 and (d) 5.

In this potential formulation, a single hole with a radius equal to 0.15 *cm* in nine different hole positions was considered to assemble the input and output data of ANN. (positions equal to (0.5;0.5) *cm*, (0.5;3) *cm*, (0.5;5.5) *cm*, (3;0.5) *cm*, (3;3) *cm*, (3;5.5) *cm*, (5.5;0.5) *cm*, (5.5;3) *cm* and (5.5;5.5) *cm*). Then, another hole of radius equal to 0.05 *cm* was also analyzed in each mentioned position.

For the elastostatics formulation, holes with radius equal to 0.05 *cm*, 0.10 *cm* and 0.15 *cm* was considered to assemble the data GA and ANN. For each radius, the x and y-coordinate of the center of the hole was varied from 0.5 *cm* to 5.5 *cm* with a step size of 0.5 *cm*. Then, 121 different positions for each radius in the plate were simulated and the respective values of the difference in the mean stress at the 9 internal points (shown as sensor locations in Figure 5(b)) were found by means of BEM and these values were stored for *a-posteriori* processing.

4.2. Analysis of the results obtained from the genetic algorithm

For the potential formulation, in the initial population of the GA, the values of the difference in the

potential were normalized before using the data directly, taking into consideration the maximum value of this difference. Finally, the initial population with 330 individuals can be formed. As the potential values near the right border (temperature equal to zero) of the plate are close to zero, the potential difference is used instead of the direct use of the potential value.

The plots of the location and size of the holes obtained from 5 different runs of the GA are presented in Figure 8. The program was run only 5 times, because there was no significant difference when this value was increased. The "real" position of the hole is represented in continuous line and the results found by the GA in non continuous lines.

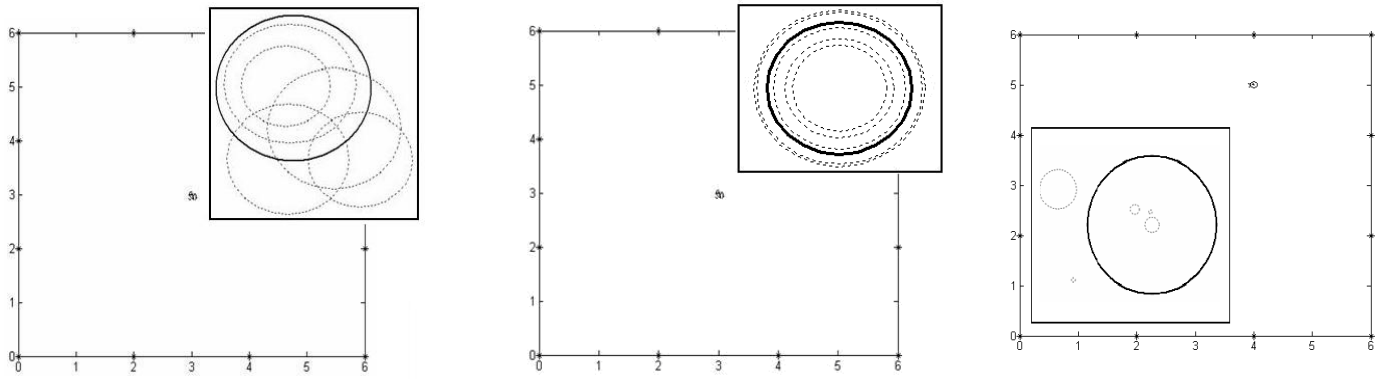

(a) (b) (c)

Figure 8. "Real" and simulated hole for potential: (a) for a central hole with elitism equal to 2; (b) for a central hole with elitism equal to 10; (c) for a hole at (4;5) *cm*. Inserts shows the region of hole in detail.

As presented previously (in section 3.3), a stopping criterion was assumed for the number of generations no to exceed 75 in the potential problem, and a stopping criterion for the tolerance (difference between two fitness functions less than or equal to 1×10^{-6}). In the results obtained, the tolerance of the problem was reached, in other words, there was no improvement in the objective function (fitness function), and the maximum number of generations was not reached, showing a good convergence of the algorithm. The crossover fraction was set as 0.8, and the mutation fraction was set as 0.2. Figure 8 (a) and Figure 8 (b) show a hole in the position (3;3) *cm*, and Figure 8 (c) shows a hole in the position (4;5) *cm*, all cases considering a radius equal to 0.06 *cm*. For the first simulation (Figure 8 (a)), the elitism was 2, and the second (Figure 8 (b)) and third simulation (Figure 8 (c)), the elitism was changed from 2 to 10, guaranteeing that 10 individuals survive in the next generation. With the change of elitism (Figure 8 (b)) the holes were concentric, and the hole position presented a small uncertainty. Moreover, the radius for every simulation was not much sensitive to the variation of the GA parameters. The crossover function considered was the heuristic function with a value of ratio equal to 1.3 (this value represents how far the child is from the better parent). Besides, the mutation function adopted was the Gaussian function. The results are different for each run of GA approach, because there is a small mutation presence and a crossover function that is different for each run of the algorithm, in other words, there is an associated occurrence probability.

In a similar manner, for the elastostatics formulation, the values of the difference in the mean stress were normalized, taking into consideration the maximum value of this difference. The values of x and y-coordinate of the center of the hole and its radius were also normalized, considering the respective maximum values. After that, the initial population with 363 individuals can be formed.

The plots of the location and size of the holes obtained from 10 different runs of the GA are presented in Figure 9. The GA, due to its own randomness, generates a different optimal solution every time it is run; nevertheless the results of the GA approach present a tendency to be concentrated near the "real" hole. Figure

9 (a) shows the results for a central hole; Figure 9 (b) shows a hole located at (2;2) *cm*; and Figure 9 (c), a hole located at (5;3) *cm*. The radius of each plot was considered equal to 0,12 *cm*. The "real" position of the hole is represented in continuous line and the results found by the GA in non continuous lines.

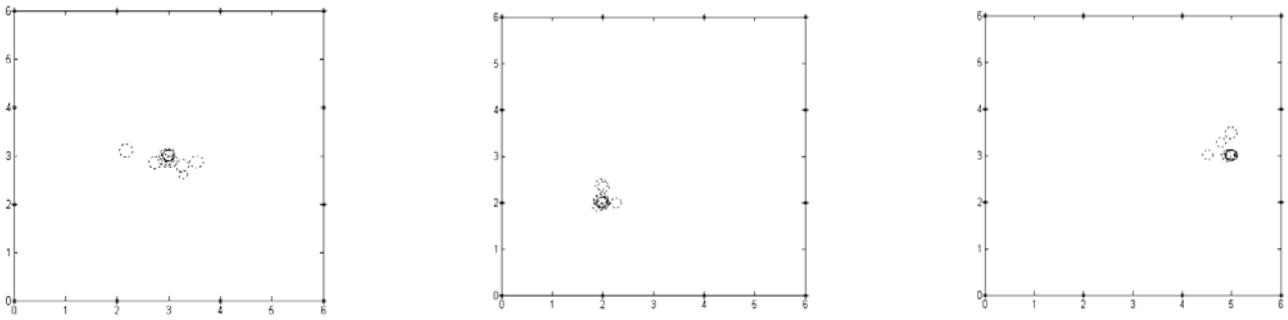

(a) (b) (c)

Figure 9. "Real" and simulated hole for mean stress: (a) for a central hole; (b) for a hole at (2;2) *cm*; (c) for a hole at (5;3) *cm*.

Stopping criteria were assumed in the elastostatics problem, both for the number of generations (no to exceed 100), and also for the tolerance (difference between two fitness functions less than or equal to 1×10^{-6}). The crossover fraction was set as 0.95, and, hence, the mutation fraction is 0.05 for the GA approach presented in this work. The elitism considered that 10 individuals survive in the next generation. The function that performs the crossover was heuristic function, considering a value of ratio equal to 0.9. The mutation function was uniform function where each gene has a probability 0.03 of being mutated. Another GA parameter configured was the migration. In this work, the migration fraction was set as 0.20, the direction of migration was set as "both" directions and 20 generations pass between migrations of individuals between subpopulations. Finally, the selection function was the roulette selection.

The GA technique requires soma extra care for its implementation, due to the required choices for the configuration of the algorithm parameters, which may be different for each problem. This choice depends on the realization of a great number of experiments and tests. Moreover, the GA also presents a high computational cost due to the several evaluations of the fitness function. The damage detection code using GA can find a region for the probable occurrence of the hole, as this algorithm generates a different optimal solution every time it is run. Thus, a confidence interval, for the different parameters being identified, can be obtained.

4.3. Analysis of the results obtained from the artificial neural network

Considering the problem of heat flow, initially the presence of a single hole in the structure was studied. Then, the influence in the results was verified when the number of sensors at the plate was decreased. However, as above mentioned, no study regarding the sensor positioning was accomplished in this work. As well as the input data, the values used to test the network were assembled following the sensor distribution scheme at the plate. A hole of radius 0.10 *cm* in different positions was considered to test the network. The best choice for the parameters of the backpropagation neural network (BPN) was 50 neurons in the input layer, 4 neurons in the hidden layer, and 4 neurons in the output layer. The other parameters of the ANN were set as:

- Threshold function in the input and hidden layers: tan-sigmoid transfer function;
- Threshold function in the output layer: linear transfer function;
- Training function: gradient descent with momentum and adaptive learning rate;

- Error goal: 1×10^{-5};
- Number of epochs: 5000;
- Learning rate: 0.05.

The influence of the reduction of the sensor number in the results found by the ANN for a hole in the position (3;3) *cm* and radius equal to 0.10 *cm* can be analyzed at Table 1. Table 2 shown the results for a hole in the position (4;2) *cm*. The problem domain is reduced when there is a decrease of the sensor number on the plate. The obtained results depend on the distribution of the sensor on the plate and of the quality of the input data.

Table 1. Influence of the reduction of the sensor number for a central hole.

"Real" hole				**Simulated hole**		
Sensors number	***x***	***y***	***r***	***x***	***y***	***r***
25	3.00	3.00	0.10	3.0035	3.0003	0.0992
15	3.00	3.00	0.10	2.9949	2.9977	0.1009
9	3.00	3.00	0.10	2.9998	2.9973	0.1002
5	3.00	3.00	0.10	3.0010	2.9959	0.1000

Table 2. Influence of the reduction of the sensor number for a non-central hole.

"Real" hole				**Simulated hole**		
Sensors number	***x***	***y***	***r***	***x***	***y***	***r***
25	4.00	2.00	0.10	3,4568	0,5676	0,0994
15	4.00	2.00	0.10	2,1225	0,5135	0,0994
9	4.00	2.00	0.10	2,4224	0,4355	0,0224
5	4.00	2.00	0.10	1,4138	0,9774	0,1000

The results obtained for a hole of radius 0.10 *cm* in the positions (3;3) *cm* (Figure 10(a)), (1;1) *cm* (Figure 10 (b)), and (5;5) *cm* (Figure 10 (c)) for 5 sensors on the plate is shown in Figure 10.

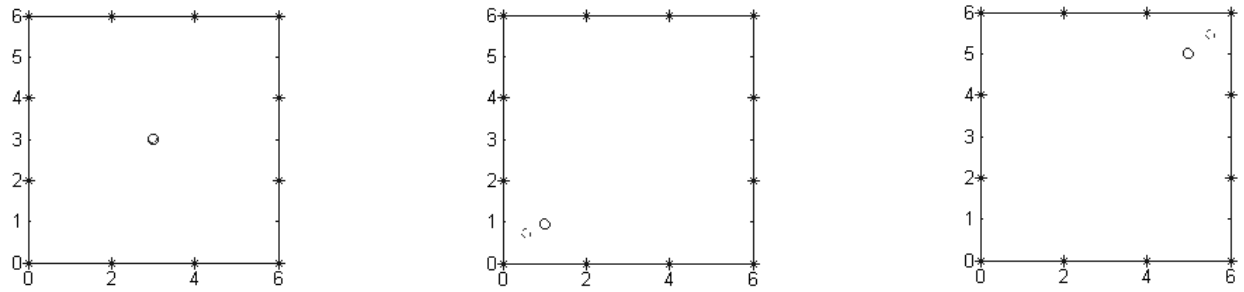

(a) (b) (c)

Figure 10. Potential problem: results from the ANN with 5 sensors for a hole at position: (a) (3;3) *cm*; (b) (1;1) *cm*; (c) hole at position (5;5) *cm*.

For the elastostatics formulation, the ANN simulates the non-linear behavior between the values of the local difference in the mean stress (between the undamaged plate and the plate with the damage) and the hole parameters (location and size). Information regarding the difference in the mean stress is supplied in the input of the network, besides the parameters of the hole are supplied in the output of the same network. Holes of

different sizes and at different places can be part of the data supplied to the net. Having defined the input and output data, the next step is to build the network and, then, this network can be trained. Finally, the network can be tested for other data of difference in the mean stress, obtaining as answer, the location and size of the hole.

As according to the initial population of GA, the values of the difference in the mean stress and the hole parameters were also normalized, before using these values directly. After training the network with these data, this network was tested for a hole of radius 0.12 *cm* in different positions. Figure 11 shows some the results obtained, considering 9 sensors on the plate and, whose distribution is presented in Figure 5(b). The network was configured with 100 neurons in the input layer, 50 neurons in the hidden layer, and 3 neurons in the output layer. Differently from the parameter configuration of ANN for potential formulation, the error goal was set as 1×10^{-2}, and the learning rate was set as 0.01.

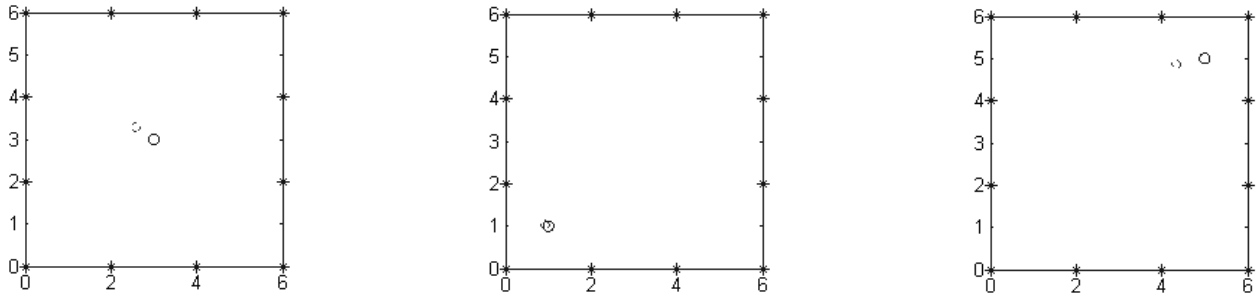

Figure 11. Elastostatics problem: results from the ANN for a hole at position: (a) (3;3) *cm*; (b) (1;1) *cm*; (c) (5;5) *cm*; and.

In Figure11, the results present a small area of uncertainty near the “real” hole; moreover, the size of the hole was obtained with good accuracy. These results were similar to those presented in Figure 10, for the potential problem, and they were obtained more quickly than in the case of using GA (as a global optimization technique). For this reason, the solution of a damage detection problem through the ANN (as a parameter identification technique) is also known as an online identification. An advantage of the use of ANN in regard to the GA is that, after training the network, holes with different sizes and in different locations can be tested without running the damage detection program again.

The damage detection problem using parameter identification technique was solved more quickly than in the case of using global optimization techniques. In this work, the solution of the problem through ANN presented good results for the several parameters being identified. In particular, the size of the hole was obtained with good accuracy, and the location of the hole was given by a fairly small area of uncertainty near the “real” hole, for the several cases tested. In part, difficulties in finding the exact area of the occurrence of the damage are due to training problems of the network, or choice of the configuration parameters of the network or the choice of the input and output data. Taking into account the advantages of each technique, a hybrid approach could be considered for future work. In this approach, the GA could be used to find the occurrence area of the damage, and then the ANN could find the exact size of this damage, reducing the search time for the optimum result.

4.4. Example of analysis of noise or measurement error in the data

To examine how the inverse method using GA herein responds to measurement error, random noises were introduced into measured data. The flowchart presented in Figure 12 shows this approach.

The random noise is a signal formed by a set of random numbers drawn from a normal distribution

with zero mean (white noise) and with COV (coefficient of variation) given as a percentage (5% or 10%) of the measurement value at the sensor location. This noise is added to the measured data, to create a set called "Measured data 2". This new measured data was normalized (as discussed in section 4.2) and then used in the GA approach for the elastostatics problem. The GA approach was run 10 times, for each case (5% and 10% noise), always considering the same configuration of parameters as in the case without noise. In each run of the GA, a different noise signal was generated, with the proper COV.

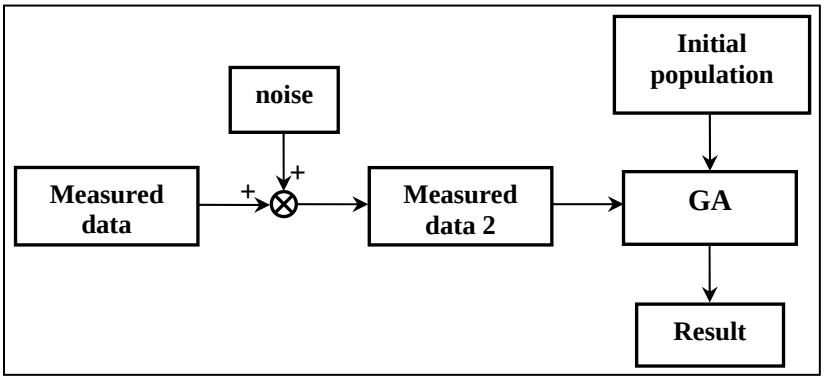

Figure 12. Flowchart for the analysis of the measurement error.

A hole in (3,3) *cm* position with a radius size equal to 0.12 *cm* was simulated for the elastostatics problem, considering a random noise with 5% and 10% introduced into measured data. The results are summarized in Table 3 and Table 4. Table 3 shows the mean results obtained through 10 runs of GA with 5% random noise in measured data, where errors around 2.10%, 3.30% and 4.17% were obtained in *x*-location, *y*-location and radius size, respectively, which are comparable with the errors for the noise-free results. These errors were small and no regularization is needed in this case. Besides, as mentioned previously, GA generates a different optimal solution every time it is run. When the GA was analyzed with 10% random noise (Table 4), the error in radius size was about 7.50%, and the errors in *x*-location and *y*-location were similar to the errors for the 5% random noise case. These results show that the GA optimization procedure, for identification and localization of the hole in the structure, presents very small sensitivities to changes in the measured values at the sensors, proving the robustness of the algorithm. A similar analysis of the measurement noise, or errors in the measured data, can be performed, to investigate the case of the inverse method using ANN, and is the object of the current research.

Table 3. Results obtained with GA for 5% random noises into measured data.

Result	noise-free	Error (noise-free) [%]	With noise of 5%	Error (with noise) [%]
x	3.069	2.30	3.063	2.10
y	2.731	8.97	2.901	3.30
r	0.127	5.83	0.125	4.17

Table 4. Results obtained with GA for 10% random noises into measured data.

Result	noise-free	Error (noise-free) [%]	With noise of 10%	Error (with noise) [%]
x	3.069	2.30	3.006	0.20
y	2.731	8.97	2.933	2.23
r	0.127	5.83	0.129	7.50

If a logarithmic transformation $J_j^{'} = \log\left(J_j + \varepsilon\right)$ (with $\varepsilon = 0.1 \times 10^{-5}$ to prevent the appearance of a $-\infty$ value in the function [1]) is done in the functional formulation (Equation (4)), the result for a central hole is slightly improved. Table 5 shows the comparison between the results without logarithmic transformation (case A) and with this transformation (case B) for a hole in (3,3) *cm* position and a radius size equal to 0.12 *cm*, and errors of simulation with regard to a "real" hole. Table 6 shows the mean results obtained through 10 runs of GA with 10% random noise in measured data, where an error about 0.57%, 2.23% and 7.50% were obtained in *x*-location, *y*-location and radius size, respectively, which are comparable with the errors for the noise-free results, considering a logarithmic transformation.

Table 5. Comparison of GA identification results using the mean stress, with and without a logarithmic transformation (cases B and A, respectively).

Result	Case A	Error case A [%]	Case B	Error case B [%]
X	3.069	2.30	2.918	2.73
Y	2.731	8.97	2.909	3.03
R	0.127	5.83	0.122	1.67

Table 6. Comparison of GA results for the mean stress with logarithmic transformation (case B), with and without 10% random noise in the measured data.

Result	Case B	Error case B [%]	With noise of 10%	Error (with noise) [%]
x	2.918	2.73	3.017	0.57
y	2.909	3.03	2.933	2.23
r	0.122	1.67	0.129	7.50

The results from Table 5 illustrate the fact that, in most cases, the use of the logarithmic transformation tends to reduce the percent error in the identification of the parameters of the damage. According to Table 5, the error in *y*-location for both cases, A and B, was larger than the error in *x*-location. A possible reason for the difference in these results is that only a central hole was simulated for the plate model presented in Figure 5. From Table 6, one can see that no significant change occurred in the results when a noise of 10% was added in the measured data. The GA approach presented in this work is robust in regard to measurement error, as only small errors were obtained at the results (radius, *x*- and *y*-location) when an error of 10% was added in the measured data. The plate is square and symmetric, as can be seen in Figure 5; however, the boundary conditions induce an asymmetry in the model. The influence of the plate's aspect ratio and boundary conditions, as well as the proximity between the hole and different sections of the boundary (for example, smooth parts of the boundary versus corners, or sections with different boundary conditions) is an object of current investigation.

The present work is limited to a simple thin plate with a circular hole. For more general problem, multiple damages can be addressed, requiring a new assembly of chromosomes (Equation (10)) of GA and also changes in the input data of ANN, to account for the presence of these multiple damages. Cracks can also be modeled, on a first approximation, as elliptical holes, so that the BEM formulation presented in this work could also be used. By doing so, a new assembly of chromosomes of the GA has to be performed, including individuals that represent elliptical hole, and new inputs have to given to ANN accordingly, allowing the identifications of circular and elliptical holes in the plate. After this first approximation for the crack is implemented, a more accurate formulation for the BEM direct model should be considered, to properly model the presence of the crack (for example, by using a BEM formulation specific for fracture mechanics, such as the dual boundary element method [21]). As part of the ongoing research, the extension of this approach to multiple damages and multiple types of damages is being undertaken, together with a proper treatment of

uncertainties, which are present not only in the measurements, but also in the numerical simulations (due to discretization errors), and in the problem parameters, such as the domain geometry variables and material properties.

4.5. GA approach for damage identification: a comparison with literature results

The method herein (that uses measurements of differences in mean stress) was compared with a result presented in [1] (that uses measurements of the boundary displacements and tractions). For both examples that were compared, a plate with external dimensions $(0.10 \times 0.10)\, m$ was simulated, and the loading was applied on the left-hand side external boundary. The material constants were considered equal to $100\ GPa$ for shear modulus and 0.3 for Poisson's ratio. In our work, the results of comparison were reached for a static loading of $1000\ MPa$ in both the horizontal and in the vertical coordinate direction, on the left-hand side external boundary, and the right-hand side was fixed. In [1], the plate was subjected to a harmonic dynamic loading in both directions at the left-hand side, and the right-hand side was also fixed.

Table 7 shows the results for GA found by [1] and the results presents in our work. In [1], the results were obtained after running GA with 200 generations, a population equal to 5 (no information is given in that text on how the individuals of the population are placed in the plate), and the plate under dynamic loading (for more details, see the reference [1]). In our work, the parameters of the GA were configured according to those parameters presented in section 4.2 for the elastostatics problem, regarding 200 generations and a population of 49 individuals. As a test, only a hole with diameter equal to 0.5 was considered in some positions where the test case ("real" hole) was not included in the initial population (the *x* and *y*-coordinate of the center of the hole was varied from 0.5 cm to 9.5 cm with a step size of 1.5 cm), hence, validating the results obtained. For a general problem, more individuals have to consider in the initial population of GA.

Table 7. GA approach: comparison with literature results.

Test	**"Real" hole**	**Results presented by [1]**			**Results in this work**		
		Calculated best element	**Average for 1000 solutions**	**Error [%]**	**Calculated best element**	**Average for 20 solutions**	**Error [%]**
x	4.0	3.9606	5.59	38.75	3.7336	3.52	12.00
y	4.0	4.0236	4.74	18.50	3.9578	3.95	1.25
diameter	0.5	0.4968	0.52	4.00	0.5000	0.53	6.00

As shown in Table 7, the GA approach used in this work has presented, for most cases, more accurate results in the identification of the "real" hole dimensions, with respect to the GA approach used in [1]. In the literature example, an average of 1000 solutions was computed, while, in this work, only an average for 20 solutions was performed. Also, for each solution, only a few seconds were needed to run the inverse program using GA on a PC. These features illustrate the accuracy and the low computational cost of the current approach.

5. Conclusions

In this work, an inverse problem of identifying damage in a plate structure was solved using both optimization and parameter identification techniques. A genetic algorithm (GA) was used as the optimization technique, and an artificial neural network (ANN) code was used as the parameter identification procedure. Two models for the direct problem were investigated, one considering a heat flow problem and another considering an elastostatics problem. In the heat flow problem, the boundary element method (BEM) for the

potential was considered for the direct problem. The BEM for the potential supplies the necessary information (potential values at internal points of the plate) to the damage detection program. In the elastostatics problem, a boundary element method (BEM) formulation was used as the direct model in this inverse problem. The refinement of the mesh for the direct BEM model was shown to play an important role, improving accuracy in the damage identification results, when a fine mesh was used. The analyses of the results indicates that the damage detection code using GA can only find a region for the probable occurrence of the hole, as this algorithm generates a different optimal solution every time it is run. The fitness function of the GA approach presented in this work has converged for the specified tolerance, before the algorithm has reached the maximum number of generations. Moreover, this GA approach was robust in regard to the measurement error, as only a small error was obtained in the results when a noise of 10% was added to the measured data. Also, this GA approach compares well, both in accuracy and in computational cost, with respect to a similar GA approach used in the literature for damage identification. The solution of the problem through ANN has also presented good results for the several parameters being identified.

An important observation is that very small holes are difficult to observe by the damage detection program, mainly when these holes are close to the borders of the plate. The optimization and the identification techniques adopted in this inverse problem can be used concomitantly, as independent procedures to identify the presence of a hole on the plate, thus providing a means to verify the numerical results obtained for the location and size of the damage in the structure, increasing the confidence in the damage identification results.

6. Acknowledgements

The authors would like to acknowledge the financial support from the Brazilian agencies CNPq – Conselho Nacional de Desenvolvimento Científico e Tecnológico, and FAPEMIG – Fundação de Amparo à Pesquisa do Estado de Minas Gerais, and also the financial support from AFOSR - Air Force Office of Scientific Research.

7. References

[1] G.E. Stravoulakis and H. Antes, *Flaw identification in elastomechanics: BEM simulation with local and genetic optimization*, Structural Optimization, Springer-Verlag. 16 (1998), pp. 162-175.

[2] M. Engelhardt, G.E. Stavroulakis, and H. Antes, *Crack and flaw identification in elastodynamics using Kalman filter techniques*, Computational Mechanics. 37 (2006), pp. 249-265.

[3] Y.C. Liang and C. Hwu, *On-line identification of holes/cracks in composite structures*, Institute of Physics Publishing, Smart Materials and Structures. 10 (2001), pp. 599-609.

[4] T. Burczynski and W. Beluch, *The identification of crack using boundary elements and evolutionary algorithms*, Engineering Analysis with Boundary Elements. 25 (2001), pp. 313-322.

[5] S.W. Liu, J.H. Huang, J.C. Sung, and C.C. Lee, *Detection of cracks using neural networks and computational mechanics*, Computer Methods in Applied Mechanics and Engineering. 191 (2002), pp. 2831–2845.

[6] T.J. Martin and G.S. Dulikravich, *Finding unknown surface temperatures and heat fluxes in steady heat conduction*, 4th InterSociety Conf: Thermal Phenomena in Electronic Systems (I-THERM IV) (Edited by A. Ortega and D. Agonafer), Washington, DC, 1994, pp. 214-221.

[7] T.J. Martin, J.D. Halderman, and G.S. Dulikravich, *An inverse method for finding unknown surface tractions and deformations in elastostatics*, Computers & Structures. 56, No. 5. (1995), pp. 825-835.

[8] P.K. Basu, A.B. Jorge, S. Badri, and J. Lin, *Higher-Order Modeling of Continua by Finite-Element, Boundary-Element, Meshless, and Wavelet Methods*, Computers and Mathematics with Applications. 46 (2003), pp. 15-33.

[9] C.A. Brebbia, J. Dominguez, *Boundary Elements - An Introductory Course*, 2nd ed., McGraw-Hill, Boston, 1992.
[10] F. Paris and J. Cañas, *Boundary Element Method - Fundamentals & Applications*, Oxford Univ. Press, New York, 1997.
[11] G. Rus, R. Gallego, *Optimizations algorithms for identification inverse problems with the boundary element method*, Engineering Analysis with Boundary elements. 26 (2002), pp. 315-327.
[12] R. Gallego and J. Suárez, *Solution of inverse problems by boundary integral equations without residual minimization*, International Journal of Solids and Structures. 37 (2000), pp. 5629-5652.
[13] J.H. Chou and J. Ghaboussi, *Genetic algorithm in structural damage detection*, Computers and Structures. 79 (2001), pp. 1335-1353.
[14] D.E. Goldberg, *Genetic Algorithms in Search, Optimization and Machine Learning*, Addison-Wesley Co, Massachusetts, 1998.
[15] J.C. Spall, *Evolutionary Computation I: Genetic Algorithms*, in *Introduction to stochastic search and optimization: estimation, simulation, and control*, John Wiley & Sons, Inc., 2003
[16] M. Mitchell, *An Introduction to Genetic Algorithms*, 5th Edition, MIT Press, Cambridge, Massachusetts-London, England, 1999.
[17] E.K.P. Chong and S.H. Zak, *An Introduction to optimization*, 2nd ed., John Wiley & Sons, Inc., 2001.
[18] H.S. Rao, V.G. Ghorpade, and A. Mukherjee, *A genetic algorithm based back propagation network for simulation of stress–strain response of ceramic-matrix-composite*s, Computers and Structures. 84 (2006), pp. 330–339.
[19] K. Gurney, *An Introduction to Neural Networks*, CRC Press, University of Sheffield, UK, 1997.
[20] A.B. Jorge, P.S. Lopes, and M.E. Lopes, On the use of boundary element methods for inverse problems of damage detection in structures, in Advances in Boundary Element Techniques IX (BETEQ 2008), R.A.A. García and M.H. Aliabadi, eds., EC Ltd, UK, 2008.
[21] A. Portela, M.H. Aliabadi, and D.P. Rooke, *The dual boundary element method: Effective implementation for crack problems*, International Journal for Numerical Methods in Engineering. 33 (1992), pp. 1269-1287.

Computation of moments and stresses in laminated composite plates by the boundary element method

Adriana dos Reis Gouvea[*,a], Eder Lima de Albuquerque[*,a], Fernando Luiz Torsani[a], Leandro Palermo[b], Paulo Sollero[a]

[a]*Faculty of Mechanical Engineering, State University of Campinas, Campinas, SP, 13083-970, Brazil*
[b]*Faculty of Civil Engineering, State University of Campinas, Campinas, SP, 13083-852, Brazil*

Abstract

This paper presents a boundary integral formulation for the computation of moments and stresses at internal and boundary points of laminated composite plates. An integral equation for the second displacement derivative is developed and all derivatives of the fundamental solution are computed analytically. Stresses on the boundary are computed by a procedure that uses integral equations, derivatives of shape functions, and constitutive relations. The obtained results are in good agreement with finite element results available in literature.

Key words: laminated composite, boundary element method, stress analysis.

1. Introduction

The attempt of developing analytical models for the representation of the behavior of plates comes since middle of 1800 with works developed by Sophie Germain, Lagrange, and Poisson [1]. Since 1978, when the first general direct formulation based on the Kirchhoff's hypothesis appeared, the boundary element method (BEM) has had large growth, being nowadays applied to several practical engineering problems. The first works discussing the use of boundary element direct formulation, in conjunction with the Kirchhoff's theory, were by Bezine [2], Stern [3], and Tottenhan [4]. Nowadays, BEM is a well-established numerical technique to deal with an enormous number of engineering complex problems. Analysis of plate bending problems using the BEM has attracted the attention of many researchers during the past years, proving to be a particularly adequate field of applications for that technique. The fundamental solution is an essencial part of the boundary element method. Bending analysis of thin plates by the BEM requires the use of two fundamental solutions: the displacement field due to a transverse point load, and the displacement field due to a point moment. Fundamental solutions for anisotropic plates utilize complex variable theory following Lekhnitskii [5]. Shi and Bezine [6], presented a boundary element analysis of plate bending problems using fundamental solutions proposed by [7] based on Kirchhoff plate bending assumptions. Rajamohan and Raamachandran [8], proposed a formulation where the singularities were avoided by placing source points outside the domain. Paiva et al [9], presented an analytical treatment for singular and hypersingular integrals of the formulation presented in [6]. Albuquerque et al [10] presented a method to transform domain integrals into boundary integrals in the formulation presented in [6]. In [11], this formulation was extended for dynamic problems. Shear deformable shells have been analyzed using the boundary element method by [13] with the analytical fundamental solution proposed by [14]. Wang and Huang [15], presented a boundary element formulation for orthotropic shear deformable plates. Later, in [16], the previous formulation was extended to laminate composite plates. Recently, [17] presented a displacement discontinuity formulation for modeling cracks in orthotropic Reissner plates.

This paper proposes numerical procedures to compute moments and stresses in internal points and at the boundary of composite laminated plates using a boundary element thin plate formulation. To the best of author's knowledge, there is no paper in literature that

[*]Corresponding authors
Email addresses: adriana@fem.unicamp.br (Adriana dos Reis Gouvea), ederlima@fem.unicamp.br (Eder Lima de Albuquerque)

presents a boundary element formulation to compute moments and stresses in anisotropic plates or shells.

2. Boundary integral equation

As shown by [10], boundary integral equations for transverse displacements of anisotropic thin plates and its derivative can be written, respectively, as:

$$
\begin{aligned}
& Kw(Q) \\
& + \int_{\Gamma} \left[V_n^*(Q,P) w(P) - M_n^*(Q,P) \frac{\partial w(P)}{\partial n} \right] d\Gamma(P) \\
& + \sum_{i=1}^{N_c} R_{c_i}^*(Q,P) w_{c_i}(P) \\
& - \int_{\Gamma} \left[V_n(P) w^*(Q,P) - M_n(P) \frac{\partial w^*}{\partial n}(Q,P) \right] d\Gamma(P) \\
& + \sum_{i=1}^{N_c} R_{c_i}(P) w_{c_i}^*(Q,P) + \int_{\Omega} g(P) w^*(Q,P) d\Omega, \qquad (1)
\end{aligned}
$$

and

$$
\begin{aligned}
& K \frac{\partial w}{\partial m}(Q) \\
& + \int_{\Gamma} \left(\frac{\partial V_n^*}{\partial m}(Q,P) w(P) - \frac{\partial M_n^*}{\partial m}(Q,P) \frac{\partial w}{\partial n}(P) \right) d\Gamma(P) \\
& + \sum \frac{\partial R_{ci}^*}{\partial m}(Q,P) w_{ci}(P) \\
& - \int_{\Gamma} \left(V_n(P) \frac{\partial w^*}{\partial m}(Q,P) - M_n(P) \frac{\partial^2 w^*}{\partial n \partial m}(Q,P) \right) d\Gamma(P) \\
& + \sum R_{ci}(P) \frac{\partial w_{ci}^*}{\partial m}(Q,P) + \int_{\Omega} g(P) \frac{\partial w^*}{\partial m}(Q,P) d\Omega. \qquad (2)
\end{aligned}
$$

where $\frac{\partial}{\partial n}$ is the derivative in the direction of the outward vector **n** that is normal to the boundary Γ; $\frac{\partial}{\partial m}$ is the directional derivative at the source point on the boundary normal direction **m**; M_n and V_n are, respectively, the normal bending moment and the Kirchhoff equivalent shear force on the boundary Γ; R_c is the thin-plate reaction of the corners; w_c is the transverse displacement of the corners; P is the field point; Q is the source point; and an asterisk denotes a fundamental solution.
The transverse displacement fundamental solution is given by:

$$
\begin{aligned}
w^*(\rho,\theta) = & \frac{1}{8\pi} \{ C_1 R_1(\rho,\theta) + C_2 R_2(\rho,\theta) \\
& + C_3 [S_1(\rho,\theta) - S_2(\rho,\theta)] \}, \qquad (3)
\end{aligned}
$$

where

$$
\rho = [(x - x_o)^2 + (y - y_o)^2]^{1/2}, \qquad (4)
$$

x and y are the coordinates of the field point P, x_o and y_o are the coordinates of source point Q,

$$
\theta = \arctan \frac{y - y_o}{x - x_o}, \qquad (5)
$$

$$
C_1 = \frac{(d_1 - d_2)^2 - (e_1^2 - e_2^2)}{GHe_1}, \qquad (6)
$$

$$
C_2 = \frac{(d_1 - d_2)^2 + (e_1^2 - e_2^2)}{GHe_2}, \qquad (7)
$$

$$
C_3 = \frac{4(d_1 - d_2)}{GH}, \qquad (8)
$$

$$
G = (d_1 - d_2)^2 + (e_1 + e_2)^2, \qquad (9)
$$

$$
H = (d_1 - d_2)^2 + (e_1 - e_2)^2, \qquad (10)
$$

$$
\begin{aligned}
R_i = & \rho^2 \left[(\cos\theta + d_i \sin\theta)^2 - e_i^2 \sin^2\theta \right] \\
& \times \left\{ \log \left[\frac{\rho^2}{a^2} \left((\cos\theta + d_i \sin\theta)^2 + e_i^2 \sin^2\theta \right) \right] - 3 \right\} \\
& - 4\rho^2 e_i \sin\theta (\cos\theta + d_i \sin\theta) \\
& \times \arctan \left(\frac{e_i \sin\theta}{\cos\theta + d_i \sin\theta} \right), \qquad (11)
\end{aligned}
$$

$$
\begin{aligned}
S_i = & \rho^2 e_i \sin\theta (\cos\theta + d_i \sin\theta) \\
& \times \left\{ \log \left[\frac{\rho^2}{a^2} \left((\cos\theta + d_i \sin\theta)^2 + e_i^2 \sin^2\theta \right) \right] - 3 \right\}
\end{aligned}
$$

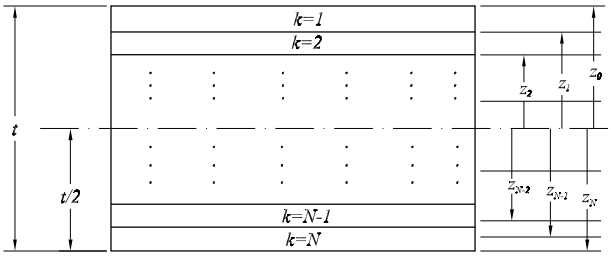

Figure 1: Staking sequence in a laminate composite plate with N plies.

$$+\rho^2\left[(\cos\theta + d_i \sin\theta)^2 - e_i^2 \sin^2\theta\right]$$

$$\times \arctan\left(\frac{e_i \sin\theta}{\cos\theta + d_i \sin\theta}\right), \quad (12)$$

d_i and e_i are the real and the imaginary part, respectively, of the roots of the characteristic polynomial:

$$D_{22}\mu^4 + 4D_{26}\mu^3 + 2(D_{12} + 2D_{66})\mu^2$$

$$+4D_{16}\mu + D_{11} = 0, \quad (13)$$

D_{11}, D_{16}, D_{12}, D_{22}, D_{26}, and D_{66} are the bending stiffness constants of an anisotropic thin plate.
The repeated index i in R_i and S_i does not imply summation. The coefficient a is an arbitrary constant taken as $a = 1$.
Other fundamental solutions are shown in works of [6] and [10].

3. Computation of stresses and moments on internal points

Laminates are fabricated such that they act as an integral structural element. To assure this condition, the bond between two plies in a laminate should be infinitesimally thin and not shear deformable to avoid the ply slip over each other, and to allow displacement continuity along the bond (see [21]). Thus, we could consider that strains are continuous along the thickness. However, as each ply is of a different material, stresses present discontinuities along laminate interfaces.
As presented by [21], stresses at each ply can be evaluated from strain by:

$$\left\{\begin{array}{c}\sigma_x\\ \sigma_y\\ \tau_{xy}\end{array}\right\} = \overline{\mathbf{Q}}\left\{\begin{array}{c}\varepsilon_x\\ \varepsilon_y\\ \gamma_{xy},\end{array}\right\}, \quad (14)$$

where matrix $\overline{\mathbf{Q}}$ is given by:

$$\overline{\mathbf{Q}} = \mathbf{T^{-1}Q(T^{-1})^t}. \quad (15)$$

The transformation matrix $\mathbf{T}$ is given by:

$$\mathbf{T} = \left[\begin{array}{ccc}\cos^2\alpha & \sin^2\alpha & 2\sin\alpha\cos\alpha\\ \sin^2\alpha & \cos^2\alpha & -2\sin\alpha\cos\alpha\\ -\sin\alpha\cos\alpha & \sin\alpha\cos\alpha & \cos^2\alpha - \sin^2\alpha\end{array}\right], \quad (16)$$

where α is the angle between the fiber direction of given ply and the global reference xy, and stiffness matrix $\mathbf{Q}$ is given in terms of engineering constants by:

$$\mathbf{Q} = \left[\begin{array}{ccc}\frac{E_L}{1-\nu_{LT}\nu_{TL}} & \frac{\nu_{LT}E_T}{1-\nu_{LT}\nu_{TL}} & 0\\ \frac{\nu_{LT}E_T}{1-\nu_{LT}\nu_{TL}} & \frac{E_T}{1-\nu_{LT}\nu_{TL}} & 0\\ 0 & 0 & G_{LT}\end{array}\right], \quad (17)$$

where E_L and E_T are elasticity moduli in the longitudinal and transversal directions, respectively, G_{LT} is the shear modulus in the plane of the ply, and ν_{LT} is the Poisson coefficient (see, for example [21]).
Moments are given by:

$$M_x = -\left(D_{11}\frac{\partial^2 w}{\partial x^2} + D_{12}\frac{\partial^2 w}{\partial y^2} + 2D_{16}\frac{\partial^2 w}{\partial x \partial y}\right), \quad (18)$$

$$M_y = -\left(D_{12}\frac{\partial^2 w}{\partial x^2} + D_{22}\frac{\partial^2 w}{\partial y^2} + 2D_{26}\frac{\partial^2 w}{\partial x \partial y}\right), \quad (19)$$

and

$$M_{xy} = -\left(D_{16}\frac{\partial^2 w}{\partial x^2} + D_{26}\frac{\partial^2 w}{\partial y^2} + 2D_{66}\frac{\partial^2 w}{\partial x \partial y}\right). \quad (20)$$

In Kirchhoff plates, strains are given by:

$$\varepsilon_x = -z\frac{\partial^2 w}{\partial x^2}, \quad (21)$$

$$\varepsilon_y = -z\frac{\partial^2 w}{\partial y^2}, \quad (22)$$

$$\gamma_{xy} = -2z\frac{\partial^2 w}{\partial x \partial y}. \quad (23)$$

where z is the distance from the point where displacements are been computed and the midplane (see Figure 1).
So, in order to obtain strains, moments, and stresses, the second order derivatives of integral equation (1) need to be computed. These derivatives are given by:

$$\frac{\partial^2 w(Q)}{\partial x^2}$$

$$= \int_\Gamma \left[\frac{\partial^2 V_n^*}{\partial x^2}(Q,P) w(P) - \frac{\partial^2 M_n^*}{\partial x^2}(Q,P) \frac{\partial w(P)}{\partial n} \right] d\Gamma(P)$$

$$+ \sum_{i=1}^{N_c} \frac{\partial^2 R_{c_i}^*}{\partial x^2}(Q,P) w_{c_i}(P)$$

$$- \int_\Gamma \left[V_n(P) \frac{\partial^2 w^*}{\partial x^2}(Q,P) - M_n(P) \frac{\partial^3 w^*}{\partial n \partial x^2}(Q,P) \right] d\Gamma(P)$$

$$+ \sum_{i=1}^{N_c} R_{c_i}(P) \frac{\partial^2 w_{c_i}^*}{\partial x^2}(Q,P) + \int_\Omega g(P) \frac{\partial^2 w^*}{\partial x^2}(Q,P) d\Omega, \quad (24)$$

$$\frac{\partial^2 w(Q)}{\partial y^2}$$

$$= \int_\Gamma \left[\frac{\partial^2 V_n^*}{\partial y^2}(Q,P) w(P) - \frac{\partial^2 M_n^*}{\partial y^2}(Q,P) \frac{\partial w(P)}{\partial n} \right] d\Gamma(P)$$

$$+ \sum_{i=1}^{N_c} \frac{\partial^2 R_{c_i}^*}{\partial y^2}(Q,P) w_{c_i}(P)$$

$$- \int_\Gamma \left[V_n(P) \frac{\partial^2 w^*}{\partial y^2}(Q,P) - M_n(P) \frac{\partial^3 w^*}{\partial n \partial y^2}(Q,P) \right] d\Gamma(P)$$

$$+ \sum_{i=1}^{N_c} R_{c_i}(P) \frac{\partial^2 w_{c_i}^*}{\partial y^2}(Q,P) + \int_\Omega g(P) \frac{\partial^2 w^*}{\partial y^2}(Q,P) d\Omega, \quad (25)$$

and

$$\frac{\partial^2 w(Q)}{\partial x \partial y}$$

$$= \int_\Gamma \left[\frac{\partial^2 V_n^*}{\partial x \partial y}(Q,P) w(P) - \frac{\partial^2 M_n^*}{\partial x \partial y}(Q,P) \frac{\partial w(P)}{\partial n} \right] d\Gamma(P)$$

$$+ \sum_{i=1}^{N_c} \frac{\partial^2 R_{c_i}^*}{\partial x \partial y}(Q,P) w_{c_i}(P)$$

$$- \int_\Gamma \left[V_n(P) \frac{\partial^2 w^*}{\partial x \partial y}(Q,P) - M_n(P) \frac{\partial^3 w^*}{\partial n \partial x \partial y}(Q,P) \right] d\Gamma(P)$$

$$+ \sum_{i=1}^{N_c} R_{c_i}(P) \frac{\partial^2 w_{c_i}^*}{\partial x \partial y}(Q,P) + \int_\Omega g(P) \frac{\partial^2 w^*}{\partial x \partial y}(Q,P) d\Omega, \quad (26)$$

where the second derivative of the transversal displacement fundamental solutions in relation to x is given by:

$$\frac{\partial^2 w^*(\rho,\theta)}{\partial x^2} = \frac{1}{8\pi} \left\{ C_1 \frac{\partial^2 R_1(\rho,\theta)}{\partial x^2} + C_2 \frac{\partial^2 R_2(\rho,\theta)}{\partial x^2} \right.$$

$$\left. + C_3 \left[\frac{\partial^2 S_1(\rho,\theta)}{\partial x^2} - \frac{\partial^2 S_2(\rho,\theta)}{\partial x^2} \right] \right\}. \quad (27)$$

Second order derivatives of other fundamental solutions in relation to x are given by:

$$\frac{\partial^2 M_n^*}{\partial x^2} = -\left(f_1 \frac{\partial^4 w^*}{\partial x^4} + f_2 \frac{\partial^4 w^*}{\partial x^3 \partial y} + f_3 \frac{\partial^4 w^*}{\partial x^2 \partial y^2} \right), \quad (28)$$

$$\frac{\partial^2 R_{c_i}^*}{\partial x^2} = -\left(g_1 \frac{\partial^4 w^*}{\partial x^4} + g_2 \frac{\partial^4 w^*}{\partial x^3 \partial y} + g_3 \frac{\partial^4 w^*}{\partial x^2 \partial y^2} \right), \quad (29)$$

$$\frac{\partial^2 V_n^*}{\partial x^2} = -\left(h_1 \frac{\partial^5 w^*}{\partial x^5} + h_2 \frac{\partial^5 w^*}{\partial x^4 \partial y} + h_3 \frac{\partial^5 w^*}{\partial x^3 \partial y^2} + h_4 \frac{\partial^5 w^*}{\partial x^2 \partial y^3} \right)$$

$$- \frac{1}{R} \left(h_5 \frac{\partial^4 w^*}{\partial x^4} + h_6 \frac{\partial^4 w^*}{\partial x^3 \partial y} + h_7 \frac{\partial^4 w^*}{\partial x^2 \partial y^2} \right). \quad (30)$$

Second order derivatives in relation to y and xy are computed by similar procedures and will not be shown herein. Derivatives of fundamental solutions of transversal displacement w can be expressed by linear combination of R_i and S_i derivatives. All derivatives of R_i and S_i up to the 4th order are presented by [6]. The 5th order derivatives are given by:

$$\frac{\partial^5 R_i}{\partial x^5} = \frac{8(\cos\theta + d_i \sin\theta)}{\Delta_1}$$

$$\times \frac{\left[\cos^2\theta + \left({d_i}^2 - 3{e_i}^2 \right) \sin^2\theta + d_i \sin 2\theta \right]}{\Delta_1}, \quad (31)$$

$$\frac{\partial^5 R_i}{\partial x^4 \partial y} = \frac{8[d_i \cos^3\theta + 3\left(d_i^2 + e_i^2\right)\sin\theta\cos^2\theta}{\Delta_1}$$

$$+\frac{3d_i\left(d_i^2 + e_i^2\right)\sin^2\theta\cos\theta + \left(d_i^4 - e_i^4\right)\sin^3\theta]}{\Delta_1}, \quad (32)$$

$$\frac{\partial^5 R_i}{\partial x^3 \partial y^2} = \frac{8}{\rho^3}\left\{\frac{\left(d_i^2 - e_i^2\right)\cos^3\theta + 3d_i\left(d_i^2 + e_i^2\right)\sin\theta\cos^2\theta}{\Delta_2}\right.$$

$$\left.+\frac{3\left(d_i^2 + e_i^2\right)^2\sin^2\theta\cos\theta + d_i\left(d_i^2 + e_i^2\right)^2\sin^3\theta}{\Delta_2}\right\}, \quad (33)$$

$$\frac{\partial^5 R_i}{\partial x^2 \partial y^3} = \frac{8}{\rho^3}\left\{\frac{d_i\left(d_i^2 - 3e_i^2\right)\cos^3\theta + 3\left(d_i^4 - e_i^4\right)\sin\theta\cos^2\theta}{\Delta_2}\right.$$

$$\left.+\frac{3d_i\left(d_i^2 + e_i^2\right)^2\sin^2\theta\cos\theta + \left(d_i^2 + e_i^2\right)^3\sin^3\theta}{\Delta_2}\right\}, \quad (34)$$

$$\frac{\partial^5 R_i}{\partial x \partial y^4} = \frac{8}{\rho^3}\left\{\frac{\left(d_i^4 - 6e_i^2 d_i^2 + e_i^4\right)\cos^3\theta}{\Delta_2}\right.$$

$$+\frac{3d_i\left(d_i^4 - 2e_i^2 d_i^2 - 3e_i^4\right)\sin\theta\cos^2\theta}{\Delta_2}$$

$$+\frac{3\left(d_i^2 - e_i^2\right)\left(d_i^2 + e_i^2\right)^2\sin^2\theta\cos\theta}{\Delta_2}$$

$$\left.+\frac{d_i\left(d_i^2 + e_i^2\right)^3\sin^3\theta}{\Delta_2}\right\}, \quad (35)$$

$$\frac{\partial^5 R_i}{\partial y^5} = \frac{8}{\rho^3}\left\{\frac{d_i\left(d_i^4 - 10e_i^2 d_i^2 + 5e_i^4\right)\cos^3\theta}{\Delta_2}\right.$$

$$+\frac{3\left(d_i^6 - 5e_i^2 d_i^4 - 5e_i^4 d_i^2 + e_i^6\right)\sin\theta\cos^2\theta}{\Delta_2}$$

$$+\frac{3d_i\left(d_i^2 - 3e_i^2\right)\left(d_i^2 + e_i^2\right)^2\sin^2\theta\cos\theta}{\Delta_2}$$

$$\left.+\frac{\left(d_i^2 - e_i^2\right)\left(d_i^2 + e_i^2\right)^3\sin^3\theta}{\Delta_2}\right\}, \quad (36)$$

$$\frac{\partial^5 S_i}{\partial x^5} = \frac{4ei\sin\theta[-3\cos^2\theta - 6di\sin\theta\cos\theta}{\Delta_1}$$

$$+\frac{\left(ei^2 - 3di^2\right)\sin^2\theta]}{\Delta_1}, \quad (37)$$

$$\frac{\partial^5 S_i}{\partial x^4 \partial y} = \frac{4e_i[\cos^3\theta - 3\left(d_i^2 + e_i^2\right)\sin^2\theta\cos\theta}{\Delta_1}$$

$$-\frac{2d_i\left(d_i^2 + e_i^2\right)\sin^3\theta]}{\Delta_1}, \quad (38)$$

$$\frac{\partial^5 S_i}{\partial x^3 \partial y^2} = \frac{4e_i[2d_i\cos^3\theta + 3\left(d_i^2 + e_i^2\right)\sin\theta\cos^2\theta}{\Delta_1}$$

$$-\frac{\left(d_i^2 + e_i^2\right)^2\sin^3\theta]}{\Delta_1}, \quad (39)$$

$$\frac{\partial^5 S_i}{\partial x^2 \partial y^3} = \frac{4e_i\cos\theta[\left(3d_i^2 - e_i^2\right)\cos^2\theta}{\Delta_1}$$

$$+\frac{3\left(d_i^2 + e_i^2\right)\sin\theta\left[2d_i\cos\theta + \left(d_i^2 + e_i^2\right)\sin\theta\right]}{\Delta_1}, \quad (40)$$

$$\frac{\partial^5 S_i}{\partial x \partial y^4} = \frac{4e_i}{\rho^3}\left\{\frac{4d_i(d_i - e_i)(d_i + e_i)\cos^3\theta}{\Delta_2}\right.$$

$$+\frac{3\left(3d_i^2 - e_i^2\right)\left(d_i^2 + e_i^2\right)\sin\theta\cos^2\theta}{\Delta_2}$$

$$\left.+\frac{6d_i\left(d_i^2 + e_i^2\right)^2\sin^2\theta\cos\theta + \left(d_i^2 + e_i^2\right)^3\sin^3\theta}{\Delta_2}\right\}, \quad (41)$$

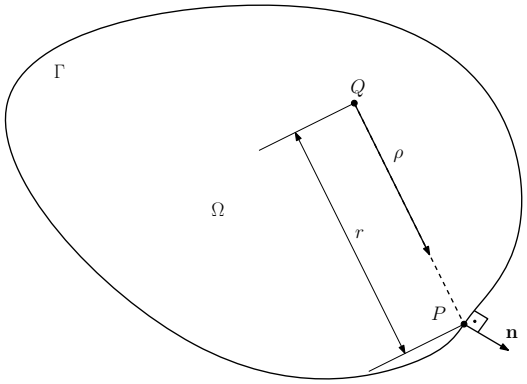

Figure 2: Variables of the transformation of the domain integral into a boundary integral.

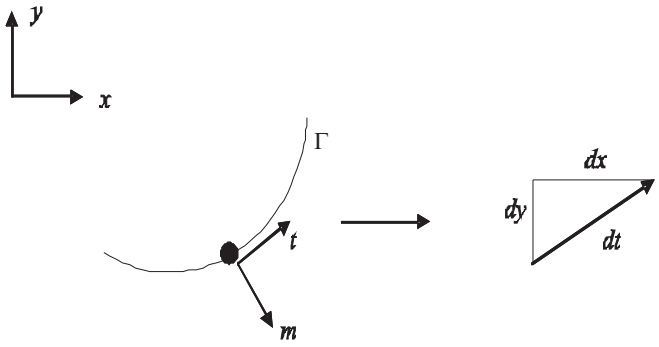

Figure 3: Normal *m* and tangential *t* directions at the source point.

and

$$\frac{\partial^5 S_i}{\partial y^5} = \frac{4e_i}{\rho^3}\left\{\frac{\left(5{d_i}^4 - 10{e_i}^2{d_i}^2 + ei^4\right)\cos^3\theta}{\Delta_2}\right.$$

$$+\frac{12d_i\left({d_i}^4 - {e_i}^4\right)\sin\theta\cos^2\theta}{\Delta_2}$$

$$-\frac{3\left({e_i}^2 - 3{d_i}^2\right)\left({d_i}^2 + {e_i}^2\right)^2\sin^2\theta\cos\theta}{\Delta_2}$$

$$\left.+\frac{2d_i\left({d_i}^2 + {e_i}^2\right)^3\sin^3\theta}{\Delta_2}\right\}, \tag{42}$$

where $\Delta_1 = \rho^3\left[\cos^2\theta + \left({d_i}^2 + {e_i}^2\right)\sin^2\theta + d_i\sin 2\theta\right]^3$ and $\Delta_2 = \left[\cos^2\theta + \left({d_i}^2 + {e_i}^2\right)\sin^2\theta + d_i\sin 2\theta\right]^3$.

The last term of equation (24) can be transformed from a domain integral to a boundary integral following the procedure proposed by [10]. Thus, considering a linear distributed load $g = Ax + By + C$, we have:

$$\int_{\Omega_g} g\frac{\partial^2 w^*}{\partial x^2}d\Omega = \int_\Gamma \frac{H^*}{r}\frac{\partial r}{\partial n}d\Gamma, \tag{43}$$

where

$$H^* = \int_0^r (Ax + By + C)\frac{\partial^2 w^*}{\partial x^2}\rho d\rho, \tag{44}$$

r is the value of ρ at the boundary (Figure 2).

4. Computation of stresses on the boundary

Equations (24), (25), and (26) present integrals whose kernels have singularities of order $\frac{1}{\rho^3}$. To compute stresses on the boundary, those equations will provide integrals that are more than hypersingular. Consequently, the computation of stresses on the boundary demands an alternative approach.

The directional derivative of equation (1) at the source point in the boundary tangential direction (Figure 3) is given by:

$$\frac{\partial w}{\partial t} + \int_\Gamma\left(\frac{\partial V_n^*}{\partial t}w - \frac{\partial M_n^*}{\partial t}\frac{\partial w}{\partial n}d\Gamma\right) + \sum\frac{\partial R_{ci}^*}{\partial t}w_{ci}$$

$$= \int_\Gamma\left(V_n\frac{\partial w^*}{\partial t} - M_n\frac{\partial^2 w^*}{\partial n\partial t}\right)d\Gamma + \sum R_{ci}\frac{\partial w_{ci}^*}{\partial t}$$

$$+\int_\Omega g\frac{\partial w^*}{\partial t}d\Omega. \tag{45}$$

Inside a quadratic discontinuous boundary element, the directional derivative of the transversal displacement in the tangential direction is given by:

$$\frac{dw}{dt} = N_1\frac{\partial w_1}{\partial t} + N_2\frac{\partial w_2}{\partial t} + N_3\frac{\partial w_3}{\partial t}. \tag{46}$$

where $\frac{\partial w_1}{\partial t}$, $\frac{\partial w_2}{\partial t}$, and $\frac{\partial w_3}{\partial t}$ are derivatives of w at boundary element nodes in the tangent to the boundary direction at the source point. N_1, N_2, and N_3 are quadratic discontinuous shape functions written as:

$$N_1 = \xi\left(\frac{9}{8}\xi - \frac{3}{4}\right), \tag{47}$$

$$N_2 = \left(1 - \frac{3}{2}\xi\right)\left(1 + \frac{3}{2}\xi\right), \quad (48)$$

and

$$N_3 = \xi\left(\frac{9}{8}\xi + \frac{3}{4}\right). \quad (49)$$

The second derivative of the transversal displacement is given by:

$$\frac{d^2w}{dt^2} = \frac{d}{d\xi}\left(\frac{\partial w}{\partial t}\right)\frac{d\xi}{dt}. \quad (50)$$

Writing $\frac{dw}{dt}$ in terms of nodal values interpolated by shape functions as given by equation (46), we have:

$$\frac{d^2w}{dt^2} = \frac{d}{d\xi}\left(N_1\frac{\partial w_1}{\partial t} + N_2\frac{\partial w_2}{\partial t} + N_3\frac{\partial w_3}{\partial t}\right)\frac{d\xi}{dt}, \quad (51)$$

or

$$\frac{d^2w}{dt^2} = \left(\frac{dN_1}{d\xi}\frac{\partial w_1}{\partial t} + \frac{dN_2}{d\xi}\frac{\partial w_2}{\partial t} + \frac{dN_3}{d\xi}\frac{\partial w_3}{\partial t}\right)$$

$$\times\left(1/\frac{dt}{d\xi}\right). \quad (52)$$

Following a similar procedure to $\frac{d^2w}{dmdt}$, it is possible to obtain:

$$\frac{d^2w}{dmdt} = \left(\frac{dN_1}{d\xi}\frac{\partial w_1}{\partial m} + \frac{dN_2}{d\xi}\frac{\partial w_2}{\partial m} + \frac{dN_3}{d\xi}\frac{\partial w_3}{\partial m}\right)$$

$$\times\left(1/\frac{dt}{d\xi}\right). \quad (53)$$

where $\frac{\partial w_1}{\partial m}$, $\frac{\partial w_2}{\partial m}$, and $\frac{\partial w_3}{\partial m}$ are derivatives of w at boundary element nodes in the normal to the boundary direction at the source point.

It was not possible to calculate $\frac{d^2w}{dm^2}$ in the same way of $\frac{d^2w}{dt^2}$ and $\frac{d^2w}{dmdt}$ because we do not have $\frac{dm}{d\xi}$. An alternative is to write equations of moments in reference system *mt*:

$$M_m = -\left(D_{11}^{'}\frac{\partial^2 w}{\partial m^2} + D_{12}^{'}\frac{\partial^2 w}{\partial t^2} + 2D_{16}^{'}\frac{\partial^2 w}{\partial m \partial t}\right), \quad (54)$$

$$M_t = -\left(D_{12}^{'}\frac{\partial^2 w}{\partial m^2} + D_{22}^{'}\frac{\partial^2 w}{\partial t^2} + 2D_{26}^{'}\frac{\partial^2 w}{\partial m \partial t}\right), \quad (55)$$

and

$$M_{mt} = -\left(D_{16}^{'}\frac{\partial^2 w}{\partial m^2} + D_{26}^{'}\frac{\partial^2 w}{\partial t^2} + 2D_{66}^{'}\frac{\partial^2 w}{\partial m \partial t}\right). \quad (56)$$

where $D_{ij}^{'}$ $(i, j = 1, 2, 6)$ are the flexural rigidities in reference system *mt*, that is:

$$\mathbf{D}^{'} = \begin{bmatrix} D_{11}^{'} & D_{12}^{'} & D_{16}^{'} \\ D_{12}^{'} & D_{22}^{'} & D_{26}^{'} \\ D_{16}^{'} & D_{26}^{'} & D_{66}^{'} \end{bmatrix} = \mathbf{T^{-1}DT}, \quad (57)$$

where

$$\mathbf{D} = \begin{bmatrix} D_{11} & D_{12} & D_{16} \\ D_{12} & D_{22} & D_{26} \\ D_{16} & D_{26} & D_{66} \end{bmatrix}. \quad (58)$$

In this system, the known variables are: M_m, $\frac{\partial^2 w}{\partial t^2}$ and $\frac{\partial^2 w}{\partial m \partial t}$, and the unknown variables are: M_t, M_{mt}, and $\frac{\partial^2 w}{\partial m^2}$.

Writing those equations in a matrix form, we have:

$$\begin{Bmatrix} M_m \\ M_t \\ M_{mt} \end{Bmatrix} = \begin{bmatrix} D_{11}^{'} & D_{12}^{'} & D_{16}^{'} \\ D_{12}^{'} & D_{22}^{'} & D_{26}^{'} \\ D_{16}^{'} & D_{26}^{'} & D_{66}^{'} \end{bmatrix} \begin{Bmatrix} \frac{\partial^2 w}{\partial m^2} \\ \frac{\partial^2 w}{\partial t^2} \\ \frac{\partial^2 w}{\partial m \partial t}. \end{Bmatrix}. \quad (59)$$

Thus, from equation (59), we have:

$$\frac{\partial^2 w}{\partial m^2} = S_{11}^{'}M_m + S_{12}^{'}M_t + S_{16}^{'}M_{mt}, \quad (60)$$

$$\frac{\partial^2 w}{\partial t^2} = S_{12}^{'}M_m + S_{22}^{'}M_t + S_{26}^{'}M_{mt}, \quad (61)$$

and

$$\frac{\partial^2 w}{\partial m \partial t} = S_{16}^{'}M_m + S_{26}^{'}M_t + S_{66}^{'}M_{mt}, \quad (62)$$

where

$$\mathbf{S}^{'} = \begin{bmatrix} S_{11}^{'} & S_{12}^{'} & S_{16}^{'} \\ S_{12}^{'} & S_{22}^{'} & S_{26}^{'} \\ S_{16}^{'} & S_{26}^{'} & S_{66}^{'} \end{bmatrix} = \mathbf{D}^{'-\mathbf{1}}. \quad (63)$$

Isolating the unknown variables, we have:

$$-\frac{\partial^2 w}{\partial m^2} + S_{12}^{'}M_t + S_{16}^{'}M_{mt} = -S_{11}^{'}M_m, \quad (64)$$

$$S_{22}^{'}M_t + S_{26}^{'}M_{mt} = \frac{\partial^2 w}{\partial t^2} - S_{12}^{'}M_m, \quad (65)$$

and

$$S_{26}^{'}M_t + S_{66}^{'}M_{mt} = \frac{\partial^2 w}{\partial m \partial t} - S_{16}^{'}M_m, \quad (66)$$

that can be written in the matrix form as:

$$\begin{bmatrix} -1 & S'_{12} & S'_{16} \\ 0 & S'_{22} & S'_{26} \\ 0 & S'_{26} & S'_{66} \end{bmatrix} \begin{Bmatrix} \frac{\partial^2 w}{\partial m^2} \\ M_t \\ M_{mt} \end{Bmatrix}$$

$$= \begin{Bmatrix} -S'_{11} M_t \\ \frac{\partial^2 w}{\partial t^2} - S'_{12} M_m \\ \frac{\partial^2 w}{\partial m \partial t} - S'_{16} M_m \end{Bmatrix}. \quad (67)$$

The unknowns $\frac{\partial^2 w}{\partial m^2}$, M_t and M_{mt} can be computed by solving the linear system (67).
Finally, the transformation

$$\begin{Bmatrix} \frac{\partial^2 w}{\partial x^2} \\ \frac{\partial^2 w}{\partial y^2} \\ \frac{\partial^2 w}{\partial x \partial y} \end{Bmatrix} = \mathbf{T} \begin{Bmatrix} \frac{\partial^2 w}{\partial m^2} \\ \frac{\partial^2 w}{\partial t^2} \\ \frac{\partial^2 w}{\partial m \partial t} \end{Bmatrix}, \quad (68)$$

can be used to compute second derivatives necessary to calculate moments and stresses.

5. Numerical Results

5.1. Laminate plate with clamped edges

Consider a cross-ply laminated graphite/epoxy composite square plate with clamped edges under uniformly distributed load of intensity q and with edge length a = 1 m. The laminate is a nine ply symmetrical cross-ply laminate with the lay-up [0/90/0/90/0/90/0/90/0]. All plies have the same thickness. The total thickness is equal to h = 0.001 m and material properties are: E_L = 207 GPa, E_T = 5.2 GPa, G_{LT} = 3.1 GPa, and ν_{LT}= 0.25. The plate was discretized using 12 quadratic discontinuous boundary elements, as shown in Figure 4. The displacement at point *A* and the moment at point *B*, shown in Figure 4, are compared with finite element results obtained by [23]. As it can be seen in Table 1, the agreement between the boundary element thin plate and the finite element shear deformable plate is very good if we considered that the finite element formulation takes into account the effects of shear deformation.

Figure 5 shows the distribution of the stress σ_x at point *B* along the thickness of the plate, from the mid-surface to the top surface. It can be seen that, as the stiffness of the material is higher in the direction of the fibers, the stress is higher in the lamina with fibers oriented parallel to the axis x ($\alpha = 0^o$).

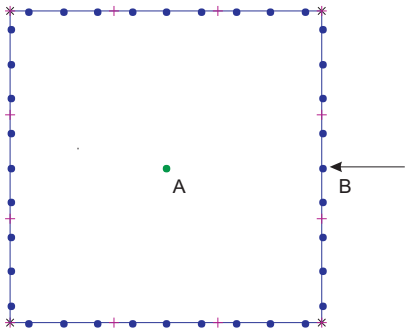

Figure 4: Discretization square plate using 3 elements per side.

Table 1: Displacements and moments in a square plate with clamped edges.

Node		This work	Reference [23]
A	$wE_T h^3/(qa^4)\times 10^3$	0.9511	0.9341
B	$M_{xx}/(qa^2)\times 10^2$	−7.0704	-6.6551

5.2. Laminated plate with simply-supported edges

Now, consider the same laminate with stacking sequence $[+\alpha/-\alpha/+\alpha/-\alpha/+\alpha/-\alpha/+\alpha/-\alpha/+\alpha]$ with $0 \le \alpha \le 45^o$. All edges are simply-supported. Material properties, dimensions, load, and the mesh used are the same of previous example. Figures 6 and 7 show the effect of the variation of θ on the displacement and resultant moments, respectively, at the centre of the plate (point A). They are compared with finite element results obtained by [23]. As it can be seen, in both cases the agreement between the boundary element thin plate and the finite element shear deformable plate is very good. Figure 8 shows the stress distribution σ_x along the thickness of the plate at point A, considering $\alpha = 45^o$. In this case, as all layers present fibers inclined with respect to x direction, variations of stress between layers are smaller than in previous case.

5.3. Orthotropic plate with clamped edges

The third example is a clamped square plate with edge length a = 0.254 m and the ratio between thicknesses and edge length h/a = 0.05. The plate is subjected to a uniformly distributed static load q. The following material parameters are used in the numerical analysis: E_T = 6.895 GPa, $E_L = 2E_T$, ν_{LT} = 0.3, and $G_{LT} = E_T/2(1+\nu_{LT})$. The mesh used is the same

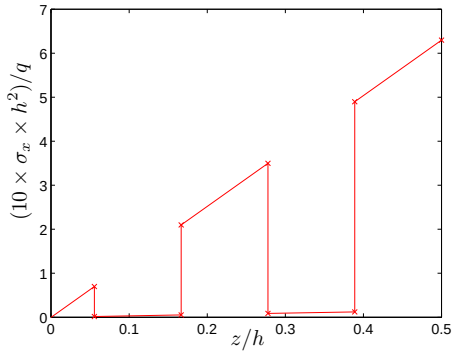

Figure 5: Stress distribution σ_x along the thickness for the cross-ply laminate at point B of the plate.

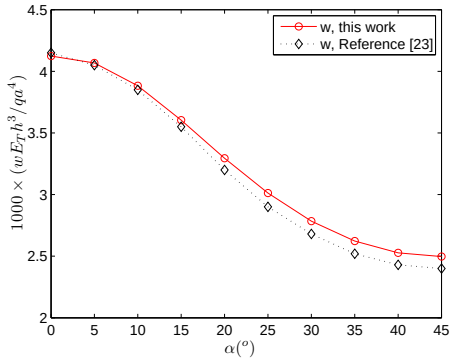

Figure 6: Effect of the fiber orientation α on the transversal displacement response at the centre of the plate.

of the first example (Figure 4). Figure 9 presents moments M_x computed by the present work and results obtained by [24], using the meshless Petrov-Galerkin method (MLPG). Results are shown along the central line of the plate, at $y = a/2$. As it can be seen, there is a perfect agreement between both results. As in [24], bending moments are normalized by the central bending moment value of isotropic plate $M_x^{(iso)}(a/2) = 3064$ Nm.

6. Conclusions

This paper presented a boundary integral formulation for the computation of moments and stresses at internal and boundary points of laminated composite thin plates. An integral equation for the second displacement derivative is developed and all derivatives of the fundamental solution are computed analytically. In the proposed approach, in order to avoid singularities that are higher than hypersingular, second derivatives of transversal displacement on the boundary were com-

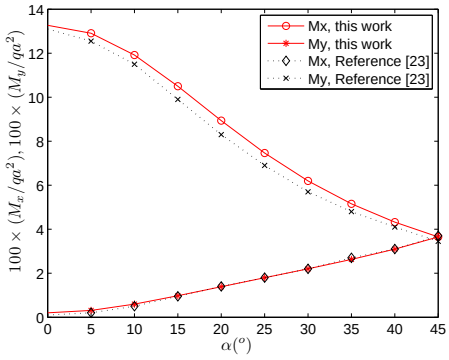

Figure 7: Effect of the orientation α on the moment response at the centre of the plate.

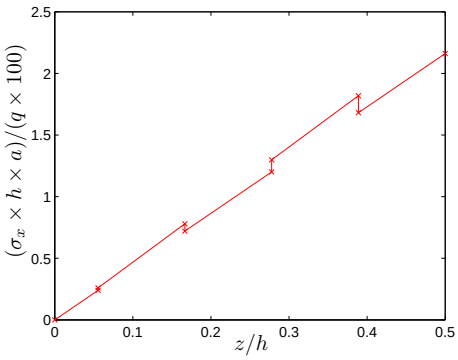

Figure 8: Stress distribution σ_x along the thickness for $\alpha = 45^o$ at the centre point of the plate.

puted using constitutive equations and shape function derivatives. The obtained results are in good agreement when compared with results available in literature.

References

[1] W.D. Pilkey and W. Wunderlich, *Mechanics of structures: variational and computational methods*, CRC Press, Inc Boca Raton, Florida, USA, (1994).

[2] G.P. Bezine. Boundary integral formulation for plate flexure with arbitrary boundary conditions, *Mech. Res. Comm.*, Vol. **5**, pp. 197–206, (1978).

[3] M.A. Stern. A general boundary integral formulation for the numerical solution of plate bending problems, *Int. J. Solids Struct.*, Vol. **15**, pp. 769–782, (1979).

[4] H. Tottenham, *The boundary element method for plates and shells*, P.K. Banerjee and R. Butterfield (Editors), Vol. I, (1979).

[5] S.G. Lekhnitskii, *Anisotropic plates*, Gordon and Breach, New York, (1968).

[6] G. Shi and G. Bezine. A general boundary integral formulation for the anisotropic plate bending problems, *J. Composite Material*, Vol. **22**, pp. 694–716, (1988).

[7] B.C. Wu and N.J. Altiero. A new numerical method for the

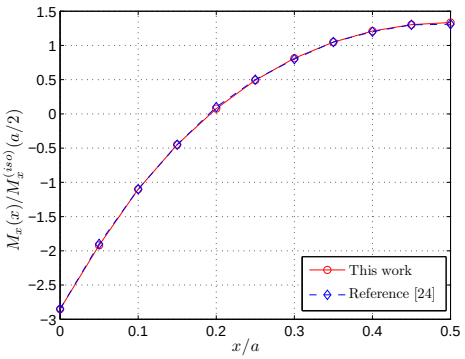

Figure 9: Variation of the bending moment along $(x, a/2)$ for a clamped square plate.

analysis of anisotropic thin plate bending problems,*Computer Meth.in Appl.Mech. and Eng.*, Vol. **25**, pp. 343–353, (1981).

[8] C. Rajamohan and J. Raamachandran. Bending of anisotropic plates charge simulation method, *Advances in Eng. Software*, Vol. **30**, pp. 369–373, (1999).

[9] W.P. Paiva, P. Sollero and E.L. Albuquerque. Treatment of hipersingularities in boundary element anisotropic plate bending problems, *Latin American J. of Solids and Struc.*, Vol. **1**, pp. 49–73, (2003).

[10] E.L. Albuquerque, P. Sollero, W. Venturini and M.H. Aliabadi. Boundary element analysis of anisotropic Kirchhoff plates, *Int. J. of Solids and Struc.*, Vol. **43**, pp. 4029–4046, (2006).

[11] E.L. Albuquerque, P. Sollero, W.P. Paiva. The radial integration method appied to dynamic problems of anisotropic plates, *Communic. in Num. Methods in Eng.*, Vol. **23**, pp. 805–818, (2007).

[16] J. Wang and K. Schweizerhof. Study on free vibration of moderately thick ortotropic laminated shallow shells by boundary-domain elements, *Appl. Math. Modelling*, Vol. **20**, pp. 579–584, (1996).

[13] J. Wang and K. Schweizerhof. Free vibration of laminated anisotropic shallow shells including transverse shear deformation by the boundary-domain element method, *Computers and Structures*, Vol. **62**, pp. 151–156, (1997).

[14] J. Wang and K. Schweizerhof. The fundamental solution of moderately thick laminated anisotropic shallow shells, *Intern. Journal Eng. Sci.*, Vol. **33**, pp. 995–1004, (1995).

[15] J. Wang and M. Huang. Boundary element method for ortotropic thick plates, *Acta Mech. Sin.*, Vol. **7 (3)**, pp. 258–266,(1991).

[16] J. Wang and K. Schweizerhof. Fundamental solutions and boundary integral equations of moderately thick symmetrically laminated anisotropic plates, *Communic. in Num. Methods in Eng.*, Vol. **12**, pp. 383–394, (1996).

[17] P.H. Wen and M.H. Aliabadi. Displacement discontinuity formulation for modeling cracks in ortotropic shear deformable plates, *Intern. Journal Fract.*, Vol. **142**, pp. 69–79, (2006).

[18] M. Ameen, *Boundary element analysis: theory and programming*, CRC Press, Inc Boca Raton, Florida, USA, (2000).

[19] J. H. Kane, *Bondary element analysis in engineering continuum mechanics*. Prentice Hall, New Jersey (1994).

[20] C. A. Brebbia and J. Domingues, *Boundary elements an introductory course*. 2nd Edition, WIT Press, Southampton (1998).

[21] B. D. Agarwal and L. J. Broutman, *Analysis and performance of fiber composites*. 2nd Edition, John Wiley and Sons Inc, New York (1990).

[22] S. Timoshenko and S. Woinowski-Kriger, *Theory of plates and shells*, 2nd. ed. New York: McGraw-Hill, 1959.

[23] H. V. Lakshminarayana and S. S. Murthy. A shear-flexible triangular finite element model for laminated composite plates. *Intern. Journal for Num. Methods in Eng.*, Vol. **20**,pp. 591–623, (1984).

[24] J. Sladek, V. Sladek, Ch. Zhang, J. Krivacek and P. H. Wen. Analysis of orthotropic thick plates by meshless local Petrov-Galerkin (MLPG) method, *Intern. Journal for Num. Methods in Eng.*, Vol. **67**, pp. 1830-1850,(2006).